University of Siena – Department of Medical Biotechnologies

Doctorate in Genetics, Oncology and Clinical Medicine (GenOMeC)

XXXIII cycle (2017-2020)

Coordinator: Prof. Francesca Ariani

CRISPR-Cas9 gene editing: a new promising treatment for Rett syndrome

Scientific disciplinary sector: MED/03 – Medical Genetics

Tutor   PhD Candidate

Prof. Ilaria Meloni   Susanna Croci

Academic Year 2019/2020

Radboudumc

Radboud university medical center
Human Genetics

P.O. Box 9101, 6500 HB Nijmegen
The Netherlands
Internal postal code 855
Geert Grooteplein 10
Radboudumc Main entrance, route 855
T +31 24 361 40 17
F +31 24 366 87 52

Head of Department
H.G. Brunner, Prof.
www.radboudumc.nl

Dutch Chamber of Commerce
trade register 41055629/4

Dott.ssa Susanna Croci, PhD Student
Doctorate in Genetics, Oncology and Clinical
Medicine
Department of medical biotechnology
University of Siena
Viale Bracci 2, 53100 Siena (SI)
Italy

Date	Our reference	Page
30 October 2020		1 of 2

Your reference	Contact

Subject
Ph.D. thesis report Susanna Croci

Dear Mrs. Croci,

It was a great pleasure to read and evaluate your thesis, entitled "CRISPR-Cas9 gene editing: a new promising treatment for Rett syndrome". I consider this thesis of a very high quality and have no hesitation to recommend it to proceed to the thesis defence and granting the doctoral degree.

The thesis starts with a comprehensive Introduction, which contains an extensive literature review about clinical and genetic aspects of Rett syndrome and its mechanisms of disease as obtained by studying cell and animal models. In addition, a relevant overview is given about CRISPR/Cas9 therapeutic approaches. This part is followed by a general Methods section. The core of the thesis consist of the results, and these are impressive. The results consist of three sections, which each are derived from already published manuscripts. Notably, you are the first author on two of these papers, which is a remarkable achievement. Each of those papers are noteworthy because of the innovative methodologies that have been applied for seemless editing of the mutated loci and the efficacy that was seen in these experiments. The innovative nature of these experiments is objectively illustrated by the fact that a patent has been granted for this technology. My excitement about these results is such that I am going to use your strategy in my own research for editing mutant loci underlying other neurodevelopmental disorders.

The results of the research reported in this thesis are an important starting point for generating novel insights into molecular and cellular mechanism underlying Rett syndrome. In addition, the tools generated might be suitable for use as a thereapeutic strategy in Rett syndrome patients. This is very well discussed in the concluding chapter of the thesis.

I have made a few textual suggestions in the thesis document, but these are minor and mainly typographical. My overall evaluation is highly postive and I like to congratulate you with this impressive work for which you fully deserve the doctoral degree.
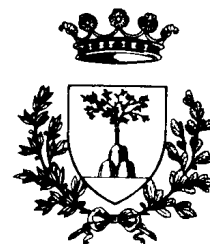
Yours sincerely,

Prof. Dr. Hans van Bokhoven

DEPARTMENT OF BIOMEDICAL AND SPECIALTY SURGERY SCIENCES
SECTION OF PHARMACOLOGY
UNIVERSITY OF FERRARA

MICHELE MORARI, PhD
Associate Professor of Pharmacology
via Fossato di Mortara 19, 44121 Ferrara
ph: +39 0532 455210; fax: +39 0532 455205
E-mail: m.morari@unife.it

Ferrara 3-11-2020

Alla cortese attenzione di
Prof.ssa Francesca Ariani
Coordinatrice
Doctorate in Genetics, Oncology and Clinical Medicine (GenOMeC)
Department of Medical Biotechnologies
University of Siena

Re: Evaluation of Susanna Croci's PhD thesis entitled "CRISPR-Cas9 gene editing: a new promising treatment for Rett syndrome"(XXXIII cycle)

During her PhD research work, the Candidate Susanna Croci, proposed to study the bichemical changes associated with Rett syndrome (RTT) and develop a novel approach of gene therapy to cure this disease. To this aim, the Candidate employed a wide array of cellular and molecular biology techniques, in particular fluorescence microscopy, Western analysis, qRT-PCR, flow cytometry, gene sequencing, gene transfection, complemented by electrophysiology recordings. The novelty of her work greatly emerged in the attempt of leveraging CRISPR/Cas9 gene editing techniques to design and validate a two-plasmid system to correct disease-relevant mutations in MECP2 and FOXG1 genes, and in its delivery to the brain via viral vectors.

The Candidate's interest in RTT is inspired by the lack of available therapies for this rare neurodevelopmental disease which essentially affects girls, among whom it represents the second cause of mental retardation. Therefore, the choice to do research in this field is widely justified and also clinically relevant. The translational potential of the Candidate's research is high given the effort to develop a novel gene therapy approach that appears very promising in light of the preliminary results presented in the thesis.

The Results Section is particularly rich and broken down on into three chapters focused on: i) the biochemical and electrophysiological characterization of iPSCs

obtained from two RTT patients carrying mutations of *MECP2* gene (Section I); the validation of a two-plasmid system capable to deliver a CRISPR/Cas9 system aimed at the correction of the c.473C>T (p.T158M) mutation of *MECP2* (Section II); the validation of a two-plasmid system capable to deliver a CRISPR/Cas9 system aimed at the correction of the c.688C>T (p.R230C) and c.765G>A (p.W255*) mutations of *FOXG1* gene, and its packing into an AAV vector (Section III).

The main findings of this thesis can be summarized as follows:

- In Section I, the Candidate developed a cellular model of RTT reprogramming neurons from fibroblasts taken from patients with *MECP2* mutations. These neurons were characterized in terms of gene expression using RNAseq and electrophysiological properties using patch-clamp. Perhaps, the most important finding was the finding of dysregulation of genes involved in GABAergic transmission (GAD1, GABA$_A$ receptor subunit alpha-1, GAD67,…), which was associated with a reduction of GABA-mediated currents and an increase in firing activity. An increase in HDAC6 expression was also found. This change was associated with a reduction in acetylated α-tubulin, that was normalized by the application of HDAC6 inhibitors.

- In Section II, the Candidate designed a two-plasmid CRISPR/Cas9 system aimed at the correction of the c.473C>T (p.T158M) pathogenic mutations of *MECP2*. The system also carries two reporter genes (mCherry e EGFP) that allows to monitor the degree of transfection and Cas9 activation. The system has been initially validated in HEK293 cells, where a small percentage (5%) was found to express active Cas9. The sequencing of fibroblasts taken from four different pT158M RTT patients confirmed the success of the correction, even though the efficiently ranged from 20% to 84%, possibly depending on the TP53 gene polymorphism. The efficiency of the correction was further confirmed measuring the levels of MECP2 protein as a readout. Indeed, the mutation is associated with an increase of MECP2 levels and *MECP2* editing resulted in their normalization. Relevant to the translatability of these findings, a significant proportion of corrected alleles (14%) was found in neurons differentiated from the fibroblasts taken from the patient showing the highest levels of correction.

- In Section III, the Candidate used the same technological approach to correct two mutations in the *FOXG1* gene, namely c.688C>T (p.R230C) and c.765G>A

2

(p.W255*). In this case, however, the final aim was to pack the correction system in AAV vectors. Therefore, in the first part of the study, the correction system was validated through a direct transfection in fibroblasts and in fibroblast-derived neurons. Cas9 showed to be activated in both cell models, although with a different degree (50% vs 4%, respectively). Nonetheless, the correction efficiency was significant in both cell models (20% and 34%, respectively). As a biochemical readout of the correction, normalization of PAX6 levels was taken. The specificity of the correction was confirmed by off-target analysis in HEK293 cells. The final part of the study focused on the choice of the more appropriate viral serotype between AAV2 and AAV9, as delivery system. Due to its greater ability to infect iPSC (6% showing Cas9 activation), AAV2 looked more promising.

The thesis is overall well written and organized, the Introduction is clear and accurate, Methods have been clearly described and data adequately discussed. As a suggestion to further improve the quality of the thesis and its readability, I would recommend some changes:

- Introduction:
    - Expand the paragraph on animal models of RTT.
    - Add a paragraph describing the basics of the CRISPR/Cas system and its physiological role. Considering the focus of this thesis (see title), a general description of this system might help the reader better understand the correction system designed by the Candidate and emphasize its relevance.
- Methods
    - Add a paragraph with statistical analysis.
- Add the Abbreviations Section.
- List references with journal title abbreviated according to the official nomenclature.

In addition, I would also suggest to:
- Check the quality of Tables and Figures. For instance, Table 1 is unreadable. Moreover, the quality of Table 4 and Figure 17b is poor.
- Check the accuracy of figure legends.
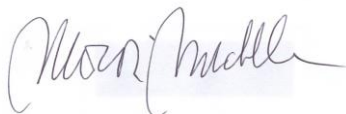- Check the consistency of abbreviations used in text.

- Correct grammar and typographical errors.

I attach to the present evaluation, a word copy of the thesis with my comments and suggestions.

In conclusion, the research activity carried out by Dr Susanna Croci fits well within the scopes of the doctorate program followed by the Candidate. The scientific findings have been presented in three papers published in peer-reviewed scientific Journals (Exp Cell Res, Eur J Hum Genet) with good impact (i.f. 3.7-3.8) in the field of cellular biology, oncology, biochemistry and molecular biology. Considering that in two of these articles, the Candidate is first Author and in the other is co-Author, I strongly believe Dr. Susanna Croci has gained the necessary work experience and professional skills to engage with competence and high motivation in the research field. In expressing my very positive opinion on the research activity carried out by Dr Susanna Croci, I compliment with the Candidate on her work and wish her a brilliant career in science.

Sincerely

Michele Morari

Associate Professor of Pharmacology

Michele Morari, PhD
Dipartimento di Scienze Biomediche e Chirurgico Specialistiche
Sezione di Farmacologia
Università di Ferrara
via Fossato di Mortara 17-19
44121 Ferrara

tel: +39 0532 455210
fax: +39 0532 455205
email: m.morari@unife.it

Index

Abstract

Rett syndrome (RTT) is a neurodevelopmental disorder affecting the central nervous system and is one of the most common causes of intellectual disability in girls, resulting in severe cognitive and physical disabilities. Mutations in *MECP2* and *FOXG1* genes cause the classic form and the congenital variant of Rett syndrome, respectively. Both genes are transcriptional regulators and both under- and over-expression of these gene cause disease in humans. To characterize the biological mechanisms implicated in disease pathogenesis, we established and characterized a human neuronal model based on genetic reprogramming of patient fibroblasts into induced Pluripotent Stem Cells (iPSCs). Functional analyses performed in MECP2 iPSC-derived neurons demonstrated that these cells closely mimic the impairment of molecular pathway characterizing the disease revealing defects in GABAergic system and cytoskeleton dynamics. Furthermore, we explored the possibility to use iPSC-derived neurons to develop and study a new treatment for RTT patients. Effective therapies are not currently available and the need for tight regulation of MeCP2 and FOXG1 expression for proper brain functioning makes gene replacement therapy risky. Therefore, gene editing would be much more effective. Gene editing based on CRISPR/Cas9 technology and Homology Directed Repair appears an appealing option for the development of new therapeutic approaches. We have engineered a two-plasmid system to correct *FOXG1* (c.688C>T (p(Arg230Cys)); C.765G>A (p.Trp255Ter)) and *MECP2* (c.473C>T-p.Thr158Met) variants.. Mutation-specific sgRNAs and donor DNAs have been selected and cloned together with an mCherry/GFP reporter system. Cas9 flanked by sgRNA recognition sequences for auto-cleaving has been cloned in a second plasmid. The system has been designed to be ready for *in vivo* delivery via Adeno-Associated Viral (AAV) vectors. NGS analysis of corrected cells from *MECP2* and *FOXG1* patients demonstrated an high editing efficiency, ranging from 20 to 80 % of HDR and confirmed that this correction strategy is feasible in neurons. Functional analyses in edited cells confirm the correction of molecular defects due to the mutation. Based on the use of AAV viruses and their capacity to cross the Blood Brain Barrier (BBB) following intravenous injection these experiments will allow us to demonstrate the full potential of gene editing as a therapeutic option for RTT and for other neurodevelopmental disorders currently lacking an effective treatment.

1. Introduction

1.1 Rett syndrome: Overview and clinical aspects

Rett syndrome (RTT OMIM# 312750) is a rare neurodevelopmental disorder that predominantly affects female subjects with an estimated prevalence of about 1:10.000 live births [1]. The story of RTT started in 1966 with Dr.Andreas Rett who first described different girl patients with clinical characteristics that today we know are typical of the disease. Only in the 80s RTT was recognized by the medical community thanks to the work of Dr.Bengt Hagberg who described 35 patients, characterized by symptoms similar to those encountered several years earlier by Dr. Rett [2,3]. In 1999, the laboratory of Dr. Huda Zoghby first identified the genetic cause of RTT as a defect in the *MECP2* gene on the X chromosome, responsible for the classic form of the disease [4]. A key factor affecting the complexity and severity of RTT symptoms is X Chromosome Inactivation (XCI), a random phenomenon that occurs during embryonic development were the X chromosome of paternal or that of maternal origin is inactivated and remains so for all subsequent cell divisions. If inactivation of X chromosome with the mutated *MECP2* gene is favored, the number of cells with malfunctioning protein is reduced, and RTT symptoms should be less severe. Conversely, if the X chromosome with the intact copy of the *MECP2* gene is mainly inactivated, the cells with the altered protein are the majority and the symptoms should be more severe. The inactivation status of the X chromosome can vary from tissue to tissue and in the case of RTT, the severity of the clinical picture will cucially depend on how the X chromosome is inactivated in brain cells [5-7]. The severity of the disease can also be modulated by the presence of mosaicism in the patient. Furthermore, different mutations at the level of the same gene can have a different severity, based on their impact on the protein that will be more or less functional depending on the domain on which the variant impacts (Figure 1). In any case, these phenomena alone do not explain the complexity of RTT and several studies have shown that other factors such as genetic polymorphisms, the expression of other genes and the alteration of processes involving miRNAs, can influence the clinic of the disease [8,9].
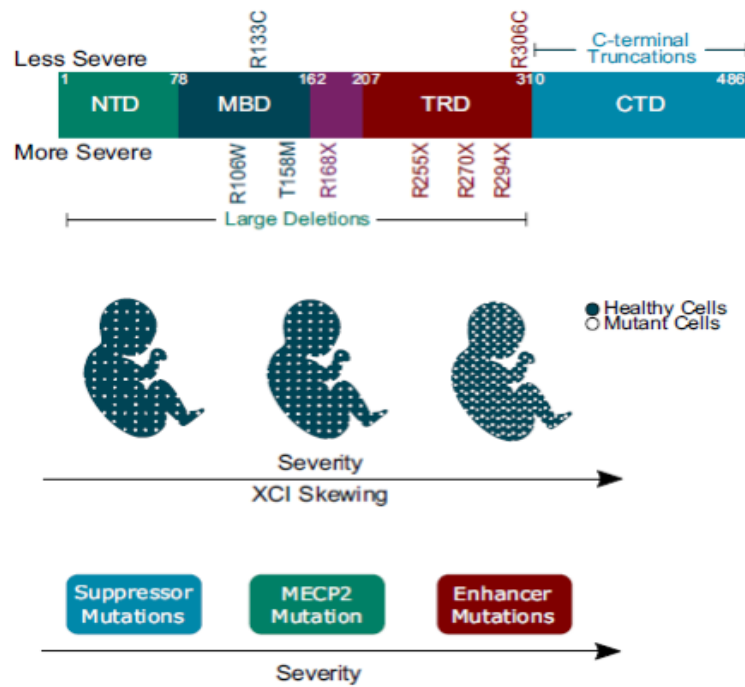
Figure 1. **Disease severity is influenced by the type of mutation and X-inactivation [10].**

RTT affects the central nervous system and is one of the most common causes of severe cognitive impairment in females. It generally occurs after the first 6-18 months of life, when subjects lose the acquired ability to speak and walk present a reduction in interpersonal contact, autistic behavior, involuntary movements, postnatal microcephaly [1].

Since the description of the first patients, RTT phenotype has been progressively expanded from the classic form to clinical variants with different degrees of severity [11-15]. It is now established that classic RTT is mainly due to mutations in *MECP2* gene, while other genes have been identified in patients affected by RTT variants, with *CDKL5*, responsible for the early-onset seizures variant, and *FOXG1*, associated to the congenital variant, being most commonly involved [16]. Methyl-CpG-binding protein 2 (MeCP2) is a DNA-binding protein highly expressed in neurons that either activates or represses transcription depending on the cellular context [17]. It is involved in chromatin compaction, regulation of mRNA splicing and brain development [18,19]. *CDKL5* encodes for a kinase protein involved in multiple functions into brain cells, including the regulation of gene expression, neuronal cell differentiation and proliferation, dendritic arborization, neuronal morphogenesis and synaptic stability [20]. *FOXG1* encodes for a transcriptional repressor that plays a fundamental role during brain development, particularly in the telencephalon, where it is involved in the timing and specification of the neuronal fate and is essential for post-mitotic neuronal survival [21].

Alterations of different pathways in the central nervous system (CNS) are the primary molecular characteristics of RTT. MeCP2 is involved in many different processes, including chromatin compaction, regulation of mRNA splicing and miRNA processing [19,22,23]. Interestingly, it has been recently involved in the regulation of autophagy [24-26]. While the underlying mechanisms are still poorly understood, a direct alteration of autophagy markers has been clearly established in Mecp2 Knock-out mice (KO) [24,25]. Such alterations are absent at birth but emerge later in life, in parallel with the appearance of symptoms [25,26] and they have also been identified in patient fibroblasts, confirming the relevance of the pathway autophagy for RTT [25]. In this context, the mTOR protein kinase act as key integrator of various environmental signals by phosphorylating a range of substrates to control major cell processes such as mRNA translation, lipid synthesis, and autophagy [27]. Intriguingly, alterations of mTOR activity have already been described in RTT models [26,28], suggesting that MECP2 may impinge on the regulation of the autophagic process by controlling the activity of mTOR and its downstream effector molecules. Also in *FOXG1* and *CDKL5* mutated cells aberrant expression of specific genes involved in brain development and neural differentiation has been reported. In particular, in *FOXG1* mutated cells the levels of PAX6, a transcription factor which interact and regulates expression of different genes during corticogenesis, is increased [29,30]. Furthermore an up regulation of *GRID1* gene, which encodes for a subunit of glutamate receptor channels, has been reported in iPSC-derived neurons from patients carrying *CDKL5*, *FOXG1* and *MECP2* variants. The alteration in mature neurons suggest a possible alteration in synapse formation and synaptic transmission in CNS [31].

Alterations in RTT primarily affect the CNS but RTT is a multisystem disease and perpheral alterations are also present in RTT patients. RTT girls present gastrointestinal and nutritional problems as difficulties with chewing, swallowing, reflux and gastric emptying defects. The most frequent and recurrent symptom is constipation. [32]. Alteration in gut microbiota can influence the homeostasis of CNS and is involved in neurological disorders as Autism Spectrum Disorders (ASD). It has been reported that impairments of MeCP2 functioning induce a dysregulation of intestinal microbial community with dysfunction in Short-chain fatty acids (SCFAs) production, onset of systemic inflammation and aggravation of constipation status [33,34].

Another systemic complication of RTT is osteoporosis. The alteration of neuro metabolites and the immaturity of the central and autonomic nervous system have repercussions at the systemic level. Osteopenia occurs early in girls and bone volume is reduced and tissue regeneration

activity is poor. Scoliosis, which is also common in RTT girls, can be aggravated by poor bone stability and hypotonia [35-37].

In RTT patients there is also an alteration of cholesterol metabolism. In the brain, cholesterol is produced in situ since circulating cholesterol cannot cross the Blood Brain Barrier (BBB). Its role is fundamental in the homeostasis of membrane trafficking and in the formation of myelin and new synapses [38-40]. Studies in Mecp2 null mice demonstrated that brain cholesterol levels are increased and the levels of alteration vary according to the type of mutation, nonetheless the mechanism by which cholesterol plays a primary role in RTT remains unknown [41].

Thanks to the clinical studies of Dr. Hagberg, a staging of the disease based on symptoms progression has been proposed. It is important to take into account that this description gives a general idea of the clinic of RTT patients and the individual variability of the symptoms and severity of the disease depends on the clinical characteristics of single subject [42]. Between 6 and 18 months of life there is the onset of the Stage I, namely Early Stagnation phase, which can last for weeks or months. During this phase, the abilities that the child has acquired are lost and there is a slowdown in psychomotor development. Hypotonia, weight loss, slowed head growth, and difficulty in maintaining posture also occur. Subsequently there is Stage II of Rapid Regression, characterized by stereotyped hand movements, among which the best known is the continuous rubbing similar to hand-washing. During Stage II, the first autistic traits emerge and the patient loses interest in the surrounding environment. This phase, which can last up to 3 years of age, involves the loss of language and movements becomes unstable with sudden and abrupt movements. In addition, the first seizures appear, accompanied by respiratory abnormalities and further progressive weight loss. Stage III, also called Pseudo Stationary phase, can last up to 10 years. The conditions of the girls become stable and there is an increase in interest in the surrounding environment and in social interaction. Despite the severe disability of the girls, eye contact and attention levels also improve. Episodes of seizures can be common and there is worsening of respiratory capacity with further gastrointestinal and cardiovascular complications. The last phase of the disease is Stage IV, known as Motor Deterioration phase, in which there is a further reduction in mobility and worsening of posture due to scoliosis. During this stage emotional contact improves and seizures are more controllable [43,44].

The stages of disease described above follow the progression of symptoms in the typical form of RTT. However, there are variants of the disease that may have a more or less severe course compared to the classic form. The first group is represented by milder atypical RTT variants

which include: the late regression variant or Hagberg's variant, characterized by moderate intellectual disability which worsens during school age with typical features of classic form; Forme Fruste, with milder symptoms and late onset, even after 4 years of age [14,44]; Zappella variant, also called Preserved Speech Variant (PSV), characterized by a mild phenotype and normal head size, in which girls recover the ability to express themselves and the partial use of hands [13]. Severe atypical RTT variants include the Hanefeld variant, associated with *CDKL5* gene that presents with early-onset seizures [11]; Rolando or congenital variant, associated with *FOXG1* gene mutations, in which symptoms arise at early stages without a period of normal psychomotor development [45]. Although RTT patients are mainly females, different publications reported cases of RTT in males, that exhibit very severe symptoms characterized by epileptic encephalopathy, usually with a fatal clinical course [46-48].

Diagnosis of RTT is based on the observation of clinical signs combined with genetic tests aimed at confirming the presence of specific mutations in the RTT associated genes. Diagnostic criteria for RTT were firstly described by Hagberg in 2002 and subsequently revised by Neul et al in 2010 [49,50]. RTT cases are mostly *de novo*. In the presence of familiarity, tests, such as Chorionic villus sampling (CVS) or amniocentesis, can be performed in the prenatal phase in order to exclude recurrence due to germinal mosaicism in one parent. Thanks to continued medical advances, the age of diagnosis of RTT has dropped to 2.7 years [51].

Currently no cure for RTT has been developed and the only treatments available are aimed at relieving symptoms. In particular, treatments are aimed to improve language, motor and social skills. It is also important to provide girls with nutritional and physical support.

1.2 Genetics of Rett Syndrome

1.2.1 RTT and *MECP2* gene

Correct neurogenesis during the embryonic stage is essential for the proper formation of the whole CNS. In the adult brain neurogenesis plays an important role in specific regions, such as the dentate gyrus of the hippocampus and the sub- ventricular zone of the lateral ventricles [52,53]. DNA methylation plays a relevant role in neurogenesis and normal brain cells and its dysfunction can have dramatic consequences on brain development and functioning [54]. Methyl-CpG-binding protein family (MBP) represents the link between DNA methylation and gene expression in the central nervous system and MeCP2 is the first MBP protein identified [55,56]. *MECP2* gene is located on the long arm of X chromosome in position q28, is composed by four exons and encodes for MeCP2. Due to an alternate splicing event of exon 2, the gene encodes for two isoforms namely MeCP2-e1 and MeCP2-e2. MeCP2-e1 is the most expressed isoform in the adult brain while MeCP2-e2 is ubiquitous and is also expressed in peripheral tissues (Figure 2). Both MeCP2 isoforms have a nuclear localization domain and are able to bind methylated DNA. In fact, MeCP2 consists of a Methyl-CpG-Binding Domain (MBD) and an NCoR domain (NID), essential for binding methylated DNA, a Transcriptional Repression Domain (TRD) for the recruitment of the co-repressor complexes that lead to condensation of chromatin, a Nuclear Localization Signal (NLS) and, finally, the C-terminal end, also involved in the condensation of chromatin [1].

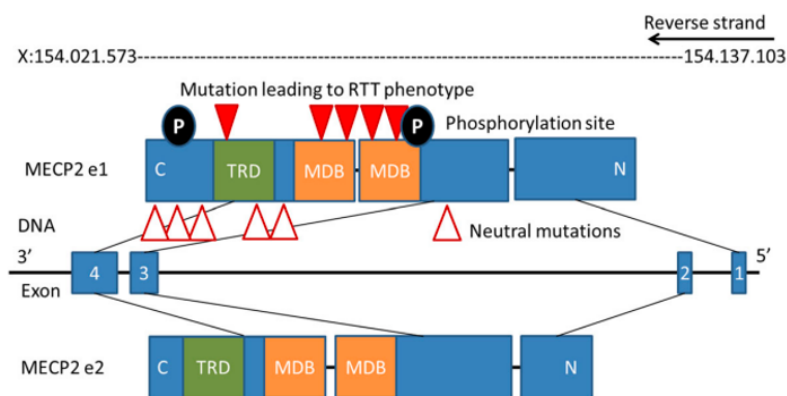**Figure 2. MECP2 gene and protein isoforms [57].**

MECP2 is highly expressed in mature neurons demonstrating its involvement in neuronal activity and synapses maturation. During development protein levels are highly variable [58]. In particular, levels are high during the embryonic stage, low at birth and growing during the postnatal development stage when neuronal maturation and synaptogenesis occur [59]. The

expression of MeCP2 protein from prenatal to adult stage reflects its fundamental and diverse role in the brain; mutations in this gene cause an alteration of neurodevelopment and brain functioning as demonstrated by the clinical course of RTT patients [60,61] (Figure 3).
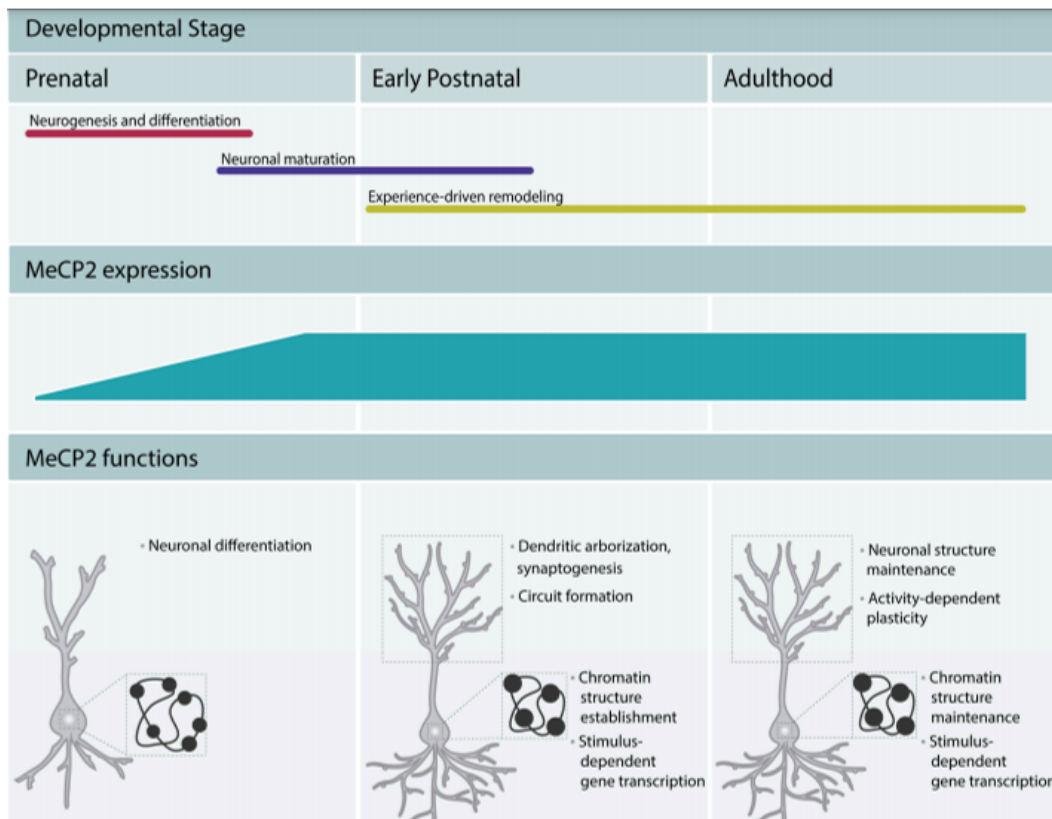
Figure 3. MECP2 expression and function during brain development [60].

MECP2 gene mutations are responsible for approximately 95% of classic RTT and most arise de novo in the paternal germline. The very large part of the mutations are sporadic, meaning that they are not of family origin but arise randomly, usually in spermatozoa. More than 200 different mutations in *MECP2* gene have been identified; recurrent mutations hotspots are R168X, R255X, R270X, R294X, R106W, R133C, T158M and R306C and account for 65% of point mutations [62]. *MECP2* facts as transcriptional regulator that can both activate and repress transcription, depending on the context. As a repressor it recruits protein complexes including histone deacetylases (HDACs). In particular, when MeCP2 binds to DNA it attracts a complex of transcriptional co-repressors composed of SIN3A, NCOR and SMRT that in turn, will recruit HDAC proteins [63]. MeCP2 also acts as transcriptional activator interacting with CREB1 (cyclic AMP-responsive element-binding protein 1) [64]. It also positively affects the expression of various genes such as BDNF, which has a primary role in survival, neuronal development, neuronal plasticity, learning and memory. Furthermore, BDNF, which is directly

regulated by MeCP2, can influence the expression of GRID1. RTT patients show abnormal expression of BDNF and GRID1 indicating the crucial role of *MECP2* [31,65,66].

1.2.2 RTT and *FOXG1* gene

FOXG1 gene is located on the long arm of chromosome 14, position q12; it is composed by five exons but contains only 1 coding exon [67]. It encodes for *forkhead box protein G1,* a 489 aminoacid protein, organized in three main functional domains:

1) the DNA-binding forkhead domain (FHD) which is involved in the binding of the protein to DNA; 2) the GROUCHO-binding domain necessary for binding with transcriptional repressor Groucho proteins; 3) the JARID1B binding domain through which the protein binds to the JARID1B transcriptional repressor (Figure 4).
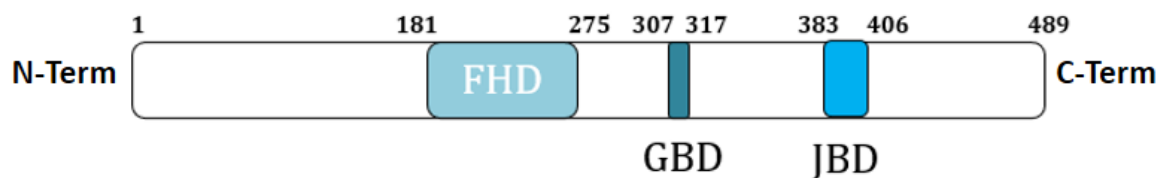
Figure 4. Structure of FOXG1 protein. Representation of the localization of DNA-binding forkhead domain (FHD), GROUCHO-binding domain (GBD) and JARID1B binding domain (JBD).

FOXG1 is essential for the correct embryonic development of the brain and in particular of the telencephalon where it promotes cell proliferation. The protein continues to be expressed in the adult brain where it promotes the survival of differentiated post-mitotic neurons [68,69]. Its action is also necessary for the correct formation of the inner ear and the olfactory system [70,71]. Mutations in the *FOXG1* gene have been identified in both female and male patients and most of them consist of a single nucleotide variant (SNV), although deletions and duplications have been found [72]. Correlation between *FOXG1* mutations and Rett syndrome was first described in 2008 [45]. The manuscript described mutations in two patients that cause early termination of the FOXG1 protein in two patients: the c.765G>A (p.(Trp255X)) variant leading to the introduction of a stop codon and disruption of the DNA binding property and the c.969delC (p.(S323fsX325)) deletion causing the loss of interaction of the JBD domain with its ligand and the misfolding of the GBD domain [45].

FOXG1 is involved in different molecular pathways. First it interacts with PAX6 and both play primary functions in regulating telencephalic cells cycle. Both genes are expressed in progenitors in the developing telencephalon, being *FOXG1* activated slightly earlier than *PAX6* [73]. Furthermore, PAX6 is involved in the development of axonal connections in the brain, in particular in the cortical thalamus through the activation of the transcription factors EMX2, TBR1, GBX2, MASH1, EBF1, FOXG1. The alteration of FOXG1 or PAX6 regulation causes the non-development of thalamic axons innervating the cortex [74,75]. During the neurodevelopment FOXG1 can influence different pathways such as WNT, NOTCH and SMAD, suggesting that it plays essential roles in cell proliferation and differentiation in the CNS (Figure 5). FOXG1 alteration also causes a dysregulation of the caspase signal suggesting a possible role in the regulation of apoptosis [76-79].
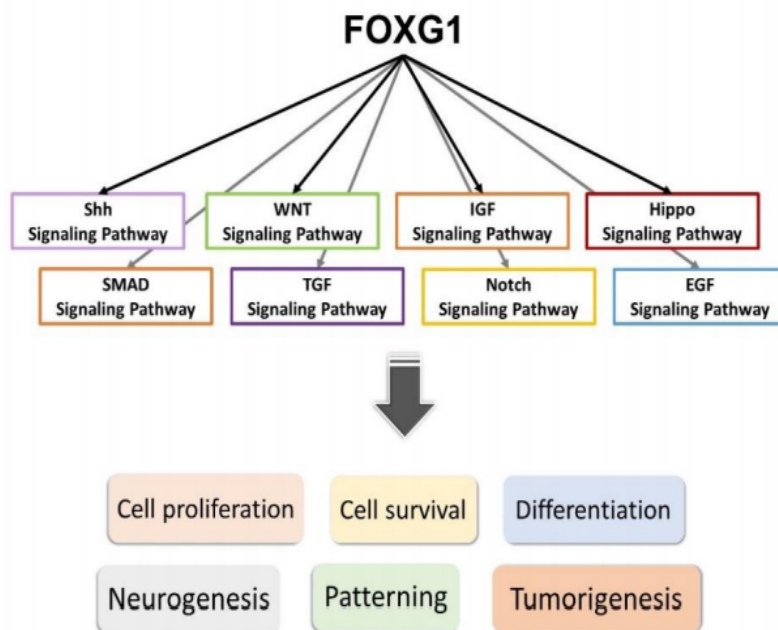
Figure 5 Molecular mechanisms regulated by FOXG1 gene [80].

1.2.3 RTT and *CDKL5* gene

CDKL5 gene (Cyclin-Dependent Kinase-like 5) is located at the level of the short arm of the X chromosome (Xp22) and consists of 24 exons but only the region between exons 2 and 21 is coding [81]. The CDKL5 protein has a catalytic domain divided in an ATP-binding site and the serine–threonine protein kinase active site. Moreover, CDKL5 presents two domains important for nuclear export and localization (Figure 6). CDKL5 is widely distributed in all tissues, but at higher levels in the brain, especially in the hippocampus and cortex. It is mainly produced in the postnatal period and is found both in the cytoplasm and in the nucleus, with transfer from one compartment to another depending on the area of the brain and the time of development. CDKL5 nuclear fraction increases in the adult brain and suggesting that it may be involved in synaptic plasticity [82,83]. In general, the expression of this protein correlates with neuronal maturation. CDKL5 both at the cytoplasm level and nuclear levels. In the cytoplasm it is involved in morphogenesis. The protein has 4 isoforms: I and II encode the same 115 KDa protein and are expressed in the central nervous system and at the peripheral level. The isoform III has a molecular weight of 120 KDa while the isoform IV is the smallest one with a molecular weight of 107 KDa. Isoforms III and IV are mainly expressed in the cerebellum, cortex and hippocampus [84,85].
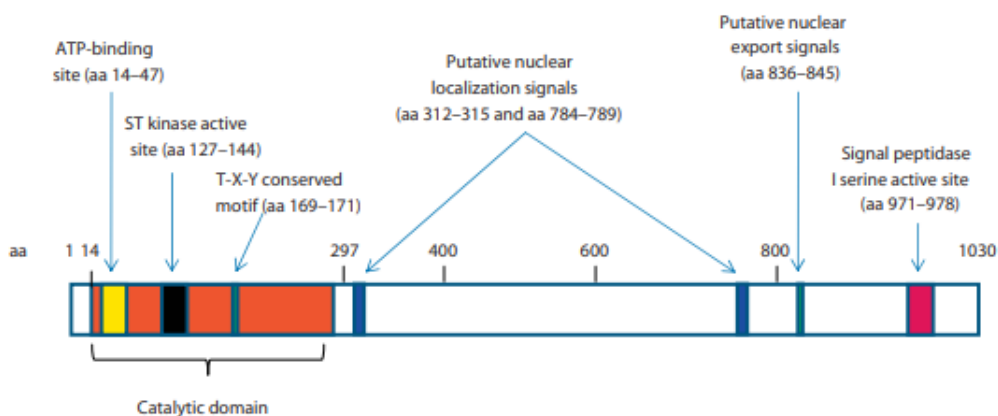
Figure 6. CDKL5 protein structure and domains [81].

Different studies demonstrated that CDKL5 interacts with MeCP2 and phosphorylates it. It also interacts with DNA methyltransferase I (DNMT1), suggesting that it can regulate DNA methylation and the binding of MeCP2 to DNA [86-88]. CDKL5 is involved in different pathway in CNS including maintenance of cellular homeostasis, cellular differentiation and

14

synapse development. In particular, CDKL5 regulates BDNF-Rac signaling and is involved in dendrite growth and dendritic spine maturation. It also regulates cell proliferation by interacting with the centrosome [89-94].

1.3 iPSC-derived neurons as a cellular model for RTT

In the study of neurodevelopmental diseases, the availability of cellular models that mimic the patient cells as closely as possible is crucial. Thanks to genetic reprogramming it is possible to obtain induced Pluripotent Stem Cells (iPSCs) directly from a skin biopsy of the patient. The first IPSCs derived from patients with Rett syndrome date back to 2010 [95]. The procedure took place through the forced expression of 4 factors called Yamanaka factors, namely Oct3 / 4, Sox2, Klf4, c-Myc [96]. This method allows to obtain stem cells identical to an embryonic stem cell with the patient mutation that can be differentiated into any type of cell, such as neurons (Figure 7).
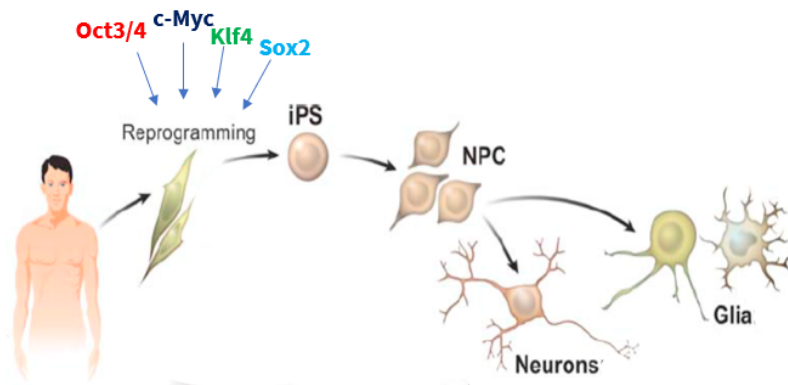
Figure 7. iPSCs reprogramming with Yamanaka factors starting from primary fibroblasts. iPSCs can be differentiated in neuronal precursor cells (NPC) and neurons.

IPSCs are widely used in precision medicine because they derive directly from the patient and there are no ethical problems regarding their use in research. With these cells, it is possible to test the efficiency and toxicity of various drug therapies, obtaining accurate results [97]. iPSC cells represent an important source to examine neuronal phenotypes. In particular, RTT iPSC-derived neurons exhibit a phenotype and metabolism comparable to those of mouse models of RTT patients [98-100]. Different studies have demonstrated that it is possible to use iPSCs to study synaptic transduction signals and the dysregulation of pathways which are involved in RTT [29,31].

1.4 RTT animal models

To date, mice represent the most used animal model for the study of Rett syndrome. After the onset of the disease, mice lose many of their locomotor skills and develop a wide variety of symptoms, from breathing defects to learning disabilities, from epileptic seizures to muscle hypotonia, scoliosis and osteopenia. The great similarity of the clinical picture found in mice and RTT girls together with the high sequence homology and the same expression dynamics of MeCP2 protein during brain development in both species make these animals first as a model for the identification of novel targets and development of innovative drugs and therapies [61;101,102]. In 2007, Guy *et al*., demonstrated that RTT is not irreversible [103]. The viability of mutated neurons in RTT patients opens up the possibility of full or partial rescue of most of the deficits caused by the disease in order to improve the patient's quality of life. Studies and research in mice represent an important possibility to select a time window for the application of possible treatments in order to intervene before the damages caused by the mutation are irreversible. KO mice still remain the mainly model used to understand cellular function related to the MeCP2 to validate new therapeutic approaches, but over the past few years many other models of the disease have been generated [100]. Due to the phenomenon of X inactivation that occurs in female mice, hemizygous Mecp2- mutant male mice still remain the most used model. While female mice develop symptoms at 4-6 months and have a normal life span, male mice develop RTT symptoms at 4 weeks and have a short lifespan that lasts no longer than 6-12 weeks [104,105]. The Mecp2$^{tm1.1Bird}$ and Mecp2$^{tm1.1Jae}$ represent the mainly used null mice models for RTT, but null mice are not the only models to be used. It must be considered that most of the mutations that cause RTT are missense and involve the translation of a more unstable or inefficient protein [104,105]. To overcome this problem, in order to study the most frequent mutations, several lines with point mutations and deletions were generated (Table 1). Mice carrying the most frequent variants found in girls (such as T158M, R168X, T308X and A140V) have been generated. These animals are often characterized by less severe symptoms, so are easier to manage and they represent a tool to understand what the different patients have in common, and could help develop "personalized" therapies for patients [101].

Allele type	Allele	Description
Null		
Mecp2[tm1.1Bird]	Null	Exon 3–4 deletion
Mecp2[tm1.1Jae]	Null; some protein product retained	Exon 3 deletion
Mecp2[tm1Pplt]	Null	MBD deletion
Human point mutations		
Mecp2[tm4.1Joez]	R106W	Missense mutation
Mecp2[tm1Nlnd]	Y120D	Missense mutation
Mecp2[tm6.1Bird]	R133C	Missense mutation
Mecp2[tm1.1Joez]	T158A	Missense mutation
Mecp2[tm4.1Bird]	T158M	Missense mutation
Mecp2[tm3.1Joez]	T158M	Missense mutation
Mecp2[tm1.1Jtc]	R168X	Stop mutation; truncation
Mecp2[tm1.1Irsf]	R255X	Stop mutation; truncation
Mecp2[tm5.1Bird]	R306C	Missense mutation
Other mutations		
Mecp2[tm2.1Jae]	S80A	Missense mutation
Mecp2[tm1Vnar]	A140V	Missense mutation
Mecp2[tm3Meg]	T308A	Missense mutation
Mecp2[tm1Hzo]	R308X	Stop mutation; truncation
Mecp2[tm1.1Meg]	S421A	Missense mutation
Mecp2[tm1.1Mitoh]	Deletion	Isoform 2 deletion
Mecp2[tm1.1Dhy]	Deletion	Isoform 1 deletion
Conditional alleles		
Mecp2[tm1Bird]	–	Exons 3–4 floxed
Mecp2[tm1Jae]	–	Exon 3 floxed
Mecp2[tm2Bird]	–	Floxed-stop upstream of exon 3

Table 1: Mouse model for RTT [10].

All animal models for FOXG1-Related Disorders (FOXG1-RD) presently available to the scientific community are KO (*Foxg1^{+/-}* - *Foxg1^{-/-}*) mice in which the entire *Foxg1* gene has been removed. KO mice were generated in 1995: homozygous mutants (*Foxg1^{-/-}*) die at birth and have a dramatic reduction in the size of the cerebral hemispheres [106]. Conversely, heterozygous haploinsufficient *Foxg1^{+/-}* mice are fertile, but show microcephaly, hyperlocomotion, impaired habituation in the open field and a severe deficit in contextual fear conditioning, thus recapitulating some features of disorders derived from deregulation of *FOXG1* [107,108].

Also, for *CDKL5*, KO mice are the most used animal model to study disease mechanisms. Mouse present only two isoforms of the protein and mice lacking the *CDKL5* gene mimic the clinical features associated with Rett syndrome by expressing autistic-like behaviors. Characterization of these mice revealed alterations in signal transduction at the synapse level [109,110].

1.5 CRISPR/Cas system

The Clustered Regularly Interspaced Short Palindromic Repeats (CRISPR) system was firstly observed and described in 1987 in *Escherichia coli* [111]. In the early 2000s, laboratories around the world began investigating the structure and function of CRISPR. In 2002 a research group observed that CRISPR locus could be composed by 25-50 nucleotides interspersed with sequences of similar size. Indeed, it has been observed that these repeats were associated with proteins with helicase and nuclease function [112]. Later it was shown that CRSPR is formed by sequences deriving from bacteriophages or extrachromosomal DNA (i.e. plasmids). Only in 2007 CRISPR has been associated with an adaptive immunity mechanism used by bacteria to defend themselves from virus infections [113,114]. The CRISPR locus is composed by several components: the first, namely Leader sequence, is positioned at the end of the locus and is rich in adenine and timine bases; repeated sequences of 23-50 base pairs (bp), and the DNA-spacer that has a length of 20-70 bp. During virus infection, bacteria acquire new spacers. Upstream of the CRISPR locus there are genes that encode for Cas proteins and their number and arrangement vary from different loci [115-117]. Bacterial defense system is divided into 3 phases: Adaptation, where the spacers sequence are inserted in the CRISPR locus; Expression, where a long transcript of RNA precursor is generated; the RNA precursor is cut by the Cas proteins into many CRISPR-RNA or crRNA. The crRNA includes the spacer sequences acquired in previous viral infections of the bacterium and the repeated sequences localized at the ends that avoid the binding of the crRNA to the bacterial DNA. In the last phase, called Interference, genome virus particles are recognized and fragmented thanks to the combined action of crRNA and Cas proteins [118,119].

1.5.1 CRISPR/Cas9 and gene therapy

CRISPR system is an adaptive immune system used by bacteria to defend themselves against invading viruses and is widely used by researchers for genome editing. In fact, CRISPR/Cas9 can be programmed to recognize a specific stretch of DNA within a cell. The system is composed by three key elements: Cas9 proteins which targets and cleave DNA; the target sequence must have a nearby protospacer adjacent motif (PAM) functioning as the binding site for Cas9; a single guide RNA (sgRNA) that drives Cas9 to the selected site. The disruption of the DNA double helix generally activates one of two endogenous DNA repair pathways: most commonly in somatic and stem cells the non-homologous end joining (NHEJ) pathway or homology-directed repair (HDR) pathway. NHEJ is an error-prone repair mechanism, as it

randomly adds or removes nucleotides in the interrupted region, generating deletions and insertions of a few base pairs. HDR uses a repair mechanism based on sequence homology either with an exogenous or endogenous complementary Donor DNA template molecule. This second mechanisms represents the base for therapeutic gene editing with CRISPR/Cas9. Indeed, after Cas9 activity on the mutated allele, the Donor DNA is used to restore wild type sequence in order to correct the specific mutation [120,121]. HDR is effective in both dividing and non-dividing cells, such as terminally differentiated neurons [122]. It is therefore suitable for use in *RTT*-related disorders in order to correct mutations avoiding alterations of gene expression. As reported in different publications, this technology has already been applied in different fields such as the study of genetic defects in patient blood cells with sickle cell anemia or in cerebral adrenoleukodystrophy [123,124]. In 2015, Liang et al demonstrated for the first time how the CRISPR/Cas9 system can effectively cut genes in three-pronuclear 3PN zygotes and how double strand breaks (DSBs) can be effectively repaired [125]. Other studies showed that CRISPR / Cas9 can correct pathogenic mutations as in the case of Beta-Thalassemia, hypertrophic cardiomyopathy (HCM) and Marfan Syndrome [126-128].

Recent works have shown that there is a pre-existing immune response to *S. pyogenes* Cas9 (spCas9) in humans [129,130]; this evidence may be of limited concern for *in vitro* gene editing but it could hinder the *in vivo* HDR repair process in future clinical trials. Unwanted off-target cuts associated with CRISPR/Cas9-based gene correction approaches in genomic regions different from the mutated allele represent another possible risk. To overcome immunological reaction and non-specific cuts derived from Cas9 activity scientists have developed strategies that limit the protein expression inside the cells and the non-specific targeting to other regions of DNA. One of the possible solutions is the use of more specific Cas9 variants that limit non-specific cuts on the DNA. For example, SpCas9-HF1 is a variant that reduces non-specific DNA contacts and has a high specificity for the on-target site comparable to the spCas9 [131]. The engineered variants are also expected not to elicit pre-existing immune response.

A key issue for a successful gene therapy of CNS disorders is the efficient delivery of the therapeutic constructs to the CNS through the Blood Brain Barrier (BBB). Adeno-Associated Viruses (AAVs) currently represent the most advanced delivery system for gene therapy approaches, due to the reduced immunogenic risk and toxicity. AAVs are non-pathogenic viruses that remain in the infected cells as episomal DNA with negligible integration rate, avoiding the risks associated with insertional mutagenesis. One potential limitation is the dilution of the transgene and consequent loss of transgene expression when infecting dividing cells [132]. Intravenously administered AAV9, or its variant PhP.B [133], can cross the BBB

and deliver genes into the CNS; AAV9 has been proven efficient for gene replacement therapy in SMA1 patients (NCT02122952), with no relevant adverse effects [134]. Although AAV vectors allow long-term transgene expression in animal models (more than 15 years in CNS in baboons) [135], no data on gene editing approaches in patients are available for long-term stability. Few data are present also for other AAV-based therapies, namely gene replacement approaches.

1.5.2 Clinical trials for Rett syndrome

Post-natal reactivation of *Mecp2* in symptomatic KO mice can revert disease phenotypes, suggesting that RTT is not irreversible [136]. At present, 27 interventional trials with 17 different drugs are registered for RTT patients, (https://clinicaltrials.gov) (Table 2), including those recently completed for Statins (NCT02563860) and IGF-1 (NCT01253317 and NCT01777542) that had given very promising results in mouse models [138,139]. Although some phenotypic improvement has been observed following IGF-1 administration, none of the treatments evaluated to date succeeded in effectively reverting RTT symptoms [137]. Studies on gene replacement therapy in mouse models are ongoing (https://www.avexis.com/research-and-development) [138] but uncertainties remain for the need of a fine native regulation of *MECP2* expression, since both down- and upregulation lead to brain impairment in humans [139].

Table 2. Clinical trial on Rett syndrome

Number	Study title	Drug	Status
	Clinical Trial of RTT/MECP2		
NCT01777542	Pharmacological Treatment of Rett Syndrome by Stimulation of Synaptic Maturation With Recombinant Human IGF-1(Mecasermin [rDNA] Injection)	IGF-1	Completed
NCT01253317	Pharmacological Treatment of Rett Syndrome by Stimulation of Synaptic Maturation With IGF-1	IGF-1	Completed
NCT02563860	Pharmacological Treatment of Rett Syndrome With 3-Hydroxy-3 Methylglutaryl-coenzyme A Reductase Inhibitor-Lovastatin (Mevacor)	Lovastatin	Completed
NCT01520363	Placebo Controlled Trial of Dextromethorphan in Rett Syndrome	Dextromethorphan	Completed
NCT00593957	Trial of Dextromethorphan in Rett Syndrome	Dextromethorphan	Terminated
NCT00990691	Pilot Study of the Effects of the Desipramine on the Neurovegetative Parameters of the Child With Rett Syndrome	Desipramine	Completed
NCT01147575	Effects of Creatine Supplementation in Rett Syndrome: A Randomized, Placebo-controlled Trial	Creatine	Completed
NCT02061137	A Phase 1 Clinical Study to Assess Safety and Efficacy of Oral Fingolimod (FTY720) in Children With Rett Syndrome	FTY720	Completed
NCT02563820	Ketamine for the Treatment of Rett Syndrome: An Exploratory Trial	Ketamine	Terminated
NCT03633058	A Randomized, Double-blind, Placebo-controlled, Cross-over Study to Assess the Safety, Tolerability and Efficacy of Oral Ketamine for Patients With Rett Syndrome	Ketamine	Recruiting
NCT02215733	Pharmacological Treatment of Rett Syndrome With Glatiramer Acetate (Copaxone)		Completed
NCT02023424	An Open Label, Exploratory Study to Investigate the Treatment Effect og Glatiramer Acetate (Copaxone ®) on Girls With Rett Syndrome	Glatiramer Acetate	Unknown
NCT02715115	A Randomized, Double-blind, Placebo-controlled, Dose-ranging Study of the Safety and Pharmacokinetics of Oral NNZ-2566 in Pediatric Rett Syndrome	NNZ-2566	Completed
NCT01703533	A Phase II Randomized, Double-Blind, Placebo-Controlled, Parallel-Group, Dose-Escalation Study of NNZ-2566 in Rett Syndrome	NNZ-2566	Completed
NCT01822249	A Phase 2A Randomized, Placebo Controlled Trial of EPI-743 in Children With Rett Syndrom	EPI-743	Completed
NCT04304482	A Double-Blind, Randomized, Placebo-Controlled, Safety and Efficacy Study of ANAVEX2-73 in Patients With Rett Syndrome		Recruiting
NCT03941444	A Double-Blind, Randomized, Placebo-Controlled, Safety and Efficacy Study of ANAVEX2-73 in Patients With Rett Syndrome		Recruiting
NCT03758924	A Double-Blind, Randomized, Placebo-Controlled, Dose Titration Study of ANAVEX2-73 in Patients With Rett Syndrome	ANAVEX2-73	Recruiting
NCT04279314	A 40-Week, Open-label Extension Study of Trofinetide for the Treatment of Girls and Women With Rett Syndrome		Recruiting
NCT04181723	A Randomized, Double-Blind, Placebo-Controlled, Parallel-Group Study of Trofinetide for the Treatment of Girls and Women With Rett Syndrome	Trofinetide	Recruiting
NCT02696044	Treatment of Mitochondrial Dysfunction in Rett Syndrome With Triheptanoin: An Open-label, 10-subject Clinical Trial of UX007 (Triheptanoin) in the Treatment of		Recruiting
NCT03059160	Open Label Trial of Triheptanoin (UX007) in Treatment of Rett Syndrome	Triheptanoin	Unknown
NCT03848832	A Randomized, Double-blind, Placebo-controlled Trial to Investigate the Efficacy and Safety of Cannabidiol Oral Solution (GWP42003-P, CBD-OS) in Patients With Rett Syndrome		Recruiting
NCT04252586	An Open-label Extension Trial to Investigate the Long-term Safety of Cannabidiol Oral Solution (GWP42003-P, CBD-OS) in Patients With Rett Syndrome	GWP42003-P, CBD-OS	Enrolling by invitation
NCT00069550	Pathogenesis of Rett Syndrome: Natural History and Treatment	dextromethorphan and	Recruiting
NCT02790034	A Randomised, Double-Blind, Placebo-Controlled 6-month Study to Evaluate the Efficacy, Safety, and Tolerability of Sarizotan in Patients With Rett Syndrome With Respiratory S	Sarizotan	Active, not recruiting
NCT04041713	A Pilot Study of an Antioxidant Cocktail vs. Placebo in the Treatment of Children and Adolescents With Rett Syndrome	Antioxidant cocktail	Not yet recruiting

2. Aim of the study

In spite of intense research efforts, the pathophysiological mechanisms of RTT spectrum disorders are far from being completely defined and no effective therapy is currently available. Different interventional trials are registered for RTT but the promising results in mouse models have not been paralleled by significant outcomes in patients (https://clinicaltrials.gov).

An important advance in the field of RTT is the availability of iPSCs reprogrammed from patient cells and widely used to obtain neurons. This approach is less invasive than *in vivo* procedures and it allows us to obtain the main affected cell type from patients with specific mutations. Starting from these considerations, at the beginning of my doctorate I collaborated in a functional study based on the employment of iPSC-derived neurons to understand molecular mechanisms involved in classic RTT.

Thanks to the excellent results obtained with this work, I used this knowledge to design and study a new technology in order to develop an innovative therapy for RTT. To reach this goal, building upon the availability of patient primary cells and neurons, I focused my attention on the application of gene editing with CRISPR-Cas9 technology based on Homology Directed Repair (HDR). With this thesis I present a novel gene therapy approach able to revert mutations and restore the correct sequence s in *FOXG1* and *MECP2* genes. Moreover, I demonstrated the feasibility and the efficacy of HDR in post-mitotic cells, such as neurons, opening new possibilities for future applications. I also tested infection with AAV2 and AAV9 viruses and I analyzed their infection efficacy in patient cells in order to choose the best serotype as delivery system for future *in vivo* studies.

Research work done during my PhD represents a proof of principle study based on gene therapy application in neurodevelopmental disorders that will open a real opportunity for the treatment of Rett syndrome and related disorders improving the quality of life of patients.

3. Material and methods

3.1 Patient selection

MECP2 patients

Four patients with classic Rett syndrome were enrolled by the medical équipe of the Medical Genetics Unit at the University Hospital of Siena, following Informed Consent signature. All patients carry the same causative mutation in the *MECP2* gene, namely c.473C>T (p.Thr158Met). The variant is present in the LOVD database (http://www.LOVD.nl/FOXG1) with ID# MECP2_000003.

Case 1 (#2204) is a 13-year-old female patient. Pregnancy and auxological parameters at birth were normal. Parents referred that the child achieved the sitting position at 6 months of age and started to say the first words at 12 months of age. At 14 months stereotypes of the hands on the midline started. The patient presented postnatal microcephaly and a MRI scan showed over and under-tentorial atrophy. She presented severe constipation, sialorrhea, cold hands and feet. She could sit down or stand up independently and presented broad-based walking. Her verbal language was limited to few words. She had no seizures. At 4 years head circumference was 45,5 cm (<< 3° percentile), weight 11 kg (<3° percentile) and length 93 cm (<3° percentile). Skin biopsy was performed at 4 years of age.

Case 2 (#304) is a 26-year-old female patient. Pregnancy and auxological parameters at birth were normal. She presented bruxism, no gastro-oesophageal reflux and constipation were reported. The language was absent. She was not able to grasp objects with her hands. She had seizures. Stereotypes of the hands were reported. She could not sit down or stand up independently and she presented broad-based walking. She had mild scoliosis. At 7 years head circumference was 48,5 cm (3° percentile), weight 16 kg (<3° percentile) and height 116 cm (10°-25° percentile). Skin biopsy was performed at 19 years of age.

Case 3 (#2271) is an 8-year-old female patient. Pregnancy and auxological parameters at birth were normal, but abnormalities in neurological development and behaviour were observed at 12 months of age. She presented verbal language limited to few words. She could not sit down or stand up independently, but she enjoyed standing with the help of her parents. The ability to grab small objects has never been acquired. No gastro-oesophageal reflux and constipation were present. Episodes of hyperventilation, bruxism and stereotypes of the hands on the midline were reported from 18 months of age. She had no seizures. At 2 years head

circumference was 48 cm (10°-25° percentile), weight 15 kg (>25° percentile) and length 94 cm (25°-50° percentile). Skin biopsy was performed at 3 years of age.

Case 4 (#2239) is a 26-year-old female patient. Clinical and molecular diagnosis were performed at 2 years of age. Pregnancy and auxological parameters at birth were normal. Parents referred that the child achieved the sitting position at 8 months of age and she started to walk at 2 years. The patient presented postnatal microcephaly. She could sit down or stand up independently. Language was absent. The ability to grab small objects was acquired, but subsequently lost. Stereotypes of the hands started at 18 months of age. No gastro-oesophageal reflux was reported. She presented severe constipation, apnea, cold hands and feet and scoliosis. At the age of 6 years, she developed seizures, characterized by a fixed gaze and then stiffness in the limbs. At 7 years head circumference was 50,3 cm (<3° percentile), weight 43 kg (<5°percentile) and length 150 cm (<5° percentile). Skin biopsy was performed at 17 years of age.

FOXG1 patients

Patients fulfilling clinical and molecular criteria for the congenital variant of Rett syndrome were enrolled at the Medical Genetics Unit of the University Hospital of Siena. Molecular diagnosis was accomplished after informed consent by performing sequencing analysis of the *FOXG1* gene. Two patients carrying two distinct causative mutations in *FOXG1* gene were selected for the study. Case 1 (#2237/17) harbours a missense variant (NM_005249.4:c.688C>T; p.(Arg230Cys)) expected to disrupt the ForkHead domain and consequently impair DNA binding. Case 2 (#156) harbours a nonsense variant (NM_005249.4:c.765G>A; p.(Trp255*)) [2]. The variants were submitted to the LOVD database (http://www.LOVD.nl/FOXG1) with the following IDs: c.688C>T ID FOXG1_000072, c.765G>A ID FOXG1_000007.

Case 1 (#2237/17), a 4-year-old male, was diagnosed with congenital variant of RTT according to the current criteria [19]. Pregnancy, delivery and auxological parameters at birth were normal. Head control was achieved at 3 weeks of age. At 3 months, the patient presented microcephaly and reduced brain size and simplified convolutions were detected by MRI scan. At 15 months, inconsolable crying crisis started and lack of response to verbal prompts was evident. He presented tongue thrusting during feeding, right eye with intermittent tendency to squint, sialorrhea, gastroesophageal reflux, constipation, disturbed sleep-wake rhythm, snoring. The ability to grab small objects was acquired at about 24 months. He was able to laugh or scream spontaneously, but he could not sit or stand independently. At 22 months of

age, head circumference was 44 cm (<3° percentile), weight and length were 11 kg (25-50th) and 85 cm (50th), respectively. Prominent metopic suture and apparent hypotonia were also detected.

Case 2 (#156), a 33-year-old female, fulfilled clinical criteria for congenital variant of RTT. Abnormalities in head growth were observed at 3 months of age. The patient displayed inconsolable crying, lack of response to verbal prompts and poor head control. She had never been able to maintain a sitting position. At about 3 years, she acquired the ability to maintain a standing position, but then she lost it. Verbal language was limited to lallation and manual apraxia was evident. An MRI scan performed at about 10 years showed underdevelopment of cerebral hemispheres and corpus callosum thinning. At the age of 14 years she developed seizures, characterized by a fixed gaze and limb-shakes. The EEG showed occipital and right central-temporal basic rhythm slowing, occipital diffuse voltage reduction, central regions paroxysmal activity. Alterations of the sleep-waking rhythm, dystonic arm movements and constipation but no gastro-oesophageal reflux and respiratory rhythm alteration were reported. The physical examination carried out at 22 years old revealed a weight of 38 kg (<5° percentile), head circumference of 49 cm (<3° percentile), sunken eyes, high nasal bridge, full lips, large mouth, small hands with wide interphalangeal joints, severe scoliosis, joint stiffness, hypotrophic left leg, bilateral flat foot. Motor stereotypes of the hands on the midline, tongue thrusting and trunk swing, bruxism, sialorrhea, sporadic episodes of hyperventilation and cold hands and feet were evident.

3.2 Cell line establishment and maintenance

Primary human fibroblasts were obtained from skin punch biopsy following signed informed consent (size 3-4 mm^3). Fibroblasts isolated from biopsies were cultured in Dulbecco's Modified Eagle's medium (DMEM) (Biochrom GmbH, Berlin, Germany) supplemented with 10% Fetal Bovine Serum (FBS) (Carlo Erba, Reagents S.r.l, Milano), 2% L-glutamine (Carlo Erba, Reagents S.r.l, Milano) and 1% antibiotics (Penicillin/Streptomycin) (Carlo Erba, Reagents S.r.l, Milano), according to standard protocols, and routinely passed 1:2 with Trypsin/EDTA (0.05%) solution (Irvine Scientific Santa Ana, California, US) [140].

Primary fibroblasts of the patient with c.473C>T (p.(Thr158Met)) *MECP2* variant and the patient with c.765G>A; p.(Trp255*)) FOXG1 variant were used to obtain induced Pluripotent Stem Cells (iPSCs) [29, 31]. iPSCs were reprogrammed using the four Yamanaka retroviral vectors [96]. Fibroblasts at passage 2 or 3 were reprogrammed following the protocol by Hotta and colleagues [141]. Briefly, fibroblasts were infected with retroviral vectors that express the

reprogramming factors (*OCT-4*, *SOX-2*, *c-MYC* and *KLF-4*). Seven days after infection, fibroblasts were passed onto mitomycin-C-inactivated mouse embryo fibroblasts (feeders). Emerging iPSCs colonies were manually picked and expanded on feeders for some passages. Established clones that maintained a good hESCs-like morphology were moved to feeders-free culture conditions on Matrigel-coated dishes (BD Biosciences, Milano, Italy) in mTeSR1 medium (Stem Cell Technologies, Grenoble, France). From this point on, cells were routinely passed by Dispase (Stem Cell Technologies, Grenoble, France).

Induced Pluripotent Stem Cells (iPSCs) from the patient with c.688C>T (p.(Arg230Cys)) *FOXG1* variant were generated and characterized in the Cell Technology Facility (CIBIO - University of Trento (https://www.cibio.unitn.it/467/cell-technology) using Sendai virus-encoded Yamanaka reprogramming factors OCT4, SOX2, KLF4, and c-MYC [96] (Fig. 8).

Cells were maintained in feeders-free culture conditions in plates coated with Geltrex matrix diluted 1:100 in DPBS with Ca^{2+}/Mg^{2+} (Gibco, Thermo Fisher Scientific, Paisley, UK). Cells were cultured with mTeSR1 medium (Stem Cell Technologies, Grenoble, France) and routinely passed using EDTA 0.5 mM diluted in DPBS without Ca^{2+}/Mg^{2+}.

HEK293 cells were cultured in Advanced DMEM (Life Technologies TM, Carlsbad, California, US) supplemented with 10% FBS, 2 mM GlutaMax (Life Technologies) and 1% penicillin/streptomycin at 37 °C with 5% CO2. Cells were routinely split when 70-80% confluent.
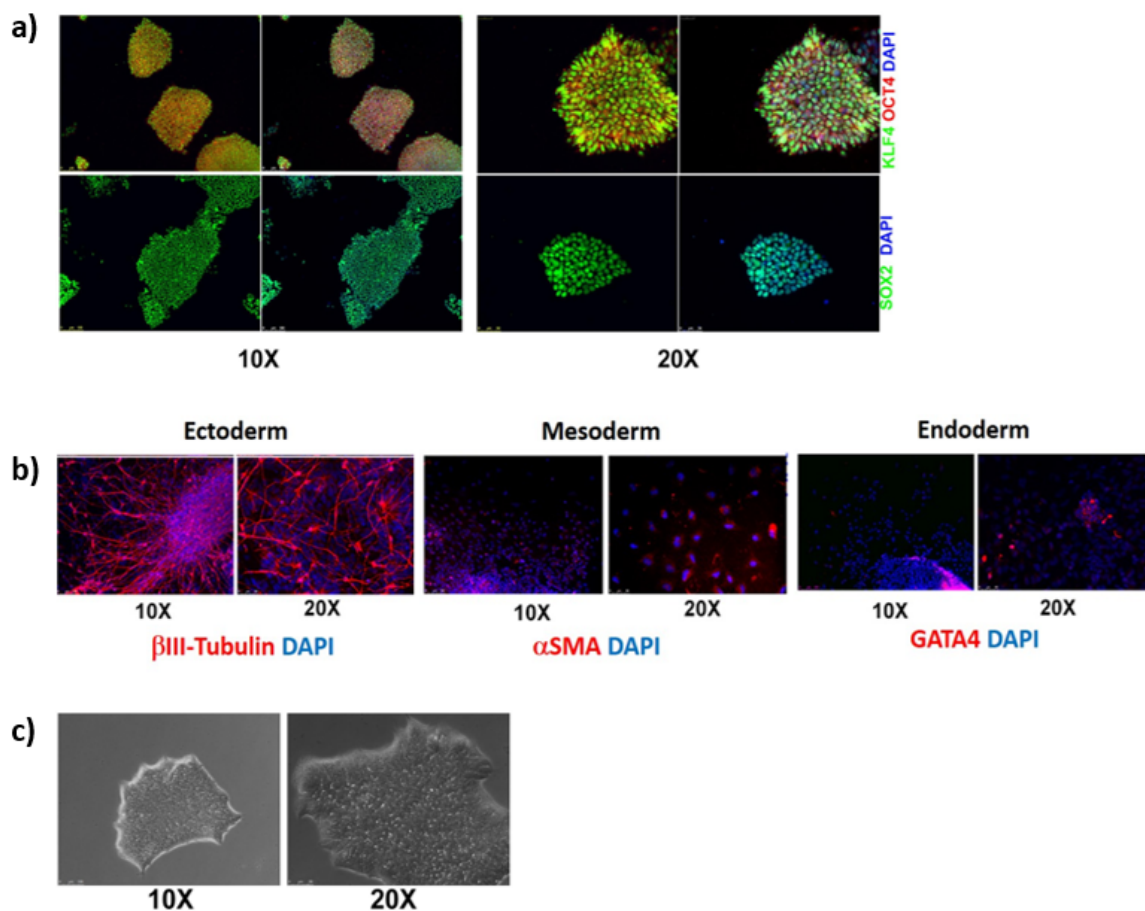
Figure 8: Characterization of human induced Pluripotent Stem Cells. a. Expression of pluripotency markers. Representative images of immunostaining for pluripotency markers showing expression of OCT4, SOX2 and KLF-4 with DAPI counterstaining. **b. Confirmation of pluripotency.** Immunofluorescence staining for human ꓳIII-tubulin, alpha-smooth muscle actin (αSMA) and GATA4 in cells derived from iPSCs by spontaneous differentiation demonstrates the capacity of the cells to differentiate into cells of the three germ layers: ectoderm, mesoderm, and endoderm. **c. Typical morphology of iPSCs clones.** iPSCs clones observed in phase contrast. Colonies have the typical human embryonic stem cell morphology with tightly-packed cells, a defined border and a round shape. Images at 10x and 20x magnification are presented.

3.3 Neuronal differentiation

Induced Pluripotent Stem Cells were differentiated into neuronal progenitors (NPCs) and neurons following the protocol routinely used in the laboratory [29]. Cell colonies were broken down into single cells with Accutase (Merck Millipore®, Burlington, Massachusetts, United States) and transferred into Aggrewell plates (Stem Cell Technologies,Vancouver, Canada) to allow the formation of Embryoid Bodies (EB)-like structures in NB medium (DMEM:F12 with Glutamax supplemented with 1% N2, 4%B27 without Vitamin A, 55 µM beta-mercaptoethanol and penicillin/streptomycin) containing 200 ng/ml Noggin (R&D System, Minneapolis, Minnesota, United States) for 2 days. The cell aggregates were then grown in suspension for 2 additional days in the same medium and then transferred onto matrigel-coated plates in the same medium for the formation of neuronal rosettes, consisting of neuroepithelial cells arranged in a tubular structure. Twentyfour hours later, the medium was changed to NB supplemented with 200 ng/ml Noggin, 200 ng/ml rh-DKK1 (R&D System, Minneapolis, Minnesota, United States) and 20ng/ml FGF2 (Thermo Fisher Scientific Waltham, Massachusetts, United states). Rosettes were manually picked, dissociated and expanded in NB medium with the addition of 10ng/ml FGF2 and EGF (Thermo Fisher Scientific Waltham, Massachusetts, United states). For subsequent neuronal differentiation, NPCs were plated onto Laminin/Poly-L-Ornithine plates in Terminal differentiation medium (DMEM:F12 supplemented with 1% N2, 4% B27 with Vitamin A, 55 µM beta-mercaptoethanol and 500 µl penicillin/streptomycin) for 30 days. In spite of the presence of Noggin and DKK that should direct differentiation toward a forebrain fate, we obtained heterogeneous cultures containing a variable percentage of non-neuronal cells. Neuronal progenitors and neuronal cells were isolated for quantitative analyses by immunomagnetic cell sorting with magnetic beads-conjugated antibodies against PSA-NCAM and CD24, respectively (Miltenyi Biotec, Calderara di Reno, Bologna, Italy). To enrich our cultures in post-mitotic neurons we also treated cells at day 15 of neuronal differentiation with Mitomycin C from Streptomyces caespitosus (2.5µg/ml) (Sigma-Aldrich, Merck, Darmstadt, Germania) which induced apoptosis in proliferating cells but did not affect post-mitotic ones.

3.4 sgRNA design and plasmid cloning

We designed a system based on two plasmids to be used in combination: one plasmid carrying the *Streptococcus pyogenes* Cas9 (SpCas9) coding sequence (CDS), and another containing the sgRNA, under the control of U6 promoter, the donor DNA to be used for HDR and an mCherry/EGFP reporter system to detect Cas9 activity in cells (targeting plasmid). The variant-

specific sgRNA was designed using the MIT CRISPR Design Tool (http://crispr.mit.edu). sgRNA and Donor DNA were cloned into BbsI and AfIII/SalI sites, respectively, in the pAAV2.1_CMV_eGFP3 plasmid backbone [142].

MECP2 plasmids

The Oligonucleotides used for the cloning are listed in Table 3. A wild type Donor DNA (#1) was designed as a 120 bp sequence centered on the mutated nucleotide, where a Protospacer Adjacent Motif (PAM) sequence with a silent variant was added. A variant-specific sgRNA was obtained by annealing and subsequent phosphorylation of single-strand oligonucleotides (#2,3). An mCherry/EGFP double reporter system was cloned between NheI/SpeI unique restriction sites replacing the eGFP3 coding sequence of the original plasmid. A target sequence, represented by sgRNA plus PAM, was interposed between mCherry and EGFP coding sequences, using a BsmbI restriction site. The same cloning was performed to obtain the mCherry/EGFP reporter harbouring the wild type target sequence (#4,5). The px330 Addgene plasmid encoding *Streptococcus pyogenes* Cas9 (SpCas9) was used for Cas9 cloning [143]. Cas9 coding sequence was amplified by PCR using specific primers (#6,7), designed to insert the sgRNA plus PAM sequences to achieve self-cleaving activity, and BamHI/SacII restriction sites at 5' and 3' end of the PCR product, respectively; the amplified product was cloned into pAAV2.1_CMV_eGFP3 backbone, under the control of CMV promoter, between BamHI and SacII restriction sites.

MECP2 mutation	Sequence feature	sequence
c.473C>T (p.(Thr158Met))	#1 Mecp2 Donor sequence	GATTGCGTACTTCGAAAAGGTAGGCGACACATCCCTGGACCCTAATGATTTTGACTTCACGGTAACgGGGAGAGGGAGCCCCTCCCGGCGAGAGCAGAAACCACCTAAGAAGCCCAAATC
	#2 Mecp2 sgRNA Fw oligo	CACCGGATTTTGACTTCATGGTAAC
	#3 Mecp2 sgRNA Rv oligo	AAACGTTACCATGAAGTCAAAATCC
	#4 Mecp2 sgRNA + PAM Wild type FW oligo	GTCGGATTTTGACTTCACGGTAACTGG
	#5 Mecp2 sgRNA + PAM Wild type RV oligo	CAGACCAGTTACCGTGAAGTCAAAATCC
	#6 Cas9 Fw primer	TAAAGGATCCGATTTTGACTTCATGGTAACTGGATGGACTATAAGGACCACGA
	#7 Cas9 Rv primer	TAAACCGCGGGATTTTGACTTCATGGTAACTGGTCAGCGAGCTCTAGGAATTC

Table 3. Sequence of oligonucleotides used for MECP2-specific plasmids construction.

The Oligonucleotides used for the cloning are listed in Table 4. Targeting construct and the genetic loads were inserted between the two Inverted Terminal Repeats (ITR): the sgRNA and Donor DNA were cloned into AflII/SacII sites, and the mCherry/EGFP reporter system [144] into NheI and SpeI sites. Variant-specific and wild-type sgRNA targets + PAM sequences (Table 3), necessary for the functioning of the fluorescent reporter system, were cloned between mCherry and EGFP sequences at the BsmBI restriction site. For Cas9, the PX551 plasmid encoding SpCas9 under the control of the *MECP2* promoter was used [143]. An additional target sequence (sgRNA + PAM) was inserted between the Cas9 coding sequence and its promoter, using an AgeI restriction site, allowing Cas9 self-cleavage, thus avoiding long-term expression.

FOXG1 mutations	Sequence feature	sequence
c.688 C>T (p.(Arg230Cys))	sgRNA	GAGGGACAGATTGTGGCAGA
	Donor DNA	GTAGTGGCGCGGCACCTTCACGAAGCACTTGTTGAGGGACAGATTGTGGCGGATAGAGTTCTGCCAGCCCTGCTTGTTCTCGCGGTAGTAAGGGAAGTTC
	Target sequence	GAGGGACAGATTGTGGCAGATGG
	Target sequence WT	GAGGGACAGATTGTGGCGGATGG
c.765G>A (p.(Trp255Cys))	sgRNA	CAAGGGCAACTACTGAATGC
	Donor DNA	TCGTGAAGGTGCCGCGCCACTACGACGACCCGGGCAAGGGCAACTACTGGATGCTAGACCCGTCGAGCGACGACGTGTTCATCGGCGGCACCACGGGCAA
	Target sequence	CAAGGGCAACTACTGAATGCTGG
	Target sequence WT	CAAGGGCAACTACTGGATGCTGG

Table 4. Sequence of oligonucleotides used for FOXG1 plasmids construction.

3.5 Plasmid extraction

Plasmids were transformed in STBL3 Competent *Escherichia coli* cells and grown in standard Luria-Bentani (LB) medium [145]; plasmids were purified using the EndoFree Plasmid Maxi Kit (Qiagen). All constructs were verified by Sanger sequencing (GA3130 Genetic Analyzer, Thermo Fisher Scientific).

3.6 Dual AAV system for plasmid delivery

The two components of the FOXG1 correction system, one encoding for self-inactivating SpCas9 and another containing the sgRNA expression cassette and the donor DNA, were packaged into either AAV2 or AAV9, known to efficiently transduce cells in vitro and neurons in vivo, respectively. AAV vectors were produced by triple transfection of HEK 293 cells as already described [146] at TIGEM AAV Vector Core (http://www.tigem.it/core-facilities/vector-core).

3.7 Cell transfection

HEK293 cells were seeded at a density of $5x10^4$ cells/well the day prior to transfection, in order to obtain cells at 70–90% confluency on the day of transfection. Transfections were performed using Polyethylenimine transfection reagent 1 μg/μl (Polysciences) according to the manufacturer's instructions. Cells were transfected with 100 ng of targeting plasmid and 400 ng of Cas9 encoding plasmid.

Fibroblasts were transfected using the Neon Transfection System with Tip100 (Thermo Fisher Scientific) according to the manufacturer's protocol. Cells were seeded 1 day before transfection and electroporated when 70-80% confluency was reached. Briefly, fibroblasts were harvested with Trypsin Solution and counted. $1x10^6$ cells were transfected with 15 ug of DNA (5μg Reporter plasmid and 10 μg Cas9 plasmid) and the following instrument parameters: 1 Pulse at 1700 Volts with 20ms pulse width. EGFP and mCherry positive cells were quantified with a Cytoflex flow (Beckman Coulter) cytometer with blue (488nm) and a yellow (560nm) lasers, using a 530/30 (EGFP) and a 585/42 (mCherry) filter.

Neurons were transfected with variant-specific plasmids on day 22 of neuronal differentiation. $2x10^5$ cells were transfected using Lipofectamine 2000 (Invitrogen Corporation, Carlsbad, California, United States) according to manufacturer's protocol. Transfection efficiency was confirmed with fluorescence microscopy and FACS analysis from 4 to 6 days post-treatment. For each experiment, non-transfected cells and cells transfected with an EGFP-encoding plasmid were used as negative and positive controls, respectively, to monitor transfection efficiency.

Neuronal precursors (NPCs) were detached from plate with Accutase (Stem Cell Technologies), diluted 1:1 with Dulbecco's modified Eagle Medium (GIBCO, Thermo Fisher scientific, Waltham, Massachusetts, United States) and transfection was performed using Neon® Transfection System with manufacturer's protocol. We used $4x10^5$ cells and 5 μg of DNA (1,25 μg Reporter plasmid and 3,75 μg Cas9 plasmid) and the instrument was set with

the following parameters: 1300 Pulse Voltage (V), 20 Pulse Width (ms) and 1 Pulse number. After treatment cells were plated on 12 well plates coated with poly-L-Ornithine and Laminin (Sigma-Aldrich, Merck Millipore®, Burlington, Massachusetts, United States) with medium without antibiotics. Transfection efficiency was confirmed at 48 hours post-treatment with by fluorescence microscopy and FACS analysis.

3.8 Infection with AAVs

Fibroblasts, iPSCs, neuronal precursors and iPSC-derived neurons were infected with AAV serotypes 2 and 9 to test their ability to transduce target cells. Fibroblasts and iPSCs were transduced with AAV9-EGFP and AAV2-EGFP control viruses respectively with a Multiplicity of Infection (MOI) of $2x10^5$. Neurons were infected with a MOI of $4x10^4$. AAV9 infection was preceded by Neuraminidase treatment in order to expose the N-Linked-Galactose that acts as AAV9 receptor. To this aim, cells were treated with 50mU of Endo-α-Sialidase (Neuraminidase, Millipore-Sigma, Darmstadt, Germany) for 2 hours at 37°C. The medium containing Neuraminidase was then removed and fresh medium containing AAV9 without FBS and antibiotics was added. The plate was centrifuged for 2 minutes at 1100 rpm and then incubated for 1 hour and 30 minutes at 4° C. Subsequently, fresh medium with FBS was added and the plate was incubated overnight at 37°C. After 24 hours the medium containing the viral particles was removed and replaced with fresh medium. No pretreatment was required for AAV2 transduction because its membrane-associated heparan sulfate proteoglycan receptor is naturally unmasked on cell surface. BD Accuri C6 flow cytometer (BD Biosciences) was used to quantify the percentage of EGFP+ cells 48 hours after transduction.

Subsequently, iPSCs and iPSC-derived neurons were transduced with AAV2 and AAV9 correction vectors, respectively. In both experiments $2x10^5$ cells/well were seeded in 12-well plates and contextually transduced with AAV-targeting and AAV-Cas9 vectors. Co-transduced iPSCs were examined by fluorescence microscopy and the percentage of mCherry/EGFP positive cells was evaluated by FACS analysis 48 hours after transduction. Treated iPSC-derived neurons were analysed by fluorescence microscopy 6 days post-infection.

3.9 Flow cytometry analysis and cell sorting

Cells were analyzed and sorted on a fluorescent-activated cell sorter FACS Aria II (Becton Dickinson) using FACS Diva software version 8.0.1 (BD Biosciences-US). To isolate EGFP-positive cells for subsequent analyses, fibroblasts and neurons were detached, resuspended in PBS/EDTA 3mM/Trypsin 2.5% and placed on ice. The cellular suspension was filtered through a 70 μm filcon filter (BD Biosciences). Fibroblasts and neurons were sorted using a 100 μm nozzle and an event rate of 1000/sec.

3.10 Ion Torrent S5 sequencing and NGS analysis

DNA was extracted from EGFP$^+$ cells and control cells using the Qiamp DNA micro kit (Qiagen, Hilden, Germany). Ion AmpliSeq 2.0TM Library Kit (Life Technologies™, Carlbad, CA) was used for library preparation. Libraries were purified using Agencourt AMPure XP system, quantified with the Qubit® dsDNA HS Assay Kit reagent (Invitrogen Corporation, Life Technologies™), pooled at an equimolar ratio, annealed to carrier spheres (Ion Sphere™Particles, Life Technologies) and clonally amplified by emulsion PCR (emPCR) using the Ion ChefTM system (Ion Chef™, Life Technologies). Ion 510™, 520™ or 530™ chip were loaded with the spheres carrying single stranded DNA templates and sequenced on the Ion Torrent S5 instrument (Life Technologies™, Carlsbad, CA) using the Ion S5™ Sequencing kit, according to manufacturer's protocol. For each patient, the FASTQ files of transfected cells and relative controls were downloaded from the sequencing platform (S5 Torrent Server VM) and uploaded to the online analysis tool Cas-Analyzer [147] together with the sgRNA and the Donor in order to obtain the percentage of HDR achieved, considering a comparison range of 15 nucleotides around the cut site. For each sample, the .bam and .bai files were uploaded on IGV Visualization Software (Broad Institute, Cambridge, United States) to precisely visualize both the replacement of the mutated base and the indels events in the neighbouring sites.

3.11 Off-target analysis

In order to investigate the genome-wide profile of off-target cleavages introduced by SpCas9 we performed GUIDE-seq analysis [148] in HEK293 cells engineered to harbor c.688C>T and c.765G>A variants.

2×10^5 HEK293 cells were transfected using Lipofectamine 3000 transfection reagent (Invitrogen) with 250 ng of each sgRNA encoding plasmid, 500 ng of SpCas9 plasmid, 10 pmol of dsODNs and 50 ng of a pEGFP-IRES-Puro plasmid, expressing EGFP and the puromycin-resistance genes. The day after transfection cells were detached and selected with

1μg/ml puromycin to eliminate non-transfected cells. Cells were collected after 48 hours and genomic DNA was extracted using the DNeasy Blood and Tissue Kit (Qiagen) following manufacturer's instructions. Genomic DNA was sheared to an average length of 500 bp using the Bioruptor Pico sonicator device (Diagenode). Library preparation, sequencing and analysis were performed according to previous works [149].

3.12 Immunoblotting

Proteins from patient-derived fibroblasts and neuronal precursors were extracted with 10-fold excess of RIPA buffer (Tris-HCl 50 mM, NP-40 1%, Na-Deoxycholate 0.5%, SDS 0.1%, NaCl 150 mM, EDTA 2mM, pH 7.4). Protease inhibitor cocktail (Sigma, Milano, Italy) was added to all lysates. Lysates were cleared by ultracentrifugation (20.000 g for 30 min at 4 °C) before Western blot analysis. Protein concentration was measured with Bradford Assay (BioRad, Hercules, CA, USA). A total of 15 μg and 30 μg of protein from cultured fibroblasts and neural precursors, respectively, were used in each lane for immunoblotting. Immunosignals were detected by autoradiography using multiple exposures to ensure that signals were in the linear range. Signals were quantified through densitometry using Adobe Photoshop 2020 software (Adobe). The following antibodies were employed for analysis: anti-MECP2 (Sigma-Aldrich, #M6818), anti-SpCas9 (Santa Cruz, Biotechnology, Inc #7A9-3A3), anti-PAX6 (Millipore, Inc #MAB5552) and anti-β-Actin (Santa Cruz, Biotechnology, Inc #sc-47778).

3.13 Real-time qRT-PCR

Total RNA was extracted with RNeasy mini kit (Qiagen). Two μg of total RNA was reverse transcribed with the QuantiTect Reverse transcription kit (Qiagen) according to manufacturer's instructions. Quantitative PCR was carried out in single-plex reactions in a 96-well optical plate with FastStart SYBR Green Master Mix (Roche) on an ABI Prism 7700 Sequence Detection System (Applied Biosystems). Experiments were performed in triplicate in a final volume of 20 uL with 25–100 ng of cDNA and 150 nM of each primer, following the SYBR Green protocol. Standard thermal cycling conditions were employed (Applied Biosystems): 2 min at 50 °C and 10 min at 95 °C followed by 40 cycles at 95 °C for 15 s and 60 °C for 1 min. The *GAPDH or GUSB* genes were used as reference. Results were analyzed using the comparative Ct method. GraphPad software was employed for statistical analysis. Unpaired Student's t-test with a significance level of 95% was used for the identification of statistically significant differences in expression levels.

3.14 Statistical Analysis

Statistical analysis was performed using Student's t-test. Data obtained from Western blot were expressed as band intensity values (mean value of 3 independent experiments and standard deviation); data obtained from edited samples were compared to mutated sample. Data obtained from Real-time qRT-PCR were expressed as absolute values (mean value of 3 independent experiments and standard deviation); data obtained from all genes in treated sample were compared with data from control sample. P values < 0.05 were considered to be statistically significant.

4. Results

4.1 Results Section 1

iPSC-derived neurons profiling reveals GABAergic circuit disruption and acetylated α-tubulin defect which improves after iHDAC6 treatment in Rett syndrome

(Published in Landucci E, *et al*. iPSC-derived neurons profiling reveals GABAergic circuit disruption and acetylated α-tubulin defect which improves after iHDAC6 treatment in Rett syndrome. *Exp Cell Res* 368(2):225-235 (2018). doi: 10.1016/j.yexcr.2018.05.001. PMID: 29730163)

4.1.1 RNA-seq analysis

RNA-seq analysis on neurons differentiated from three clones from 2 different MECP2 mutated patients with c.473C>T (p.(Thr158Met)) and c.916C>T (p.(Arg306Cys)) variants and 2 control iPSC clones revealed that about 17,000 transcripts are significantly expressed (FPKM=1) both in controls and MECP2-mutated samples. The distribution of reads corresponding to coding sequences (CDS), 5'UTRs, 3'UTRs, introns and intergenic regions did not show a statistically significant difference between control and mutated samples. Differentially expressed genes were identified comparing the log ratio of gene's expression (FPKM value) in mutation bearing samples against that of controls. We identified about 900 deregulated genes, with the proportion of down regulated genes being almost double the amount of up-regulated transcripts (Fig. 9). A direct or indirect effect of MeCP2 on the expression level for some of the identified deregulated genes (BDNF, RELN, TNR, NEFL, NRXN1, NRXN3, ID1-3 and EGR2) has been previously reported, confirming the reliability of our disease model [150-154].

To clarify MECP2 function in directly regulating the identified altered genes, given its role as transcriptional regulator, we investigated a possible action through binding at the promoter regions. Thus, we interrogated published MeCP2-ChIP-chip data. Among the 937 genes deregulated in our dataset, 38 genes were reported by Yasui and colleagues to be modulated by MeCP2 binding at their promoters in human cells [152] (Table 5). Evaluation of the significance of this overlap by Hypergeometric probability, indicates that it is statistically

significant (p < 0.0001). Then, to further investigate a possible role of MeCP2 as transcriptional repressor through the binding to non-promoter genomic regions, we surveyed the few MeCP2 ChIP-seq available datasets from studies of Mecp2-mutant mice, asking if genes up-regulated in our MECP2-mutated cell lines have been previously described as direct Mecp2 targets. Among the 342 up-regulated transcripts in our dataset, we identified 17 transcripts previously reported by Gabel to be consistently repressed by Mecp2 binding to methylated CA sites in different mouse studies (Table 6) [150]; none of these 17 transcripts was present among those common to Yasui list (compare Table 4 to Table 5). Hypergeometric probability analysis indicates that also this overlap is statistically significant (p < 0.0005). The fact that many dysregulated genes in our dataset may not be directly regulated by MeCP2 binding at promoter and non-promoter regions suggests that MECP2 regulates gene expression by both direct and indirect mechanisms. In line with this idea, further interrogation of datasets of deregulated genes identified in expression profiling studies in different MECP2 patient material (post-mortem brain, primary lymphocytes, lymphoblasts, fibroblasts) found no relevant overlap [155-158].
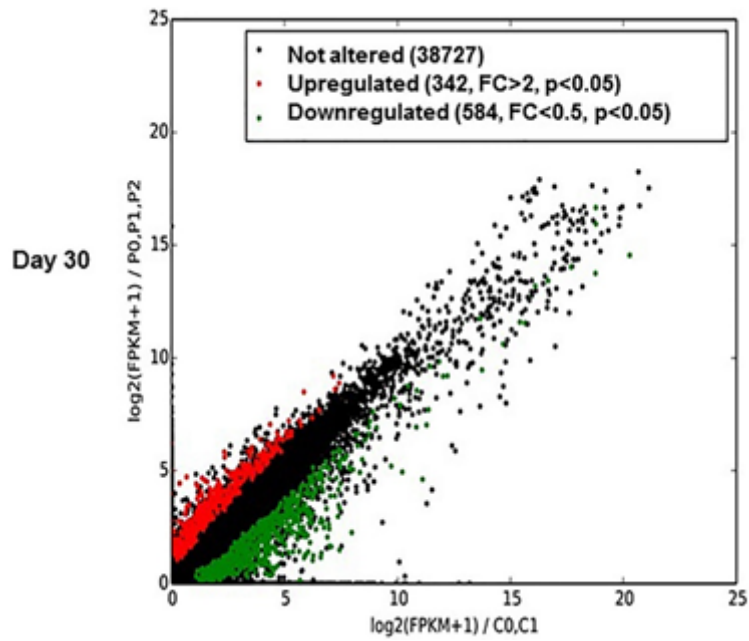
Figure 9. RNAseq data analysis. Scatter plot of log2 transformed RNAseq expression level (FPKM) of MECP2-derived cells (P0, P1, P2) versus controls (C0, C1) in terminally differentiated neurons (day 30) is shown. Red and green spots indicate significantly ($p < 0.05$) up-regulated and down-regulated genes, respectively.

Gene symbol	Change direction in present study	Fold Change (M/C)	p value
AATF	UP	3.52	0.01675
BDNF	UP	3.47	0.04875
CDKL2	UP	7.12	0.00325
GAN	UP	2.49	0.02810
HSPA4	UP	2.57	0.02685
MAGEE2	UP	4.42	0.04320
NCAM1	UP	2.77	0.01545
NEFL	UP	4.15	0.00545
PCDH1	UP	2.99	0.04655
PIK3R3	UP	2.47	0.02110
SLC38A1	UP	2.25	0.04300
STXBP5	UP	3.37	0.00840
VGF	UP	4.43	0.01665
ADRB2	DOWN	0.05	0.00825
ANTXR1	DOWN	0.30	0.01020
B4GALT1	DOWN	0.12	0.00115
CD164	DOWN	0.19	0.01100
DLEU1	DOWN	0.25	0.00965
EGFR	DOWN	0.29	0.01430
FAM46C	DOWN	0.04	0.00115
FRZB	DOWN	0.08	0.00020
GULP1	DOWN	0.33	0.02010
HIST1H4B	DOWN	0.33	0.02245
ID3	DOWN	0.22	0.01225
IGFBP5	DOWN	0.06	0.00025
IL11RA	DOWN	0.20	0.00520
IQGAP3	DOWN	0.24	0.00215
LAPTM4A	DOWN	0.15	0.00460
OLFML2B	DOWN	0.29	0.01700
PBXIP1	DOWN	0.29	0.01135
PDGFRA	DOWN	0.12	0.02755
PPP1R1B	DOWN	0.21	0.03115
RGS16	DOWN	0.32	0.01410
SNAP23	DOWN	0.26	0.01935
SNX3	DOWN	0.30	0.01370
SPAG8	DOWN	0.27	0.03980
TNFRSF19	DOWN	0.39	0.04860
UQCRB	DOWN	0.32	0.04625

Table 5: Deregulated genes in iPSC-derived neurons known to be regulated by MECP2 in Human cells.

Gene symbol	Change direction in present study	Fold Change (M/C)	p value
AK5	UP	3.41	0.02020
CABP1	UP	14.53	0.01055
CHGB	UP	3.28	0.01635
DPP10	UP	3.65	0.00560
HSPA12A	UP	6.91	0.00040
KCNK2	UP	3.38	0.04340
KRT222	UP	7.94	0.04015
LRRTM4	UP	3.69	0.00515
NPNT	UP	4.72	0.01960
SCN1A	UP	13.94	0.01035
SH3GL2	UP	6.23	0.00585
SLC4A10	UP	3.00	0.02035
SORBS2	UP	2.75	0.03125
TFRC	UP	2.78	0.03035
TNR	UP	13.35	0.01065
TPD52	UP	3.02	0.02930
ZBTB7C	UP	4.72	0.00025

Table 6. Deregulated genes in iPSC-derived neurons known to be repressed by Mecp2 in the mouse.

4.1.2 GABAergic circuits up-regulation

GO analysis revealed a statistically significant enrichment among up-regulated transcripts for genes related to neuron development/differentiation, synaptic transmission axonogenesis and dendrite development (Table 7). Further inspection of these genes revealed a substantial number of GABA pathway genes including GABA receptors and other GABA circuit related genes as represented by the heatmap in Fig. 10a. A trend toward up-regulation was noticed also for GAD1, the rate-limiting enzyme the production of GABA from L-glutamic acid. The up-regulation was confirmed by Real-Time qRT-PCR and Western blot analyses on neurons from independent differentiation experiments (Fig. 10b). Furthermore, we found a significant increase in mRNA levels of NRG1 and NRG3 that encode proteins expressed mainly in interneurons controlling the development of GABAergic circuits and promoting the formation of excitatory synapses onto the dendrites of GABAergic interneurons [159-161]. Specifically, NRG1 signaling can affect NMDA receptor activity by acting on the NR2 subunit of the receptor. We thus surveyed our RNA-seq data for the expression levels of GRIN2B, the gene encoding for the NR2B subunit of NMDA receptors, and found a trend toward an up-regulation

(Fig. 10a); Real Time qRT PCR analysis on cDNAs from an independent differentiation experiment confirmed the up-regulation of GRIN2B (Fig. 10c). A statistically significant up-regulation was also detected for Neurexin1 (NRXN1) and Neurexin3 (NRXN3), transcripts essential for modulating GABAergic transmission by direct binding to GABAA-receptors [162] and important for their concurrent role in axon path-finding.
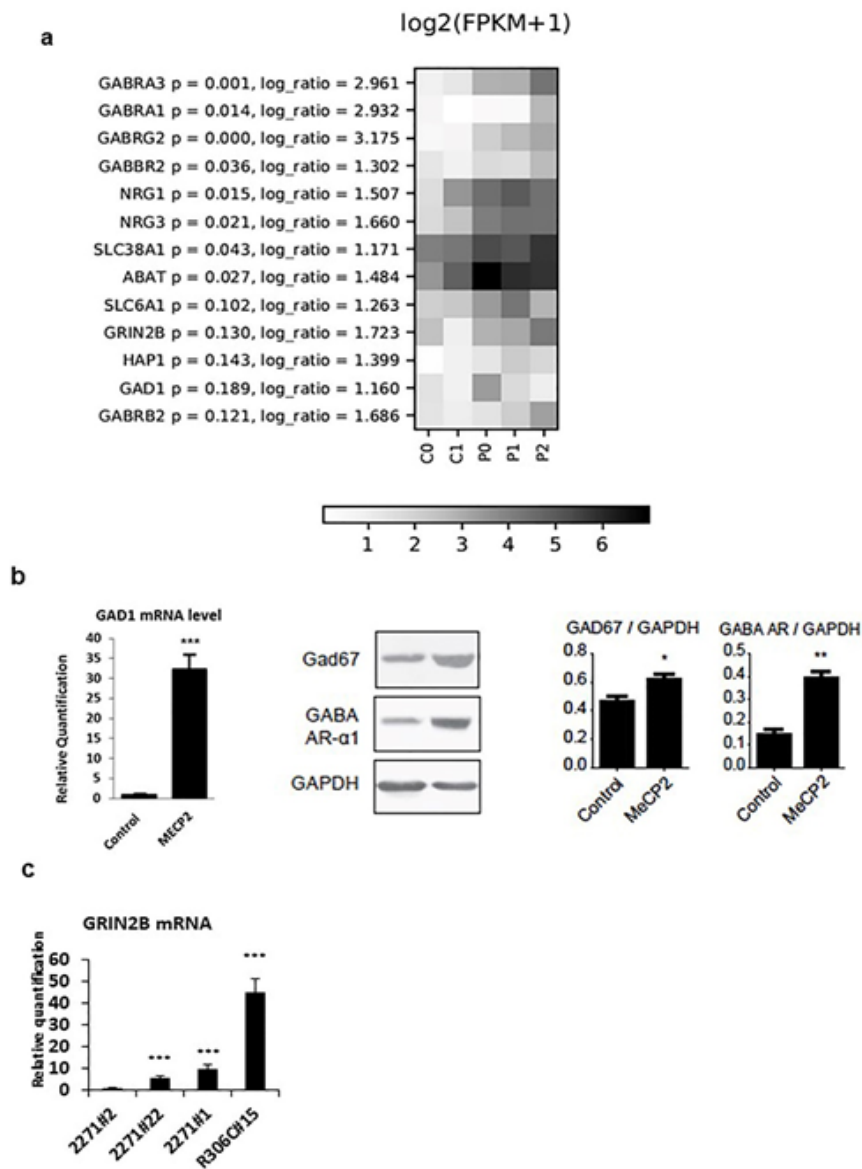

Figure 10. Up regulation of GABAergic axis. a. HeatMap of GABAergic pathway genes. For each gene, log ratio and related p-values are shown. b. Validation of RNAseq data**.** Validation experiments on neurons from and independent differentiation experiment demonstrate a significant upregulation of GAD1 mRNA and protein levels and of GABA-R receptor alpha 1 (GABA-AR) protein in MECP2-mutated neurons compared to controls. GAPDH was used as loading control for Western blot analysis. n=3. **c.** Upregulation of GRIN2B mRNA. GRIN2B mRNA was significantly increased in neurons from the 3 MECP2-mutated clones respect to neurons from the partial isogenic control clone (2271#2). Statistical significance was determined using unpaired Student's t-test (*$p < 0.05$; **$p < 0.001$; ***$p < 0.0001$).

GO Term	p Value	Genes	Fold Enrichment	Bonferroni-corrected p value	Benjamini-corrected p value	FDR-corrected p value
GO:0007268~synaptic transmission	1.83E-11	SYT1, TAC1, GABBR2, ADORA1, RIMS1, HCRTR2, CTTNBP2, SLC1A2, SHC3, SLC1A1, GABRG2, KCND2, NRXN3, GABRA3, SLC12A5, LIN7C, NRXN1, GRIA4, NAALAD2, GRIA2, GRIA1, TMOD2, GHRL, ABAT, CACNA1E, NCAN	5.32	2.83E-08	2.83E-08	3.06E-08
GO:0030182~neuron differentiation	1.31E-10	CDK5R1, LPPR4, IRX5, SOX5, PAX3, KLHL1, ALDH1A2, BDNF, S1PR1, ANK3, PAX7, TNR, GBX2, ROBO3, OLFM3, DCX, NEFL, DSCAM, APC, GNAO1, MCF2, NRXN3, PTPRZ1, DOCK7, NRXN1, ASCL1, MAP2, GHRL, RELN, NTM	4.17	2.02E-07	6.74E-08	2.19E-07
GO:0048666~neuron development	1.54E-09	CDK5R1, LPPR4, GNAO1, IRX5, MCF2, PTPRZ1, NRXN3, DOCK7, NRXN1, KLHL1, ASCL1, BDNF, ANK3, TNR, MAP2, GBX2, GHRL, RELN, ROBO3, OLFM3, DCX, NEFL, NTM, DSCAM, APC	4.49	2.38E-06	5.95E-07	2.57E-06
GO:0031175~neuron projection development	7.30E-09	CDK5R1, LPPR4, GNAO1, MCF2, PTPRZ1, NRXN3, DOCK7, NRXN1, KLHL1, BDNF, ANK3, TNR, MAP2, GBX2, GHRL, RELN, ROBO3, DCX, NEFL, DSCAM, APC	5.00	1.13E-05	2.25E-06	1.22E-05
GO:0007267~cell-cell signaling	4.43E-08	SYT1, TAC1, GABBR2, VGF, ADORA1, RIMS1, HCRTR2, CTTNBP2, PCDH1, SLC1A2, BDNF, SHC3, SLC1A1, GABRG2, KCND2, NRXN3, GABRA3, SLC12A5, LIN7C, PCDH8, NRXN1, GRIA4, NAALAD2, WNT7B, GRIA2, GRIA1, TMOD2, ABAT, GHRL, CACNA1E, NCAN	3.15	6.83E-05	1.14E-05	7.39E-05
GO:0030030~cell projection organization	6.61E-07	CDK5R1, LPPR4, GNAO1, ONECUT1, MCF2, PTPRZ1, NRXN3, DOCK7, NRXN1, KLHL1, BDNF, ANK3, TNR, MAP2, GBX2, GHRL, RELN, ROBO3, DCX, NEFL, DSCAM, APC	3.64	1.02E-03	1.45E-04	1.10E-03
GO:0032940~secretion by cell	1.54E-06	SYT1, CPLX2, NRXN3, LIN7C, SYT6, VGF, RIMS1, CADPS, BDNF, GNPTAB, STXBP5, GHRL, EXOC6, SYTL2, DOC2B, SCAMP5	4.71	2.37E-03	2.97E-04	2.57E-03
GO:0048667~cell morphogenesis involved in neuron differentiation	1.73E-06	CDK5R1, LPPR4, PTPRZ1, NRXN3, DOCK7, NRXN1, BDNF, ANK3, TNR, GBX2, RELN, ROBO3, DCX, NEFL, DSCAM, APC	4.67	2.66E-03	2.96E-04	2.89E-03
GO:0048812~neuron projection morphogenesis	2.19E-06	CDK5R1, LPPR4, PTPRZ1, NRXN3, DOCK7, NRXN1, BDNF, ANK3, TNR, GBX2, RELN, ROBO3, DCX, NEFL, DSCAM, APC	4.58	3.38E-03	3.38E-03	3.66E-03
GO:0048858~cell projection morphogenesis	2.68E-06	CDK5R1, LPPR4, ONECUT1, PTPRZ1, NRXN3, DOCK7, NRXN1, BDNF, ANK3, TNR, GBX2, RELN, ROBO3, DCX, NEFL, DSCAM, APC	4.23	4.12E-03	3.75E-04	4.47E-03
GO:0007409~axonogenesis	3.41E-06	CDK5R1, LPPR4, PTPRZ1, NRXN3, DOCK7, NRXN1, BDNF, ANK3, TNR, GBX2, RELN, ROBO3, DCX, NEFL, APC	4.74	5.25E-03	4.38E-04	5.69E-03
GO:0046903~secretion	8.76E-06	SYT1, CPLX2, NRXN3, LIN7C, SYT6, TPD52, VGF, ADORA1, RIMS1, CADPS, BDNF, GNPTAB, STXBP5, GHRL, EXOC6, SYTL2, DOC2B, SCAMP5	3.66	1.34E-02	9.64E-04	1.46E-02
GO:0000904~cell morphogenesis involved in differentiation	1.14E-05	CDK5R1, LPPR4, PTPRZ1, NRXN3, DOCK7, NRXN1, BDNF, ANK3, TNR, GBX2, RELN, ROBO3, DCX, NEFL, DSCAM, APC	4.00	1.74E-02	1.17E-03	1.90E-02
GO:0016358~dendrite development	1.94E-05	BDNF, MCF2, MAP2, GHRL, DCX, KLHL1, DSCAM	12.19	2.95E-02	1.87E-03	3.23E-02

Table 7: Biological processes enriched in over-expressed genes.

42

4.1.3 Functional studies reveal altered GABAergic transmission and increased excitability of mutant cells

To investigate the functional consequences of MeCP2 mutation in iPSC-derived patient neurons we first assessed general biophysical neuronal parameters such as resting potential (Fig. 11a), membrane capacitance (Fig. 11b), membrane resistance (Fig. 11c). None of these parameters was significantly different between control and mutant neurons. Then, we studied neuronal excitability by measuring the peak of the V-gated Na+ current and depolarization evoked firing (Fig. 11d-e). Evoked firing resulted to be significantly affected by MeCP2 mutation. Indeed, mutant cells produced more action potentials than wild type cells in response to different depolarizing steps. No difference was present in Na+ current peaks. To explore the functional differences in GABAergic transmission caused by MeCP2 mutations, we recorded spontaneous GABAergic currents using patch-clamp in whole cell configuration in the presence of 6,7-dinitroquinoxaline-2,3-dione (DNQX) to inhibit excitatory glutamatergic transmission. Spontaneous currents were abolished by bicuculline confirming the GABAergic nature of the recorded currents (Fig. 11f-g). We found that spontaneous current amplitude (Fig. 11h) and frequency (Fig. 11i) were significantly lower in MeCP2 cells (187 cells) with respect to control cells (28 cells). No significant difference was present in current decay time (Fig. 11j). These data indicate at functional level that alterations in the GABAergic transmission are present in *MECP2*-mutated neurons and report enhanced excitability of mutant neurons.
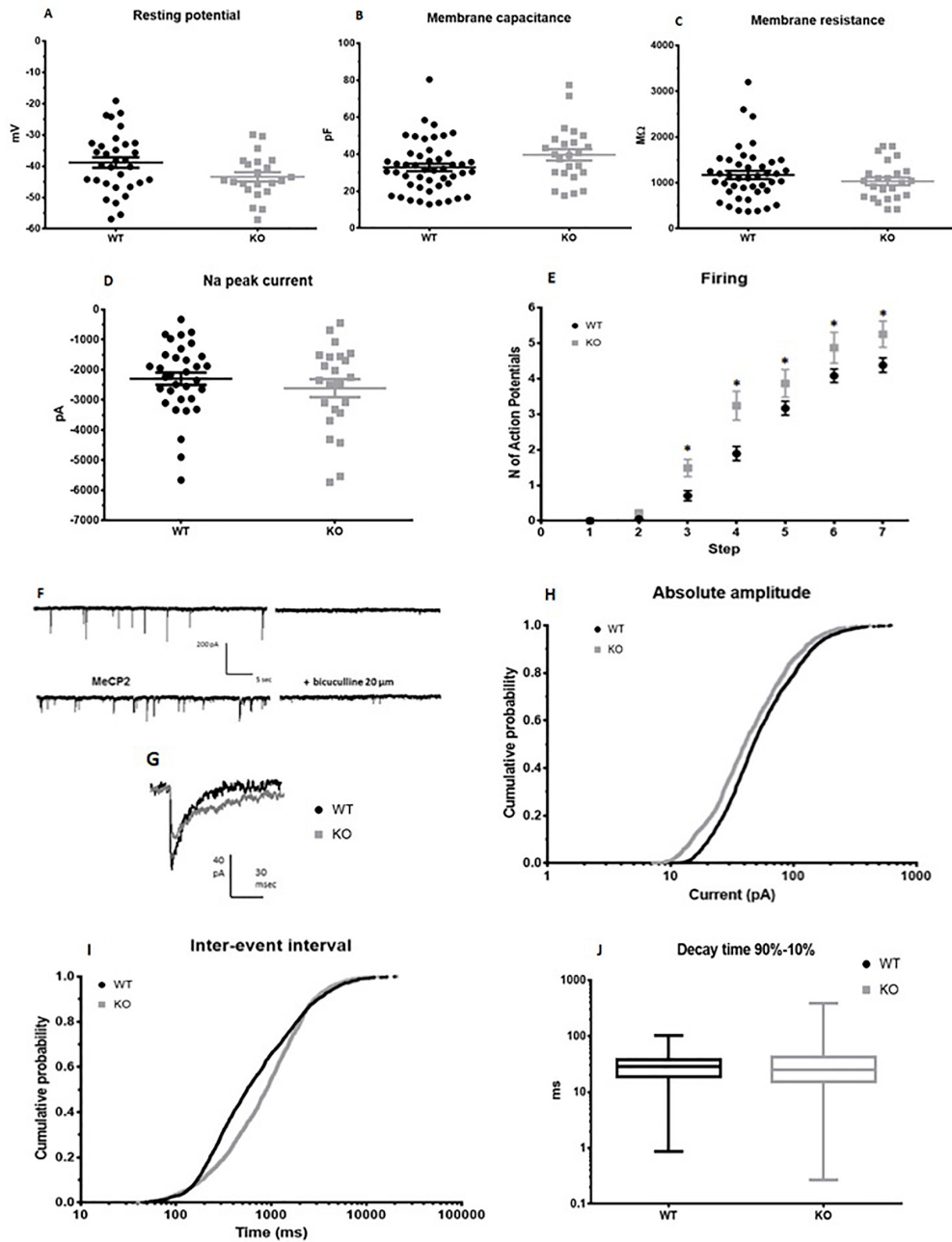
Figure 11. Altered functional properties of MeCP2 mutant neurons. **a)** Membrane resting potential (mV). Student t-test: p = 0.093, n wt = 32, n ko = 22. **b)** Membrance capacitance (pF), p = 0.063, n wt = 48, n ko = 24. **c)** Membrane resistance (M.). Student t test: p = 0.31, n wt = 43, n ko = 24. **d)** Maximum peak of Na current recorded in voltage clamp. Student t-test: p = 0.373, n wt = 33, n ko = 23. **e)** Firing: number of action potentials evoked by +10 mV steps of the membrane potential starting from -70 mV. Two way ANOVA, * p < 0.05, n wt = 27, n ko = 20. **f)** Example of traces for control and MECP2 mutated cells; traces from the same cell in the presence of bicuculine are shown on the right. **g)** Average sIPSCs in a control (CNT) and a mutant cell. **h)** Cumulative 5t distribution of sIPSC amplitude (pA). Mann-Whitney: p < 0.001; wt median: 47.0, 25th-75th percentile = 30.0-87.0; ko median: 40.1, 25th-75th percentile = 24.5- 73.0. **i)** Cumulative distribution of sIPSCs inter-event interval (ms). Mann-Whitney: p < 0.001; wt median: 56.4, 25th-75th percentile; ko median: 895.0, 25th-75th percentile 392.6-1764.0. **j)** Whisker plot of sIPSC decay kinetics (90-10% decay time). Mann-Whitney: p = 0.078; wt: median: 28.6, 25th-75th percentile 18.6-37.7; ko median: 25.3, 25th-75th percentile 15.2-41.8. Measurements for h, i and j were collected from 28 control neurons and 18 MECP2-mutated neurons. Data are reported as mean ± SEM. Each circle in a-d represents a cell.

4.1.4 Microtubules system impairment, selective over-expression of HDAC6 and increase of acetylated α-tubulin levels after iHDAC6 treatment

Intriguingly, RNA-seq data analysis revealed an over-expression of the histone deacetylase 6 (HDAC6) gene, encoding for a cytoplasmic deacetylase whose main substrate is acetylated α-tubulin, in MECP2- mutated neurons. Western blot analysis revealed a significant reduction in acetylated α-tubulin in MECP2-mutated neurons compared to controls, likely as a consequence of the increase in HDAC6 activity ($p < 0.05$) (Fig. 12a). The levels of acetylated tubulin are of fundamental relevance for many functions in neuronal cells, including vesicle trafficking, neuronal migration and axon polarization and elongation [163]. Therefore, this finding indicates that an impairment of the microtubule network together with a reduction of acetylated α-tubulin mediated by HDAC6 overexpression could be reflected in axonogenesis alterations. To validate the direct correlation between HDAC6 overexpression and acetylated tubulin reduction, we treated mutated neurons with a new potent and selective heterocyclic inhibitor of HDAC6 (compound #1, HDAC1/HDAC6 IC50 ratio = 47). Specifically, differentiating neurons were treated for 5 days with 40 µM drug concentration (Fig. 12b). Western blot analyses on mutated and control neurons showed that the treatment significantly increases acetylated α-tubulin levels (Fig. 12c). A literature search for commercial HDAC6 inhibitors revealed a molecule, ACY-1215 (HDAC1/HDAC6 IC50 ratio = 12), presently under evaluation for Multiple Myeloma treatment [164]. We thus decided to test also this second molecule for its ability to modulate acetylated α-tubulin levels in our model. Since the selected dose for inhibitor #1 resulted in a significant increase in acetylated α-tubulin also in control cells, for ACY-1215 we evaluated lower drug doses (20 µM and 40 µ M). This treatment also resulted in a marked increase in the levels of acetylated α-tubulin (Fig. 12c), confirming the direct link between HDAC6 activity and microtubule network status.
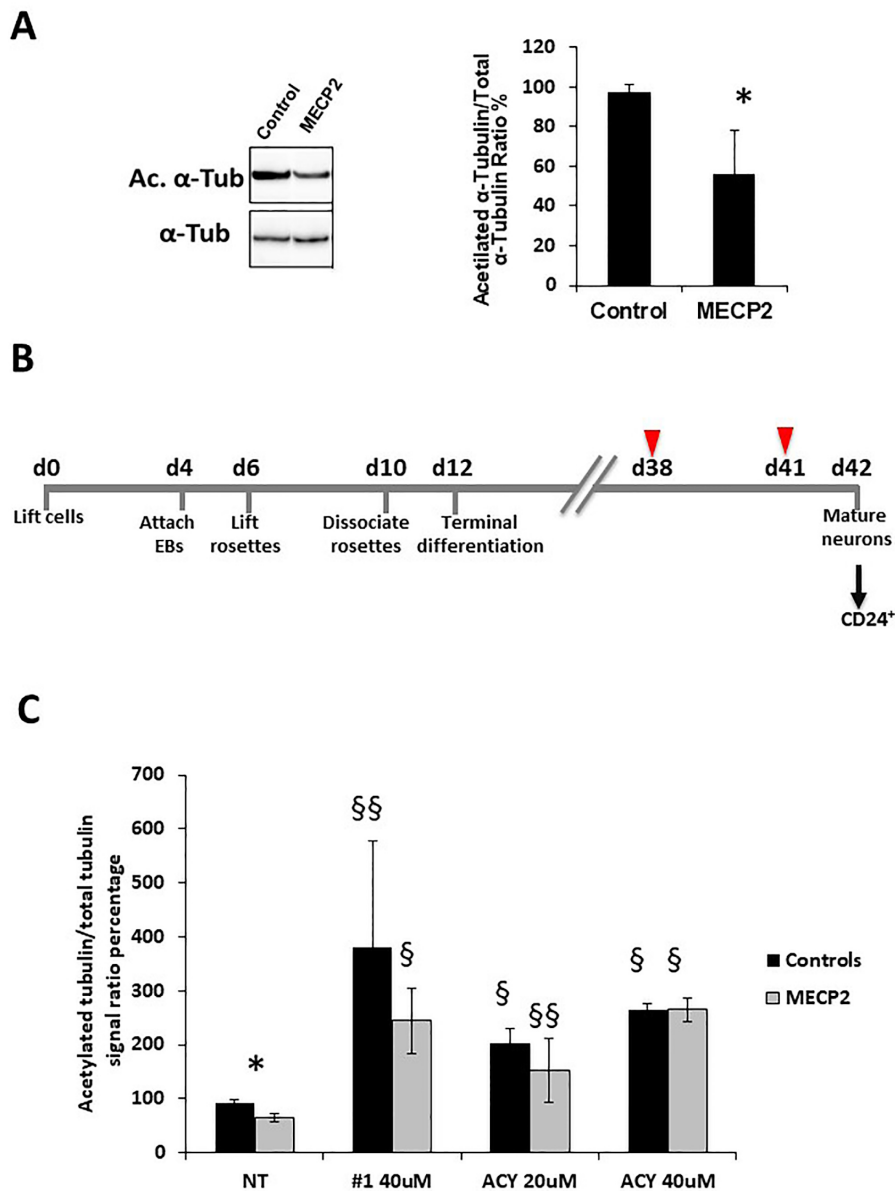
Figure 12. Reduction in acetylated α-tubulin levels and treatment with selective HDAC6 inhibitors. a) A reduction in acetylated α-tubulin levels was observed by Western Blot analysis in MECP2-derived neurons (n=3 clones) compared to control ones (n=2 clones).* p < 0.05. b) Overview of the neuronal differentiation protocol with critical time-points indicated below the time lane. Cells were differentiated in Terminal Differentiation medium for 30 days; differentiating cells were treated twice (arrowheads) with either the selective inhibitor (Compound #1 or ACY-1215) or vehicle and then neurons were isolated (arrow) by immunomagnetic sorting with anti-CD24 antibodies for further analyses. c) Treatment with compound #1 (40 uM) or ACY-1215 (ACY 20 uM or ACY 40 uM) resulted in a significant increase in acetylated α-tubulin levels in both MECP2-mutated and control neurons. Data are expressed as the mean +SEM from 3 independent experiments performed on 3 control and 3 MECP2-mutated clones. *p < 0.05 between mutated and control neurons; §p < 0.0001 and §§p < 0.005 compared to the corresponding untreated neurons. Statistical significance was determined using unpaired Student's t-test.

4.2 Results Section 2

High rate of HDR in gene editing of p.(Thr158Met) *MECP2* mutational hotspot.

(Published in Croci, S., *et al.* High rate of HDR in gene editing of p.(Thr158Met) *MECP2* mutational hotspot. *Eur J Hum Genet* 28, 1231–1242 (2020). doi: 10.1038/s41431-020-0624-x. PMID: 32332872).

4.2.1 Plasmids design and validation

To validate CRISPR/Cas9 application as therapeutic strategy for the correction of pathogenic *MECP2* variants, we tested its potential for the correction of the most common variant found in RTT patients, the c.473C>T (p.(Thr158Met) missense variant. To this aim, we selected a sgRNA that exclusively targets the mutated allele and an appropriate donor DNA harbouring the WT sequence (Figure 13a). An adjacent spCas9 PAM sequence (NGG) is present and a silent nucleotide substitution was inserted in the PAM sequence; this modification prevents a secondary cut by Cas9 and helps to identify the corrected alleles. We designed a dual-vector approach for contemporary delivery of the correction machinery components to the cells (Figure 13b): one plasmid expresses SpCas9 under the control of *CMV* promoter, and the second one harbours the variant -specific sgRNA, under the control of U6 promoter, and the Donor DNA along with the mCherry/EGFP reporter system, under the control of *CMV* promoter. The variant-specific sgRNA sequence plus a PAM sequence has been cloned in the Cas9 vector between the promoter and Cas9 coding sequence, allowing Cas9 auto-cleaving and thus avoiding its long-term expression.
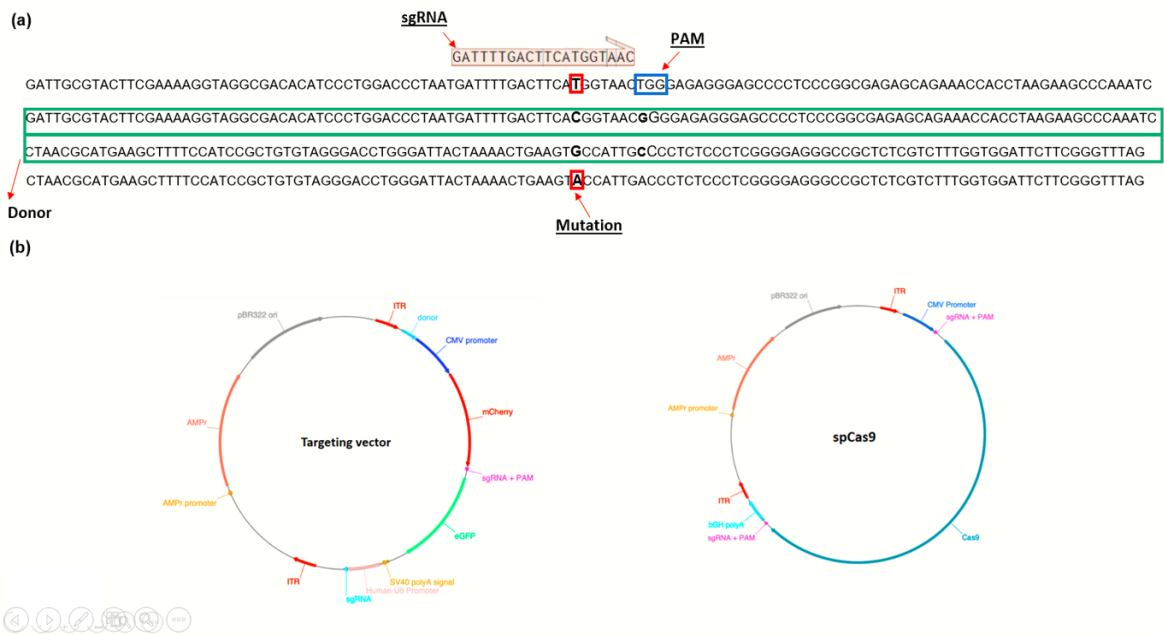
Figure 13. Design of sgRNA and donor for MECP2 variant c.473C>T (p.(Thr158Met)). a) The red box indicates the variant and the grey sequence above is the sgRNA which directs the Cas9 specifically to the target sequence. The PAM sequence, required for Cas9 activity, is marked by the blue box. After Cas9 activation, the donor sequence, indicated by the green box, is used as template to restore the wild type sequence. **b)** Representation of the plasmids structure by ApE tool http://biologylabs.utah.edu/jorgensen/wayned/ape. The relevant components are reported.

The double reporter system included into the targeting vector is designed to visualize transfected cells and monitor Cas9 activation. Indeed, mCherry is constitutively expressed, while EGFP expression requires Cas9 protein synthesis and activity. Once expressed, Cas9 is able to recognize and cut the target sequence between mCherry and EGFP bringing EGFP coding sequence in frame and resulting in the expression of an mCherry/EGFP fusion protein (Figure 14 a, b).
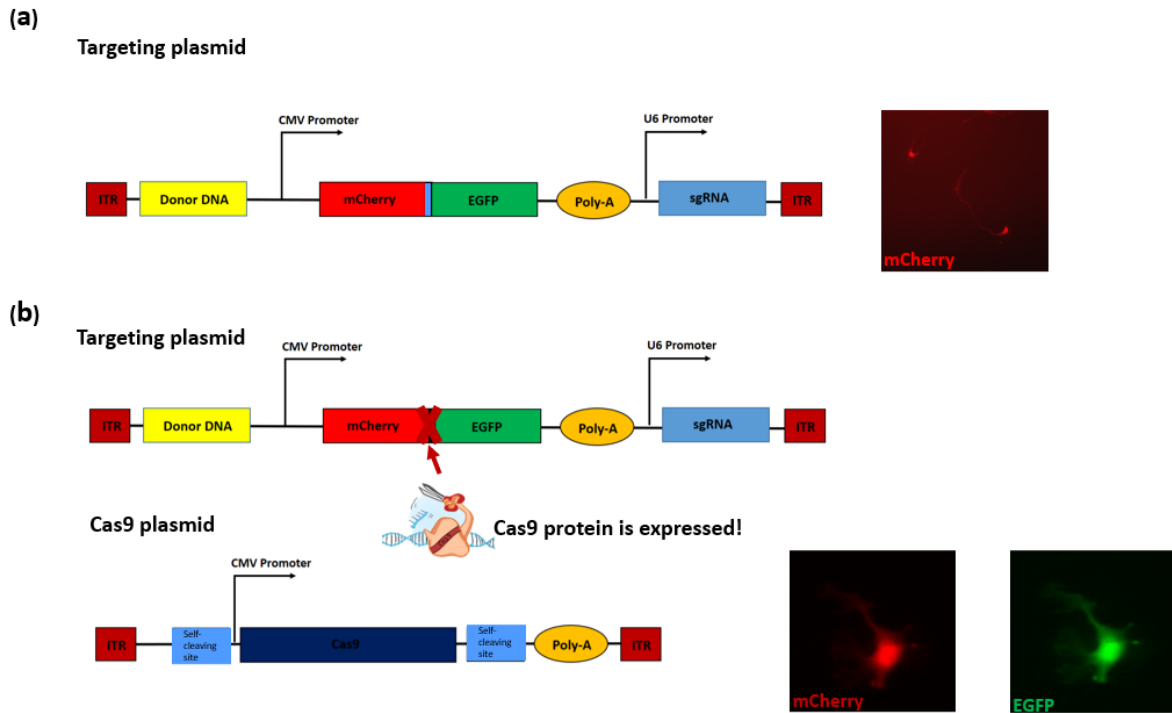
Figure 14. Plasmids strategy a) The targeting construct brings sgRNA, Donor DNA and the Reporter system composed by mCherry and EGFP. If the Targeting plasmid is transfected into the cells, mCherry is expressed constitutively and the cells acquire red fluorescence. **b)** The Cas9 construct encodes Cas9 and two self-cleaving targets (light blue boxes) composed by sgRNA + PAM sequence. When a cell is transfected by both Targeting and Cas9 plasmids, Cas9 is expressed and cuts the target sequence interposed between mCherry and EGFP (light blue box); this allows EGFP expression resulting in double mCherry+/EGFP+ cells. The same specific nuclease activity ensures Cas9 auto-cleaving, avoiding long-term expression.

To test the functionality of the reporter system, HEK293 cells were transfected with the targeting vector alone or in combination with the Cas9 vector; mCherry+ and EGFP+ population was investigated by FACS analysis 48 hours after transfection (Figure 15a). About 50 % of cells transfected only with the reporter system were mCherry+/EGFP-. Conversely, 4.86% of cells co-transfected with reporter and Cas9 plasmid are mCherry+/EGFP+, proving Cas9 activation and plasmids functionality (Figure 15a).

The specificity of the sgRNA was confirmed in HEK293 cells, by transfection with the Cas9 plasmid and a targeting plasmid in which the target sequence between mCherry and EGFP harbours either the wild type or the variant-specific sgRNA. After 48 hours green fluorescence was confirmed to be expressed only in cells co-transfected with the Cas9 plasmid and the reporter plasmid with variant -specific sgRNA (Figure 15b). No EGFP+ cells were observed when the wild type sgRNA is interposed between mCherry and EGFP sequence (Figure 15b), confirming the specificity of the variant-specific sgRNA for the mutated allele.

Correction plasmids were also transfected in mutated iPSC-derived neurons and fluorescence was visualized *in vivo* 5 days post-transfection. Efficient co-expression of mCherry and EGFP confirmed the correct activation of the vectors in this type of cells (Figure 15c).
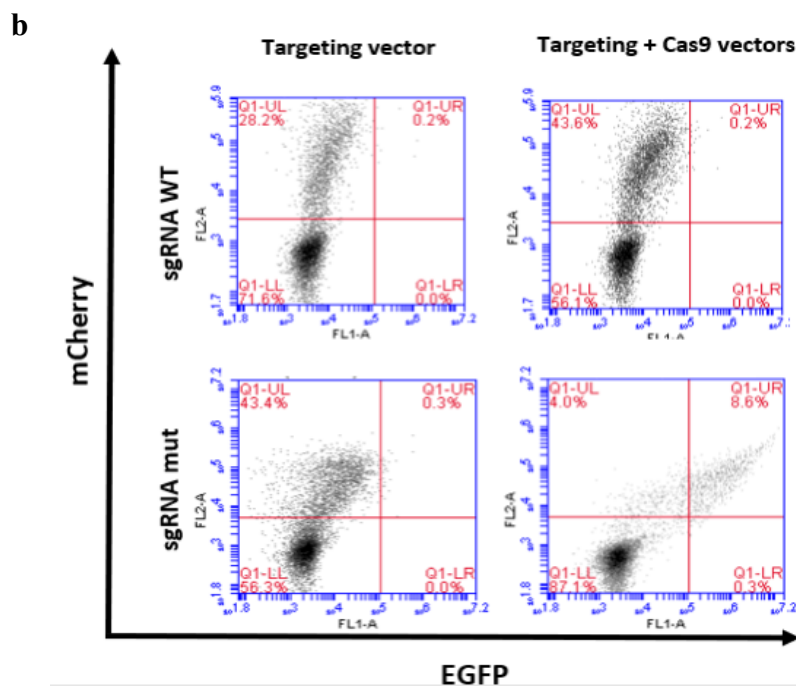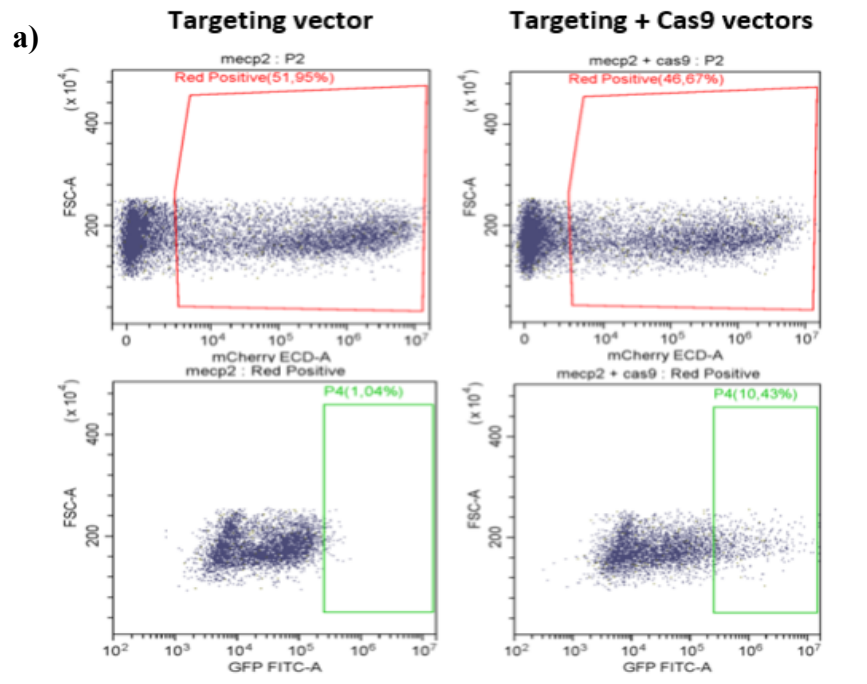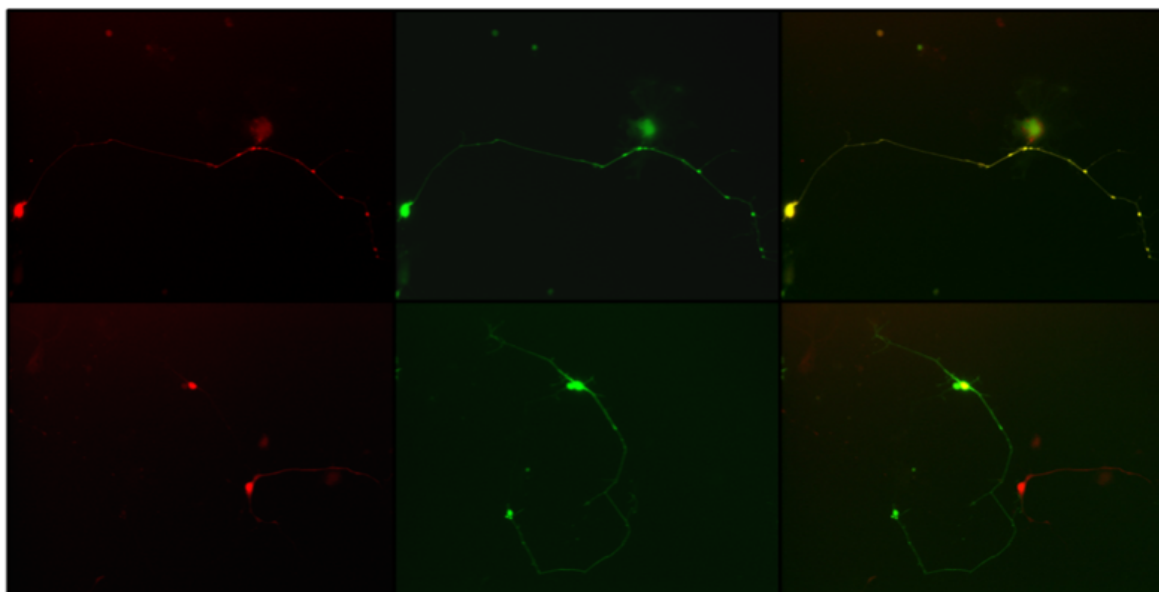
c)

Figure 15. sgRNA specificity and plasmid functionality in HEK293 cells and *MECP2* neurons. a) Representative FACS analysis on HEK293 cells 48 hours after transfection with constructs for the c.473C>T p.(Thr158Met)) *MECP2* variant. Cells were transfected with the Targeting vector alone or in combination with Cas9 vector and fluorescence was quantified. Transfection with the targeting plasmid alone results in 51.95% of mCherry$^+$ cells and no EGFP$^+$ cells. As expected, following co-transfection 10.43% of mCherry$^+$ cells were also EGFP$^+$, confirming the functionality of the system. **b)** Specificity of the mutation-specific sgRNA was demonstrated by transfecting HEK293 cells with the reporter plasmid expressing the wild type or mutated sequence between mCherry and EGFP. The mCherry$^+$/GFP$^+$ population is gated in the UR quadrant. The double fluorescence (8,6%) expressed by cells co-transfected with targeting vector comprising the mutation-specific sgRNA and Cas9 plasmid, but not by those transfected with the vector harbouring the WT sequence, demonstrates the specificity of the selected sgRNA. **c)** *In vivo* fluorescence microscopy images of mutated iPSC-derived neurons 5 days after transfection showing double mCherry and EGFP expression. Images are 20X magnification.

4.2.2 Gene correction in patient's cells

To establish the efficiency of the correction plasmids in patient-derived cells, we transfected fibroblasts obtained from 4 independent RTT patients harbouring the c.473C>T (p.(Thr158Met)) variant and quantified fluorescence 48 hours post-transfection by FACS analysis. In line with results in HEK293, fibroblast cells transfected with Targeting plasmid alone expressed mCherry but not EGFP. Results from replicate experiments (n=3) in which cells were co-transfected with Targeting and spCas9 plasmids showed a consistent cell population which expressed mCherry (~23%), with a ~33% of these cells expressing also EGFP. This result indicates proper plasmids activation in patient's cells. Co-transfected mCherry$^+$/EGFP$^+$ fibroblasts were recovered by cell sorting 48 hours later and analysed using Next Generation Sequencing (NGS) (Figure 16a). NGS data were uploaded to the Cas-Analyzer tool to assess HDR frequency. This analysis demonstrated the efficiency of the

correction plasmids, in particular we obtained 64.2% of edited alleles for case 1 (#2204), 50% of edited alleles for case 2 (#304), 83.6% of edited alleles for case 3 (#2271) and 20.4% of edited alleles for case 4 (#2239) (Table 8).

Case	Patient code	Mutation	Sample	Total reads	HDR efficiency	Ins/dels frequency	C (WT)	T (M)
1	2204	c.473C>T (p.(Thr158Met))	Fibroblasts	22165	64,2 %	0.1%	83% (18284)	17% (3857)
2	304	c.473C>T (p.(Thr158Met))	Fibroblasts	2689	50%	0,2%	68,3% (1833)	31,5% (842)
3	2271	c.473C>T (p.(Thr158Met))	Fibroblasts	104	83.6%	0%	98% (102)	2% (2)
3	2271	c.473C>T (p.(Thr158Met))	iPS-derived Neurons	2935	14%	0%	56% (1643)	44% (1292)
4	2239	c.473C>T (p.(Thr158Met))	Fibroblasts	1873	20.4%	0,5%	59,8% (1120)	39,7% (744)

Table 8. Editing efficiency in patients' cells.

For case 3 (#2271), *MECP2*-mutated neurons differentiated from iPSCs were also analysed. Co-transfected mCherry⁺/EGFP⁺ neurons were recovered by cell sorting 6 days after transfection and analysed using NGS (Figure 16b). Data analysis in neurons demonstrated that 14% of mutated alleles has been correctly reverted to the wild type sequence (Table 7). Editing experiments in fibroblasts and neurons demonstrated a negligible rate of indels generation. Manual analysis of sequencing reads with IGV for the inclusion of the silent nucleotide change on the PAM sequence (TGG to TAG) demonstrated it is presence in a high proportion of the corrected alleles (about 90%).

In the mouse model, the (p.(Thr158Met)) variant is associated with a ~70% reduction of the levels of Mecp2 protein [98]. We thus asked whether a similar reduction occurred also in human cells and whether it was corrected following gene editing. Western blot analysis was performed on whole protein extracts isolated from wild type fibroblasts, patient fibroblasts and co-transfected mCherry+/EGFP+edited fibroblasts. In patient cells we observed a decrease of MeCP2 protein levels (Figure 16c). Following editing, a statistically significant increase in the expression of MeCP2 was observed compared to native patient cells (Figure 16c).
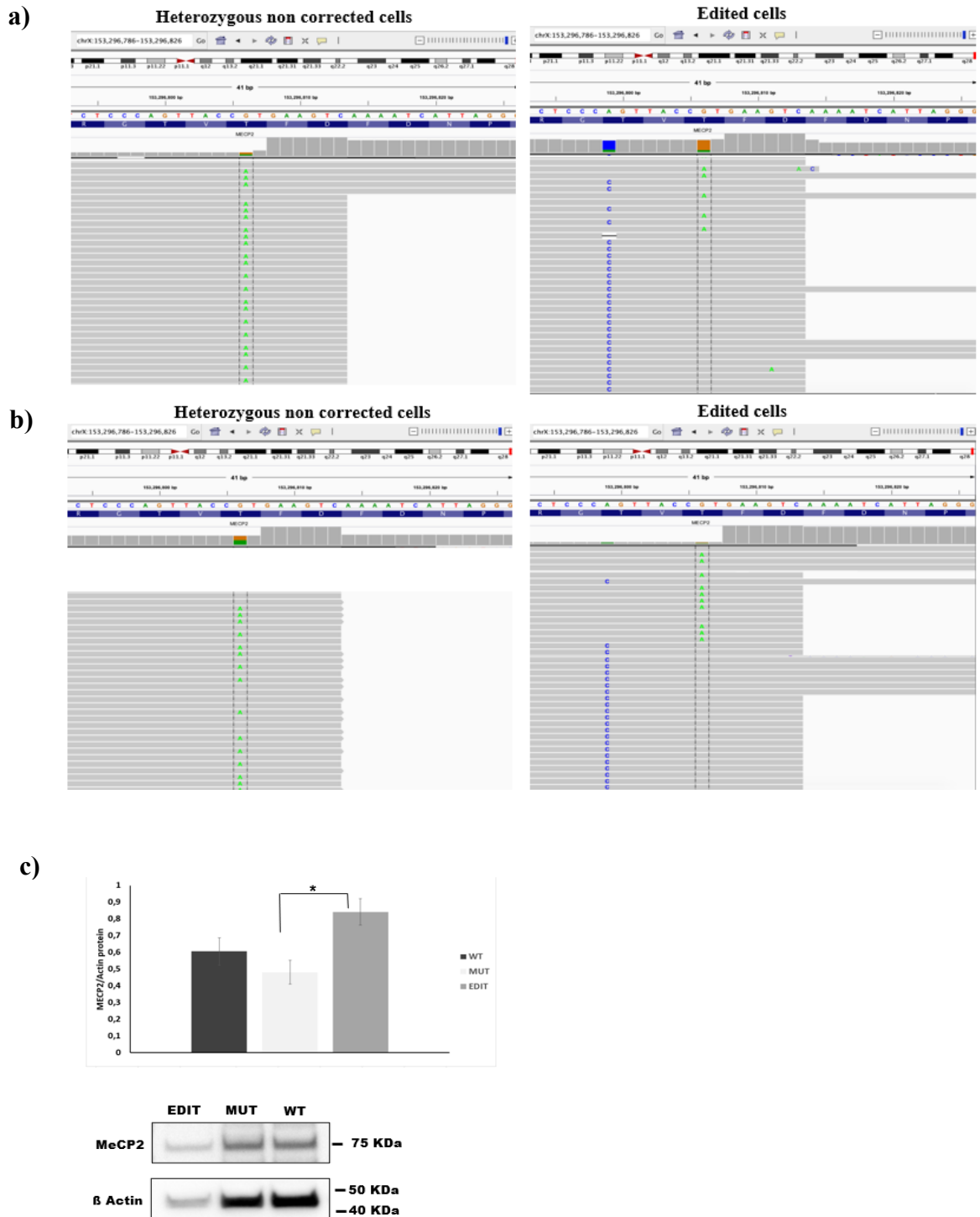
Figure 16. Efficient editing in *MECP2* mutated cells. a, b) Representative NGS results for edited fibroblasts from Case 1 (#2204) (**a**) and iPSC-derived neurons from Case 3 (#2271) **b)**. Sequencing results have been visualized by IGV (Integrative Genomic Viewer). The mutated nucleotide is placed between dashed lines. In edited cells, the silent A>C change removing the PAM 7 nucleotides upstream to the variant is present in edited alleles. **c)** MeCP2 protein levels were analysed by immunoblotting on extracts obtained from wild type, mutated and edited fibroblasts. Protein levels were quantified with Photoshop 2020 software MeCP2 levels significantly increase in edited samples compared to mutated not-edited cells. Values on the y axis are the averages of percentage of proteins relative to WT normalized to b-Actin expression. n=2. Statistical significance was determined using unpaired Student's t-test (*p<0.05: edited sample vs mutated sample).

4.2.3 TP53 polymorphism characterization

It is well known that the activation of the DNA repair machinery following Cas9-induced double-strand breaks involves tumor protein 53 (TP53) activation and that TP53 inhibition increases the rate of homologous recombination [165]. The functional TP53 polymorphism c.215C>G (p.(Pro72Arg)) at amino acid position 72 is known [166]. We reasoned that editing efficiency might be influenced by this TP53 polymorphism. The genotype analysis of our patients at this locus revealed homozygosity for the Arg72 allele in 3 patients (Table 9). The fourth patient, displaying the lower editing efficiency, resulted homozygous for the Pro72 allele.

Case	Patient code	Pro72Arg genotype
1	2204	Arg/Arg
2	304	Arg/Arg
3	2271	Arg/Arg
4	2239	Pro/Pro

Table 9. TP53 polymorphism characterization in MECP2 mutated patients.

4.3 Results Section 3
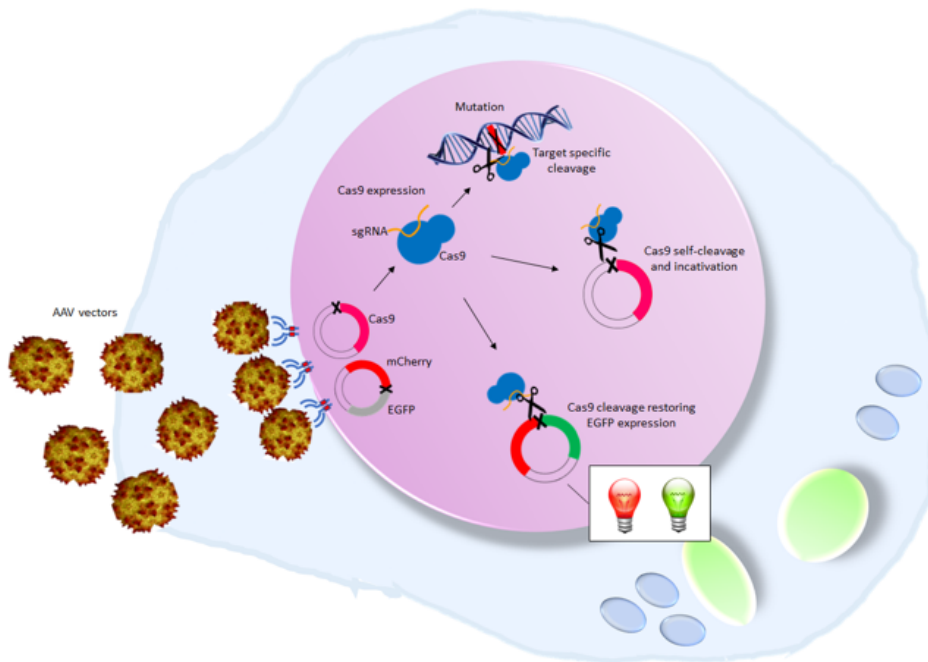
AAV-mediated FOXG1 gene editing in human Rett primary cells

4.3.1 Strategy for gene correction and plasmid design

In order to deliver SpCas9 together with its sgRNA and a donor DNA to mutated cells exploiting AAV vectors, we designed a dual plasmid correction system to overcome the size limits of the AAV genome [167]. The system is thus based on an SpCas9 expressing vector to be delivered in combination with a targeting vector (Fig. 17a).
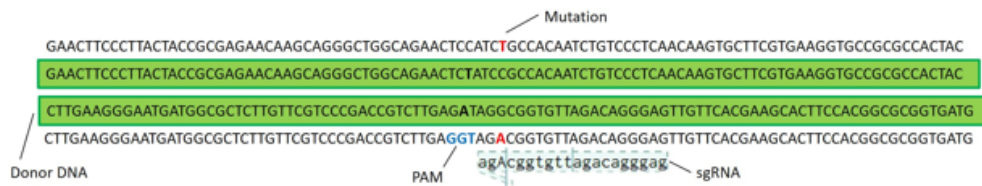
The targeting plasmid contains a cassette expressing a variant-specific sgRNA to direct Cas9 selectively to the mutated allele and a 100bp donor DNA centered on the variant that should act as template for Homology-Directed Repair (HDR) to restore the wild type sequence. In order to avoid targeting of the donor sequence by SpCas9 we have disrupted the Palindromic Adjacent Motif (PAM) in the donor with a silent nucleotide substitution (TGG to TAG) (Fig. 17b). We tested the system for the following two *FOXG1* variants: c.688C>T and c.765G>A. The targeting plasmid also includes a fluorescent reporter system to monitor both transduction/transfection efficiency and SpCas9 activity (Fig. 17a). The reporter is based on an mCherry/EGFP cassette were mCherry is constitutively expressed, while EGFP expression is prevented by the insertion of a sequence which keeps the EGFP out of frame and which contains a variant-specific target sequence for Cas9 (sgRNA + PAM). Indels generated by SpCas9 cleavage on this site can lead to frameshifts that restore EGFP expression (Fig. 17a, c). To limit the temporal window of SpCas9 expression, a target sequence represented by the variant-specific sgRNA plus a PAM sequence was inserted between the promoter and the CDS of the nuclease (Fig. 17c).

a)

b)

FOXG1 mutation: c.688C>T - p. Arg230Cys

```
Mutation
GAACTTCCCTTACTACCGCGAGAACAAGCAGGGCTGGCAGAACTCCATCTGCCCACAATCTGTCCCTCAACAAGTGCTTCGTGAAGGTGCCGCGCCACTAC
GAACTTCCCTTACTACCGCGAGAACAAGCAGGGCTGGCAGAACTCTATCCGCCACAATCTGTCCCTCAACAAGTGCTTCGTGAAGGTGCCGCGCCACTAC
CTTGAAGGGAATGATGGCGCTCTTGTTCGTCCCGACCGTCTTGAGATAGGCGGTGTTAGACAGGGAGTTGTTCACGAAGCACTTCCACGGCGCGGTGATG
CTTGAAGGGAATGATGGCGCTCTTGTTCGTCCCGACCGTCTTGAGGTAGACGGTGTTAGACAGGGAGTTGTTCACGAAGCACTTCCACGGCGCGGTGATG
```
Donor DNA   PAM   agAcggtgttagacagggag ← sgRNA

FOXG1 mutation: c.765G>A - p. Trp255*

sgRNA → caagggcaactactgAatgc   PAM
```
TCGTGAAGGTGCCGCGCCACTACGACGACCCGGGCAAGGGCAACTACTGAAATGCTGGACCCGTCGAGCGACGACGTGTTCATCGGCGGCACCACGGGCAA
TCGTGAAGGTGCCGCGCCACTACGACGACCCGGGCAAGGGCAACTACTGGATGCTAGGCCCGTCGAGCGACGACGTGTTCATCGGCGGCACCACGGGCAA
AGCACTTCCACGGCGCGGTGATGCTGCTGGGCCCGTTCCCGTTGATGACCTACGATCTGGGCAGCTCGCTGCTGCACAAGTAGCCGCCGTGGTGCCCGTT
AGCACTTCCACGGCGCGGTGATGCTGCTGGGCCCGTTCCCGTTGATGACTTACGACCTGGGCAGCTCGCTGCTGCACAAGTAGCCGCCGTGGTGCCCGTT
```
Donor DNA   Mutation

c)

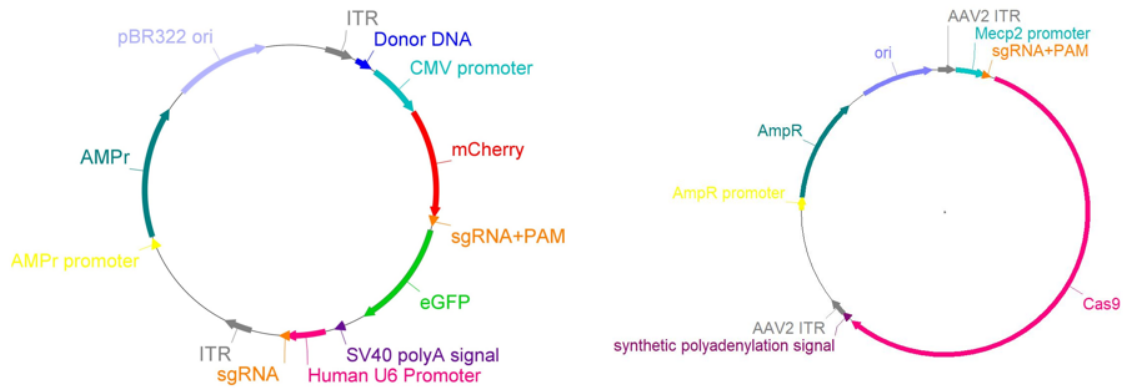**Figure 17: Plasmid strategy and design. a)** System functioning. Cells are infected with correction AAVs and constructs are expressed inside the cells. The targeting plasmid encodes three elements: the mutation-specific sgRNA leading Cas9 towards the target mutated site; the donor DNA used as template for Homology Directed Repair to restore the wild type sequence; the reporter system composed by mCherry and EGFP fluorescent proteins used to confirm of plasmids expression inside the cell. Since mCherry is constitutively expressed, cells transfected with the targeting plasmid will be mCherry[+], irrespective of Cas9 expression When cells are exposed to both targeting and Cas9 plasmids, Cas9 is expressed and it cleaves the target sequence between mCherry and EGFP. This allows EGFP expression, resulting in mCherry[+]/EGFP^{+} cells. One self-cleaving site allows for regulation of Cas9 expression. **b)** sgRNA and donor DNA design. The diagram shows for each mutation the selected sgRNA and donor DNA aligned to the mutated *FOXG1* sequence. The mutated nucleotide is marked in red and the PAM sequence in blue. The silent nucleotide substitution inserted to abolish the PAM is reported in bold in the donor sequence. **c)** Overview of plasmids structure. The general structure of the targeting plasmid (left), for the delivery of the sgRNA and HDR donor template, and the Cas9 plasmid (right) are illustrated. AMPr = Ampicillin resistance gene; pBR322ori = bacterial replication origin; ITR = Inverted Terminal Repeats.

Western blot analysis on whole protein extracts isolated from fibroblasts co-transfected with the targeting plasmid and a Cas9 plasmid encoding either the auto-cleaving Cas9 or a non-autocleaving variant (i.e. Cas9 in which the auto-cleaving site was not included), indicate that the presence of the auto-cleaving site indeed limits SpCas9 expression (Fig. 18).
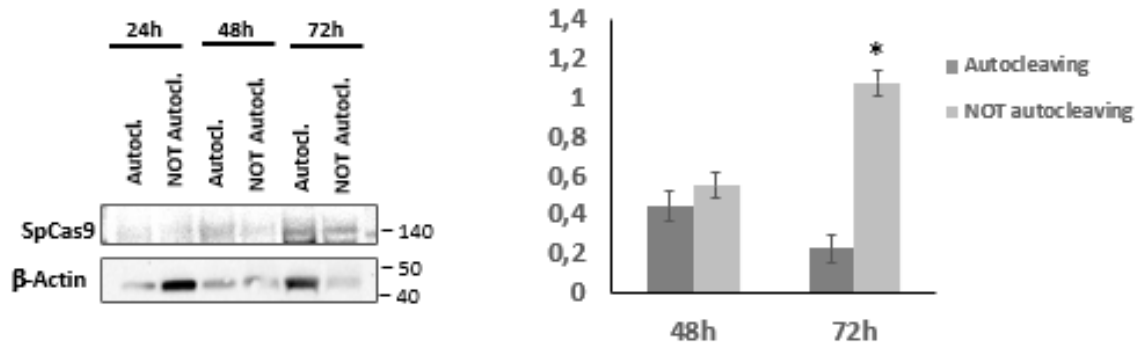

Figure 18: SpCas9 protein levels in the presence or absence of an auto-cleaving site. Protein levels of SpCas9 were analysed by immunoblotting in extracts obtained from fibroblasts cultures 24,48 or 72 hours after transfection with either the autocleaving Cas9 plasmid or the non-autocleaving variant. Detectable SpCas9 levels were present starting from 48 hours. Values on the y axis are the averages of signal intensity expressed in arbitrary units normalized to b-Actin expression. n=2. Statistical significance was determined using unpaired student's t test (*p<0.05).

4.3.2 Fibroblasts and iPSC-derived neurons transfection efficiency

The specificity of the sgRNAs was tested by transient transfection in HEK293 cells (Fig. 19a). To this aim, we designed modified targeting plasmids in which the target sequence between mCherry and EGFP contained the WT nucleotide instead than the c.765G>A or the c.688C>T variants. As expected, cells transfected with targeting plasmids harbouring the wild-type sequences inside the reporter system remained EGFP negative since the variant-specific sgRNA did not allow this sequence to be cut by Cas9. Cells transfected with the targeting plasmids containing the mutant target sequence between mCherry and EGFP showed a marked increase in EGFP fluorescence, indicating the activation of Cas9 (Figure 19a). The presence of an mCherry+/EGFP+population around 50% after co-transfection in fibroblasts proves that our strategy can be successfully applied to patient-derived primary cells (Fig. 19b, c). Additionally, we achieved 3.7+ 1.9% EGFP positivity after co-transfection of iPSC-derived neurons (n=3), supporting the feasibility of transfection in a disease-relevant neural cellular model (Fig. 19d).
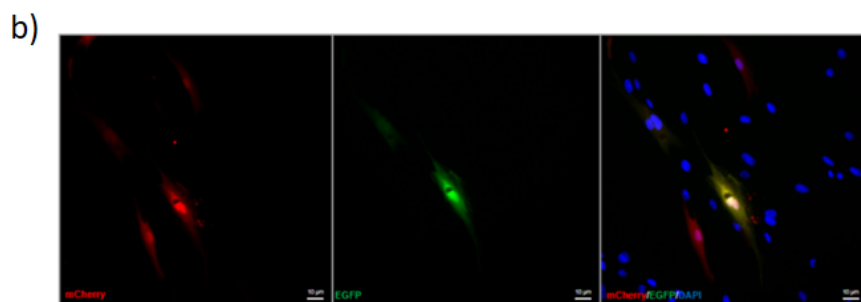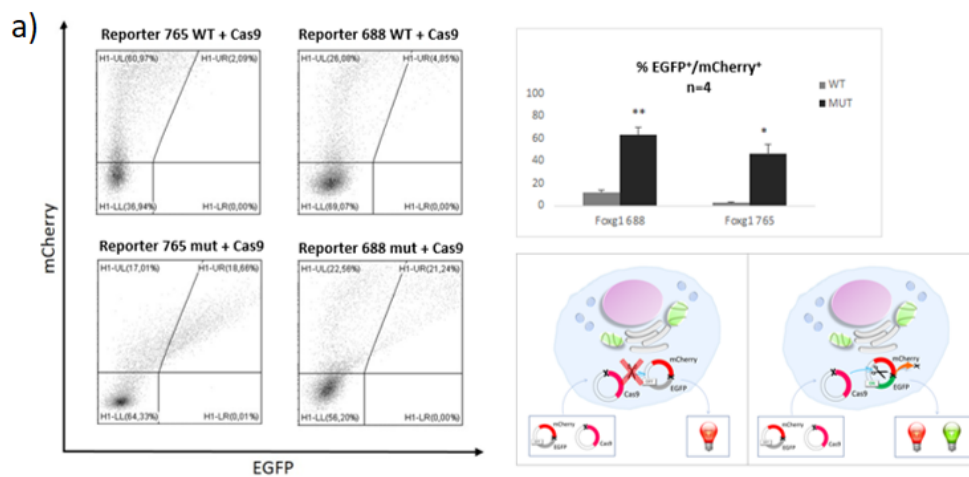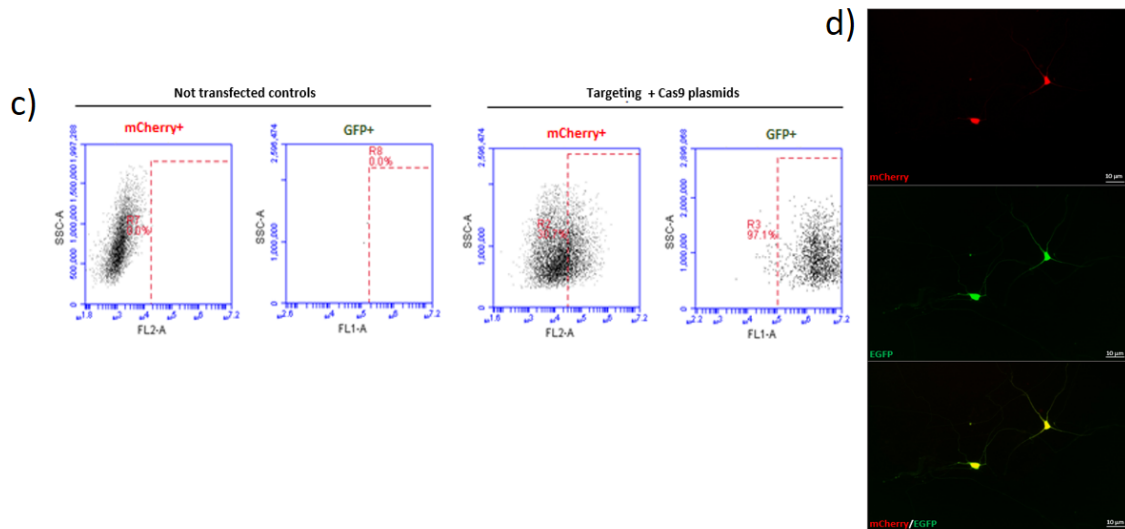
Figure 19: Transfection experiments. a) Plasmids functionality and sgRNA specificity. Representative results of FACS analysis on HEK293 cells 48 h after transfection with Cas9 plasmid and mCherry/EGFP targeting plasmid in which the target sequence between mCherry and EGFP harbours either the mutation-specific (lower panel) or the wild type sequence (upper panel), for c.765G>A and c.688 C>T pathogenic variants, respectively. The population of mCherry$^+$/EGFP$^+$ cells is gated in the UR quadrant. Significant double mCherry/EGFP fluorescence is present only in the cells co-transfected with the targeting plasmid with the specific mutation and the Cas9 plasmid (18,66 % and 21,24 % for c.765G>A and c.688 C>T, respectively demonstrating the specificity of the sgRNA. The presence of an mCherry+/EGFP+ population on the plots of cells transfected with the targeting plasmids harboring the Wild type target sequence between mCherry and EGFP is due to a residual aspecific activity of Cas9. The percentage of double positive population showed on histogram, confirms the sgRNA specificity only for the mutation-specific sequence. Statistical significance was determined using unpaired Student's t-test (*p<0,05, **p<0,005). A cartoon illustrating the approach is presented on the right. **b-c**) Plasmids activation in fibroblasts. Fibroblasts harboring the c.688 C>T mutation were analysed by *in vivo* fluorescence microscopy 48 h after co-transfection showing the presence of double mCherry$^+$/EGFP$^+$ cells (b), also confirmed by FACS quantitation **c)** A percentage of 50,7% of cells transfected with targeting and Cas9 plasmids in combination is mCherry$^+$; 97,1% of mCherry$^+$ cells are also EGFP$^+$. Globally, 48,75% of cells are double mCherry$^+$/EGFP$^+$. Untransfected fibroblasts, used as negative control, are shown on the left. The y axis shows SSC (side scatter), and the x axis shows fluorescence intensity (FL2-A = mCherry; FL1-A = GFP). The dashed rectangle represents the gating for positive cells. The percentage of positive cells is indicated inside the graphs. **d)** *In vivo* fluorescence imaging of iPSC-derived neurons. *In vivo* fluorescence microscopy images of iPSC-derived neurons from the patient harbouring the c.688 C>T mutation 6 days after transfection showing double mCherry (upper panel) and EGFP (lower panel) expression. Images are 20x (b) and 40X (d) magnification.

4.3.3 Gene editing efficiency

In order to demonstrate that the CRISPR/Cas9 system is able to effectively correct *FOXG1* variants in patient-derived cells, co-transfected mCherry[+]/EGFP[+] fibroblasts from both patients were isolated and analysed by deep sequencing (n=2 for each patient). NGS in native cells showed that the reads harbouring the wild type allele and those harbouring the mutant allele were approximately the same, as expected in heterozygous samples. In transfected cells, the percentage of reads harboring the wild type allele increased indicating that correction occurred (Fig. 20a, b). HDR efficiency was assessed by Cas-Analyzer [168] using NGS data, taking into account a region of 100 nucleotides around the cut site. Correct editing count by Cas-Analyzer assessed HDR efficiency over 20% for both patients (21.0 ±1.8 % and 23.6±2.4 % for case 1 and case 2 respectively) with 50% indels for case 1 and 20% for case 2. In order to test correction efficiency in a disease-relevant cellular model, we co-transfected iPSC-derived neurons harbouring the c.688C>T variant. NGS/Cas-Analyzer analysis of mCherry[+]/EGFP^{+} neurons demonstrated a high efficiency of editing, with ~ 34% of mutated alleles reverted to WT sequence and 38% indels (Fig. 20c).
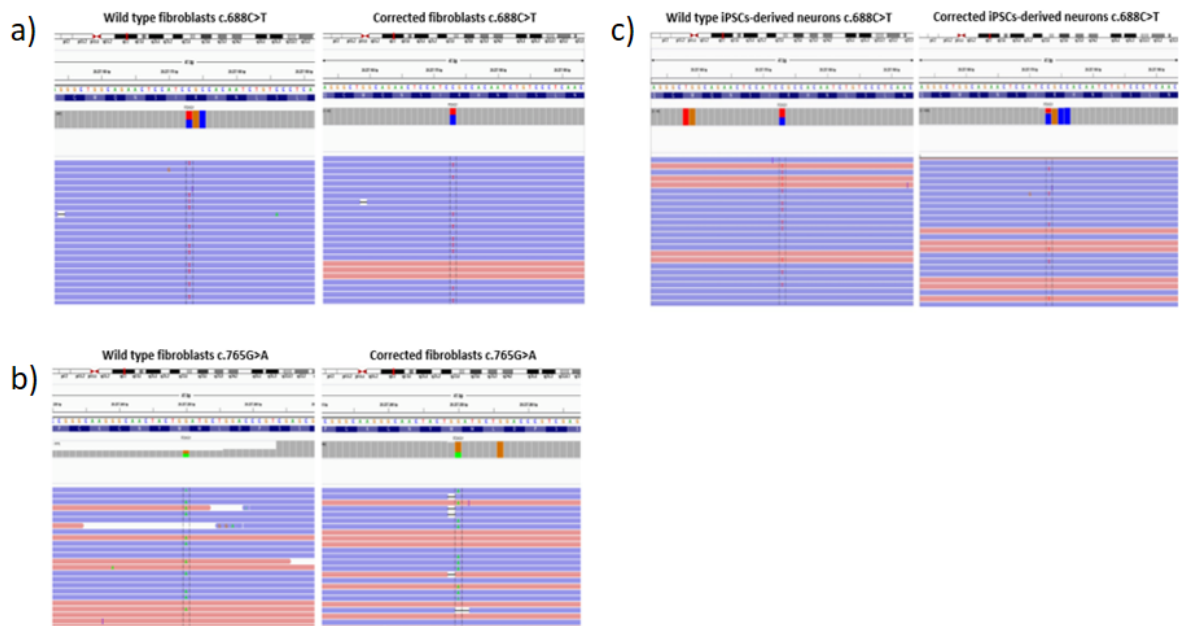
Figure 20: Sequencing analysis in edited patient-derived cells. a-c) IGV visualization of NGS results in edited patient fibroblasts. Next-generation sequencing results for fibroblasts harboring the c.688C>T and c.765G>A variants visualized with IGV tool is shown. The reference sequence is represented by colored letters, with the standard color code: adenine in green, cytosine in blue, guanine in yellow, and thymine in red. Right below, the coverage track displays reads depth for each nucleotide as a gray bar chart. Where a nucleotide differs from the reference sequence, the bar is colored accordingly, in proportion to the read count for each base. Each horizontal row (or track) represents one read, red for positive rightward (5' to 3') DNA strand, blue for negative leftward (reverse-complement) DNA strand. The regions encompassing the c.688 C>T and c.765G>A variants are shown for native (left panel) and edited cells (right panel). The mutated nucleotide is reported between dashed lanes. The percentage of reads harboring the wild type allele, measured as the percentage ratio between the read count of base C and the total number of reads, increases from 54% to 82% for the c.688C>T variant and from 51% to 65% for the c.765G>A variant. **c**) IGV visualization show efficient editing in iPSC-derived neurons harboring the c.688 C>T mutation with 34% mutated alleles reverted to WT sequence and 38% indels.

4.3.4 Off-target analysis

To evaluate the specificity of the correction plasmids, off-target analysis was performed by Guide-seq in HEK293 cells harboring the variants. This analysis pointed out 13 off-target sites for the c.688C>T variant and 6 off-target sites for the c.765G>A variant, all located in intronic or intergenic regions (Table 10 and 11). To exclude an effect on gene expression, mRNA levels of genes interested by intronic off-targets were measured. Gene expression in mutant HEK293 cells transfected with the correction plasmids was analyzed and compared to gene expression in untreated cells using qRT-PCR. No statistically significant difference was observed (Fig. 21).

Chromosome	Gene	Function	Reads
6	Intergenic		1179
14	FOXG1	Mutant allele (c.688C>T)	586
20	BFSP1 (intronic region)	Encodes the protein Filensin in humans	309
14	FOXG1	Wild type allele	187
14	CEP128 (intronic region)	Encodes Centrosomal Protein 128	165
16	Intergenic		99
1	Intergenic		62
1	DPYD (intronic region)	Antisense RNA 1 (Non-Protein Coding)	49
20	E2F1 (intronic region)	Encodes the Transcription Factor E2F1 playing an important role in the control of cell cycle	44
9	SARDH (intronic region)	Encodes the mitochondrial enzyme Sarcosine Dehydrogenase that catalyzes the oxidative demethylation of sarcosine	31
12	BICD1 (intronic region)	Encodes the protein Bicaudal Homolog 1 implicated in COPI-independent membrane transport from the Golgi apparatus to the endoplasmic reticulum	27
11	Intergenic		21
8	Intergenic		16
12	CCDC91 (intronic region)	Encodes the Coiled-coil Domain-containing protein 91 involved in the regulation of membrane traffic through the trans-Golgi network (TGN)	11

Table 10. Guide-seq results in HEK 293 cells harboring c.688C>T mutation.

Chromosome	Gene	Function	Reads
10	TLL2 (intronic region)	Encodes Astacin-like zinc-dependent Metalloprotease	506
14	FOXG1	Mutant allele (c.765G>A)	186
3	ADAMTS9-AS2 (intronic region)	Non coding RNA	97
14	FOXG1	Wild type allele	92
1	Intergenic		57
10	SYT15 (intronic region)	Encodes a member of the Synaptotagmin (Syt) family of membrane trafficking proteins	47
X	SATL1 (intronic region)	Encodes Spermidine/spermine N1-acetyl transferase-like 1	14

Table 11. Guide-seq results in HEK 293 cells harboring c.765G>A mutation.
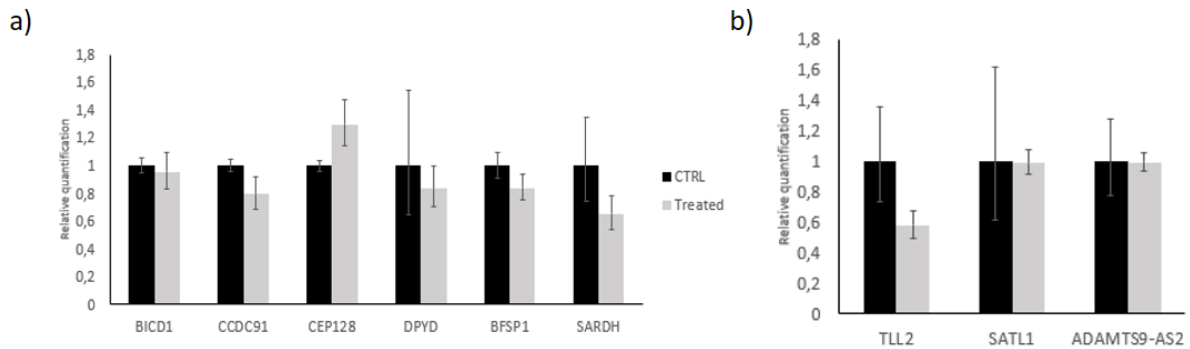
Figure 21. Expression analysis of potential off-targets. mRNA levels for genes corresponding to intronic off-targets were evaluated by real time qRT-PCR. Expression levels in untreated cells and cells transfected with correction constructs for the c.688C>T **(a)** or the c.765G>A **(b)** variants were compared. E2F1 and SYT15 were not analysed since they are not expressed in HEK293 cells. Values in the y axis represent 2exp (-ddCt). Data are presented as mean $\pm$ SD. No statistically significant differences were observed.

4.3.5 PAX6 expression analysis

It has been demonstrated that PAX6 protein levels are increased in patient-derived neuronal progenitor cells harbouring *FOXG1* mutations [29]. We thus tested if a similar alteration was also observed in the c.688 C>T (p.(Arg230Cys)) variant and if it was possible to restore the normal protein levels with gene editing by using our correction plasmids. Western blot and qRT-PCR analyses were performed on whole protein extracts and total RNA, respectively, isolated from wild type, mutated, and transfected mCherry+/EGFP+ edited neuronal precursors. In the mutated cells we observed an increase of PAX6 mRNA and protein levels compared with WT cells. Following editing, a statistically significant decrease in the expression of *PAX6* was observed with normalization to WT levels (Figure 22a,b).
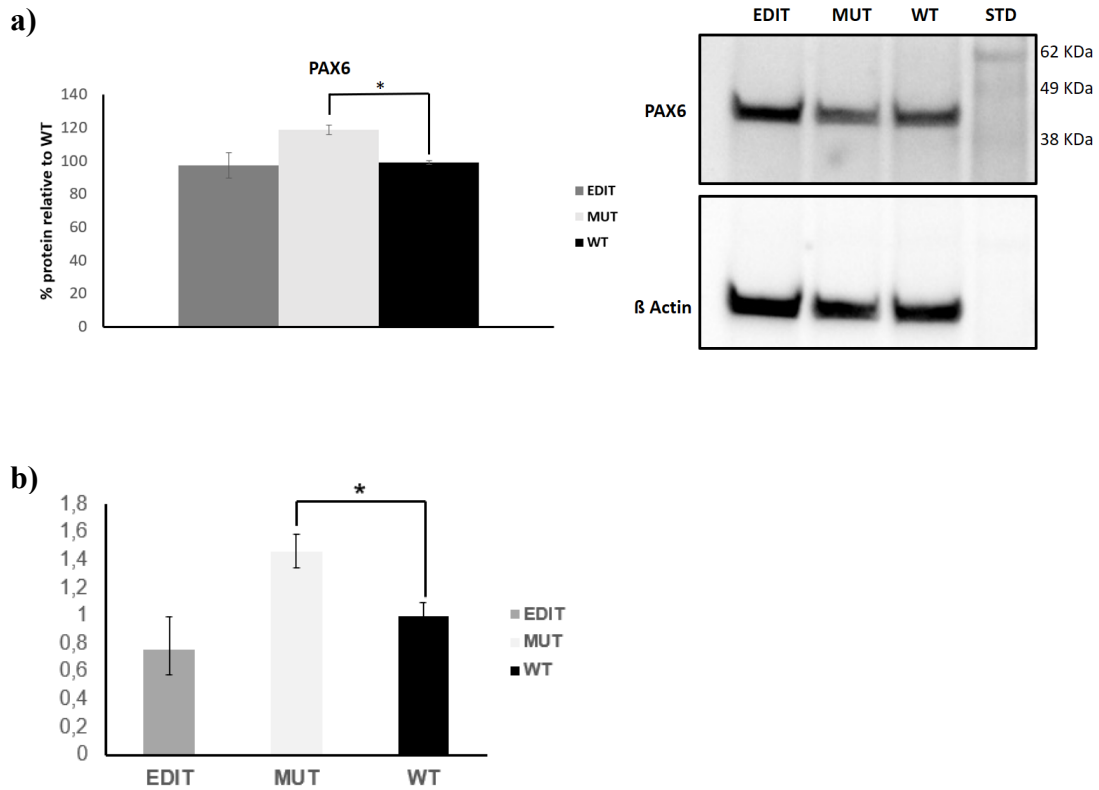
Figure 22. PAX6 analysis. a) PAX6 protein expression. PAX6 protein levels were analysed by immunoblotting on extracts obtained from wild type, mutated and edited neuronal precursors. Protein levels were quantified with ImageJ. PAX6 levels significantly increase in mutated samples compared to WT and edited cells. Values on the y axis are the averages of percentage of proteins relative to WT normalized to b-Actin expression. n=3. **b)** PAX6 mRNA levels. PAX6 mRNA levels were evaluated by qRT-PCR. Data are presented as mean ± SD. The analysis confirmed an increase of PAX6 expression in mutated cells and a normalization in edited ones. Statistical significance was determined using unpaired Student's t-test (*p < 0.05).

4.3.6 AAV2 vs AAV9: serotype-cell type correlation

We evaluated the most effective serotype for each cell type by testing AAV2 and AAV9 control viruses, encoding EGFP, in fibroblasts, iPSCs and iPSC-derived neurons (Fig. 23). Serotypes 2 and 9 were selected since they have been proven efficient in both mitotic and postmitotic cells [123; 168].

FACS analysis 48 hours after infection demonstrated that AAV2 is more efficient for iPSCs, with approximately 25% of EGFP$^+$ cells compared to 7% with AAV9. On the contrary, about 15% fibroblasts and neurons were EGFP$^+$ following AAV9 infection while AAV2 yielded less than 10% EGFP$^+$ cells.
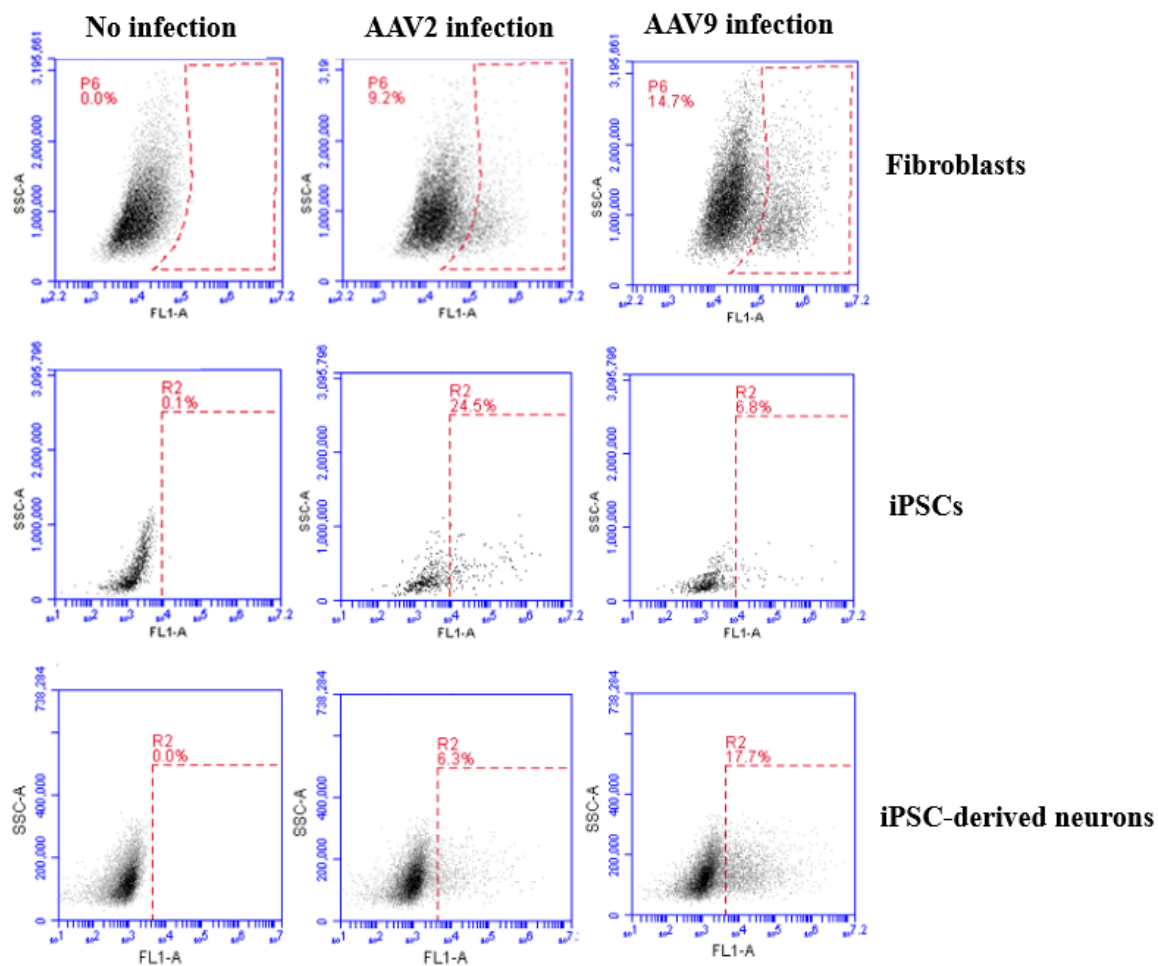
Figure 23: AAV serotype selection. FACS analysis of fibroblasts, iPSCs and iPSC-derived neurons harboring the c.688 C>T mutation after infection with EGFP-AAV2 or EGFP-AAV9 control viruses. The y axis shows SSC (side scatter), and the x axis shows fluorescence intensity. The dashed rectangle represents the gating for positive cells. The percentage of positive cells is indicated in the figure. AAV2 is more efficient for iPSCs, with 24,5% of EGFP$^+$ cells compared to 6,8% with AAV9. 14,7% of fibroblasts and 17,7% of neurons were EGFP$^+$ following AAV9 infection while AAV2 yielded only 9.2% and 6.3% EGFP$^+$ cells, respectively. No-infection controls are shown on the left.

4.3.7 iPSCs and iPSC-derived neurons infection efficiency

We succeeded in proving the significant potential of AAV co-infection as delivery strategy for the CRISPR/Cas9 gene editing constructs. Specifically, iPSCs harboring the variant were infected with AAV2 correction vectors and examined by fluorescence microscopy and FACS sorting. Double mCherry$^+$/EGFP$^+$ cells were observed starting from 24 hours post infection. Quantitation by FACS at 48 hours showed 12,57% mCherry positive cells, 49,12% of which was also EGFP positive (Fig. 24a). iPSC-derived neurons harboring the variant were infected with AAV9 correction vectors and analyzed by *in vivo* fluorescence microscopy. Results show that cells which express mCherry are also positive for EGFP, corroborating that these cells can be effectively co-infected (Fig. 24b).

c)
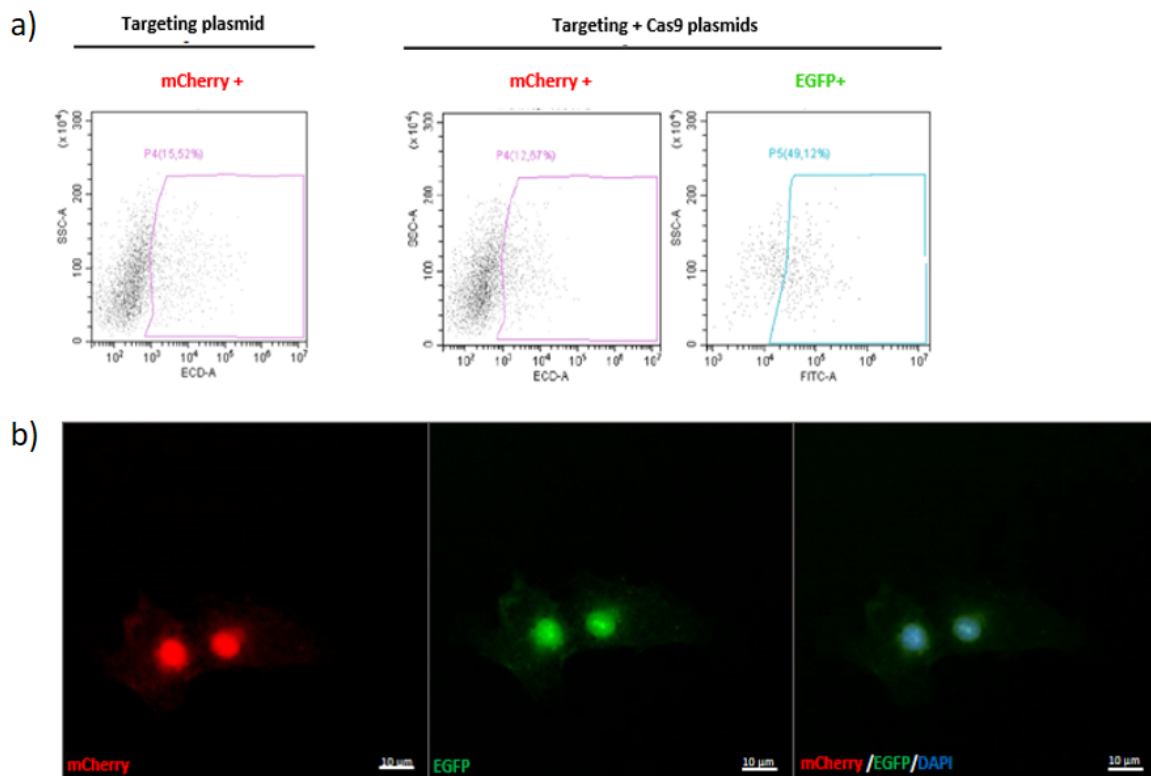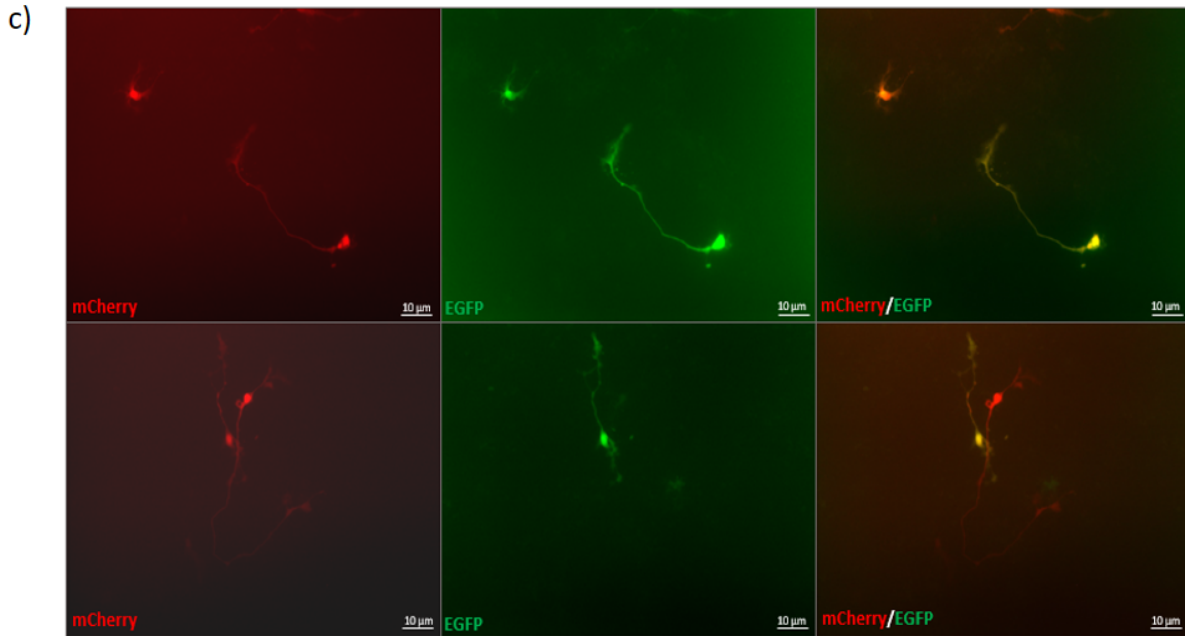
Figure 24: Infection in patient-derived cells. a,b) iPSCs infection. FACS quantitation (upper panel) and *in vivo* fluorescence imaging (lower panel) of infected iPSCs harboring c.688 C>T mutation 48 h post-infection are presented. The percentage of red and green fluorescent cells determined by FACS is indicated inside the graphs. A percentage of 12.67% of cells infected by targeting and Cas9 AAVs in combination is mCherry+; 49,12% of mCherry+ cells are also EGFP+. Globally, 6,22% of cells are mCherry+/EGFP+. **c)** Infection of iPSC-derived neurons. *In vivo* fluorescence imaging of infected iPSC-derived neurons harboring the c.688 C>T mutation 5-6 days post-infection showing co-expression of mCherry and EGFP. Images are 20x magnification.

5. Discussion and future perspectives

RTT is a rare incurable X-linked neurodevelopmental disorder that affects females. Mutations in *MECP2* gene represent 95% of RTT cases and lead to classic form of the disease. Another gene implicated in RTT is *FOXG1,* which leads to the congenital variant, one of the most severe forms of the disease.

An important model for the study of CNS disorders is represented by neurons differentiated from induced pluripotent stem cells (iPSCs) generated from patient cells. The improvement of *in vitro* differentiation protocols allows to obtain cell types, such as neurons, that can be used as a model for diseases and that would otherwise be difficult to obtain and investigate. Results obtained in our works are based on the use of iPSC-derived neurons and have allowed us to characterize alterations of molecular pathways involved in RTT. In particular, functional analysis on molecular pathways and electrophysiology data obtained in *MECP2* neurons have shown a dysregulation in the expression of different genes related to neuron development/differentiation, synaptic transmission, axonogenesis and dendrite development and demonstrated an alteration of GABAergic transmission. With these cells we have also proven the efficacy of drugs like HDAC6 inhibitors that act on the microtubule network. These results highlight an increase in α-tubulin levels which are lowered as a consequence of an over-expression of HDAC6 [29,170]. Results obtained showed that iPSC-derived neurons are an important cellular model for studying and understanding the complex molecular processes involved in RTT.

A few studies have shown that it is possible to apply CRISPR/Cas9-based gene editing in human primary cells, such as fibroblasts, and in iPSCs, including cells from patients with different genetic disorders [171-173]. Interestingly, Le and colleagues recently applied an similar approach that described in this manuscript for editing the *MECP2* locus in iPSCs, including the correction of another *MECP2* variant hotspot, c.808C>T (p.(Arg270*)). They obtained an editing efficiency of 20-30%, confirming that *MECP2* gene can be efficiently modified in different cell types [172]. Gene therapy using a gene replacement approach, as the one recently tested in patients affected by SMA [174], has been extensively tested in RTT mouse models causing, however, toxicity due to excessive Mecp2 expression [175-177]. Indeed, this approach relies on the insertion of an additive copy of the gene within the genome and it is thus effective when a tight regulation of the target gene is not needed, as in the case of enzymatic defects. A fine native regulation is essential for *FOXG1* and *MECP2* since both down- and up-regulation lead to brain impairment in humans and even small deviations from

the native expression of these genes can disrupt brain function, outlining the importance of setting up a therapeutic approach that maintains native gene expression. For these reasons, gene replacement may not represent the therapeutic approach of choice in RTT. CRISPR/Cas9-mediated gene editing has been chosen over gene replacement since it has the unique advantage of preserving native regulation. Although our variation-specific gene editing system clearly requires to be shaped on the targeted variant, since a specific sgRNA needs to be designed, it offers the major benefit of correcting the endogenous mutated allele thus maintaining its native regulation.

Our work showed that gene editing with CRISPR/Cas9 is an efficient tool for the precise correction of the most common *MECP2* hotspot variant, c.473C>T (p.(Thr158Met)) and for two missense variants c.688C>T; p.(Arg230Cys)), c.765G>A; p.(Trp255*)) in *FOXG1* gene in cells deriving from RTT patients, including iPSC-derived neurons. Sequencing results obtained in *MECP2* and *FOXG1* cells demonstrate that the number of wild type alleles switch from 50%, as expected for an heterozygous mutation, to 70-80 %, indicating that more than 60% of mutated alleles were correctly reverted to WT, with a limited number of ins/del. Specifically, editing results showed an high HDR levels with an efficiency ranging from 20 % to up 80% in fibroblasts and from 14% to 34% in iPSC-derived neurons.

To extend our results, we performed functional analysis to confirm that correction of the mutations results in correction of associated molecular defects. Brown and colleagues demonstrated that in T158M mouse models there is a ~70% reduction in the expression of Mecp2 protein levels compared with wild type mice [101]. Our analysis of MeCP2 expression in patient's cells suggests that protein expression is reduced also in patient fibroblasts, although to a lower extent, and that editing results in an increase in protein levels, confirming the correction of protein expression. Previous data indicate *PAX6* overexpression in *FOXG1* mutated neuronal precursors (NPCs) derived from patient iPSCs harbouring *FOXG1* mutations [29]. To assess the functional outcome of gene correction with our toolkit we thus analysed *PAX6* expression in mutated and edited NPCs and we confirmed the increase in *PAX6* expression in mutated cells and the normalization of protein levels in the edited ones. FOXG1 plays an important role in progenitor proliferation in the telencephalon through cell autonomous mechanisms including the regulation of *PAX6* expression. Pax6 downregulation in *Foxg1*$^{-/-}$ dorsal telencephalic cells in mice has been previously reported but this difference is likely due to the complex Pax6 regulation in the developing central nervous system [30].

The Blood Brain Barrier (BBB) represent one of the major obstacles for the treatment of neurological diseases and for the delivery of genetic cargos to CNS due to the presence of a

physical barrier composed by tight junctions between brain microvascular endothelial cells [177]. With the perspective of employment in clinical trials, we designed a toolkit based on Adeno-associated viral vectors (AAVs) that are promising tools for *in vivo* gene delivery [178,179]. Indeed, AAVs are immune-tolerated and some serotypes are capable of crossing the BBB, an essential feature for in vivo gene therapy of CNS disorders via intravenous injection [179,181]. However, the packaging of SpCas9, sgRNA, donor DNA template and reporter system in a single AAV vector was not feasible due to the limited packaging capacity of AAVs (4.7Kb) [182]. Several groups have previously packaged Cas9 and sgRNA into separate AAV vectors increasing overall packaging capacity [182, 183]. We thus designed an approach based on a correction system that employs two plasmids to be used in combination. In agreement with literature data, our results demonstrate that co-transfection and subsequent gene editing can be efficiently obtained, confirming the feasibility of the proposed strategy. Results from the phase I trial for SMA1 suggest that intravenous delivery of AAV9 particles might have relevant outcomes in patients with an improvement in motor skills [169,174]. However, it will be important to perform correction experiments in mouse models, in order to confirm that efficient correction can be obtained also *in vivo*. It will be also important to test different administration routes, including intrathecal or intracerebroventricular, to establish the more efficient way for CNS delivery; these routes, although more invasive, would have the advantage to inject the correction machinery directly into the CNS without immunity reaction or organ toxicity [185,186]. Finally, the need of 2 viral particles for the delivery of the correction machinery likely reduces the effectivity of our toolkit. To overcome this issue, modified AAV particles with increased infectivity for brain cells could be employed [187]. Alternatively, SaCas9, a shorter nuclease derived from Staphylococcus aureus, could be employed to allow packaging in a single AAV particle, provided a specific PAM is available close to the variant. This approach has recently been tested for Leber Congenital Amaurosis, in both cellular and animal models and a PhaseI/II trial is currently ongoing [188] (ClinicalTrials.gov Identifier: NCT03872479).

The application of CRISPR/Cas9 technology and HDR-mediated repair in the context of gene therapy represents an important innovation in the scientific field. Few studies have attempted to apply gene editing techniques to primary cells, mainly for their short lifespan and extreme sensitivity to treatment [172, 189, 190,191]. Moreover, HDR is active primarily during the S phase of cell cycle, limiting its application in post-mitotic cells [192,193]. However, recent works have demonstrated that HDR is effective also in non-dividing cells, such as terminally differentiated neurons, allowing its application to disorders affecting tissues with limited

regeneration/renewal capacity, including the CNS [122, 194]. In particular, Nishiyama and colleagues compared the editing efficiency in mammalian neurons using an approach based on either one or two AAV-based vectors for *in vivo* delivery to the brain [122]. They demonstrated that editing of neurons can be obtained in both cerebral cortex and organotypic hippocampal slice cultures with an efficiency of 6-15% and that the single and dual vector systems give comparable results. In line with these data, the results we obtained in iPSC-derived neurons demonstrate that accurate gene editing can be obtained in the primarily affected cells in RTT. The percentage of HDR we obtained in neurons is lower compared to fibroblasts from the same patient, but, interestingly, our results fit with what reported from Nishiyama and colleagues in mouse brain, suggesting that we might expect a similar editing efficiency also *in vivo* [122]. In the perspective of future clinical trials our editing results in patient-derived cells represent a proof of concept demonstrating that the application of HDR-CRISPR/Cas9 gene therapy is possible also in post-mitotic cells with encouraging results. Pre-clinical studies in the mouse models will help evaluate which extent the obtained correction efficiency allows correction of disease phenotype.

In spite of the presence of the same *MECP2* variant, editing efficiency in the four patients analysed is variable, ranging from 20% to more than 80%. Based on a recent publication demonstrating that TP53 can affect HDR efficiency [195], we hypothesized that the reported differences in HDR efficiency might be partly explained by TP53 genotype. TP53 maintains genome integrity and prevents cell cycle transition to the S phase in the presence of DNA damage [196]. Cell cycle affects HDR machinery, which is mainly activated in S/G2 phase [197]. Recent publications have shown that TP53 inhibition can increase HDR frequency and precise genome editing efficiency [165, 198,199]. It is known that c.215C>G polymorphism in TP53, resulting in a Proline-to-Arginine substitution at position 72, can influence TP53 stability and activity [166]. It is possible that this polymorphism could influence the final correction efficiency in patient cells. Our analysis has shown that the three patients with a higher editing efficiency are homozygous for the less stable Arg72 variant, while the patient having the lowest efficiency is homozygous for Pro72 variant. Although the number of patients is limited, these data suggest a possible correlation between TP53 polymorphism and correction efficiency. Further analyses in a larger cohort of patients will be essential to validate this hypothesis and assess the impact of TP53 functionality on therapeutic gene editing.

The importance of target selectivity is crucial when using gene editing approach, especially for therapeutic and clinical applications [200]. In order to reduce cellular toxicity and ensure specificity of CRISPR/Cas9 system we employed a Cas9 self-cleaving target with an sgRNA

recognition sequence for autocleavage. Thanks to the Cas9 self-inactivation, a reduced expression and avoid persistence of Cas9, potentially leading to off-target effects, was obtained. The negligible percentage of in/del obtained in *MECP2* cells indicates the safety of the approach. In *FOXG1* cells, the percentage of in/del is higher and for this reason we assessed Cas9 off-target activity in the 2 investigated variants. Consistent with the specificity of the design sgRNAs, a limited number of off target sites that were exclusively placed in either intergenic or intronic regions was found, which does not appear to impact on known regulatory elements. Although this phenomenon could be of biological relevance and pinpoints that the toolkit could be potentially improved, we consider it unlikely to be of clinical relevance.

The approach described in this thesis is currently being tested in the laboratory for other diseases, such as the Alport syndrome. For this disease, we performed editing analysis of two missense mutations localized in the *COL4A3* and *COL4A5* genes and also in this case results showed a high correction efficiency ranging from 44 to 58% with a low percentage of in/del [201].

Our gene editing-based therapeutic approach based on CRSPR/Cas9 technology and HDR system has been patented (Italian Priority application n. 102018000020230 of 12/19/2018 and PCT extension n. PCT/EP2019/085659 of 12/17/2019, patent pending).

Overall, our findings provide further evidence that HDR-mediated gene editing with CRISPR/Cas9 represents a promising therapeutic tool for targeting pathological variants in patients with Rett spectrum disorders for whom no effective therapeutic alternatives are available. In order to confirm these preliminary data, our data, 3D culture cells and RTT mouse models will be used. Both models closely mimic human brain development and represent a unique opportunity to study brain development at the molecular and functional levels, associated disorders and respective therapies outside the human body.

6. References

1) Chahrour, M., & Zoghbi, H. Y. (2007). The story of Rett syndrome: from clinic to neurobiology. *Neuron*, 56(3), 422-437.

2) Rett, A. (1966). On a unusual brain atrophy syndrome in hyperammonemia in childhood. *Wien Med Wochenschr* (1946), 116(37), 723.

3) Hagberg, B., Aicardi, J., Dias, K., & Ramos, O. (1983). A progressive syndrome of autism, dementia, ataxia, and loss of purposeful hand use in girls: Rett's syndrome: report of 35 cases. *Ann Neurol,* 14(4), 471-479.

4) Amir, R. E., Van den Veyver, I. B., Wan, M., Tran, C. Q., Francke, U., & Zoghbi, H. Y. (1999). Rett syndrome is caused by mutations in X-linked MECP2, encoding methyl-CpG-binding protein 2. *Nat Genet*, *23*(2), 185-188.

5) Weaving, L. S., Williamson, S. L., Bennetts, B., Davis, M., Ellaway, C. J., Leonard, H., ... & Christodoulou, J. (2003). Effects of MECP2 mutation type, location and X-inactivation in modulating Rett syndrome phenotype. *Am J Med Genet A*, *118*(2), 103-114.

6) Bao, X., Jiang, S., Song, F., Pan, H., Li, M., & Wu, X. R. (2008). X chromosome inactivation in Rett Syndrome and its correlations with MECP2 mutations and phenotype. *J Child Neurol*, *23*(1), 22-25.

7) Schanen, C. (2001). Rethinking the fate of males with mutations in the gene that causes Rett syndrome. *Brain Dev*, *23*, S144-S146.

8) Xiol, C., Vidal, S., Pascual-Alonso, A., Blasco, L., Brandi, N., Pacheco, P., ... & Armstrong, J. (2019). X chromosome inactivation does not necessarily determine the severity of the phenotype in Rett syndrome patients. *Sci Rep.*, *9*(1), 1-9.

9) Ip, J. P., Mellios, N., & Sur, M. (2018). Rett syndrome: insights into genetic, molecular and circuit mechanisms. *Nat Rev Neurosci*, *19*(6), 368-382.

10) Vashi, N., & Justice, M. J. (2019). Treating Rett syndrome: from mouse models to human therapies. *Mamm Genome*, *30*(5-6), 90-110

11) Hanefeld, F. (1985). The clinical pattern of the Rett syndrome. *Brain Dev*, *7*(3), 320-325

12) Rolando, S. (1985). Rett syndrome: report of eight cases. *Brain Dev*, *7*(3), 290-296.

13) Zappella, M. (1992). The Rett girls with preserved speech. *Brain Dev*, *14*(2), 98-101.

14) Hagberg, B. (1995). Rett syndrome: clinical peculiarities and biological mysteries. *Acta Paediatr*, *84*(9), 971-976.

15) Zappella, M. (1997). The preserved speech variant of the Rett complex: a report of 8 cases. *Eur Child Adolesc Psychiatry*. 6 Suppl 1:23-5.

16) Bahi-Buisson, N. (2013). Genetically determined encephalopathy: Rett syndrome. *Handb Clin Neurol*. 111:281-6. doi: 10.1016/B978-0-444-52891-9.00031-2.

17) Lagger, S., Connelly, J. C., Schweikert, G., Webb, S., Selfridge, J., Ramsahoye, B. H., ... & Walkinshaw, M. D. (2017). MeCP2 recognizes cytosine methylated tri-nucleotide and di-nucleotide sequences to tune transcription in the mammalian brain. *PLoS genetics*, *13*(5), e1006793.

18) Kyle, R. A., Larson, D. R., Therneau, T. M., Dispenzieri, A., Kumar, S., Cerhan, J. R., & Rajkumar, S. V. (2018). Long-term follow-up of monoclonal gammopathy of undetermined significance. *N Engl J Med*, *378*(3), 241-249.

19) Young, J. I., Hong, E. P., Castle, J. C., Crespo-Barreto, J., Bowman, A. B., Rose, M. F., ... & Zoghbi, H. Y. (2005). Regulation of RNA splicing by the methylation-dependent transcriptional repressor methyl-CpG binding protein 2. *Proc Natl Acad Sci U S A .102*(49), 17551-17558.

20) Valli, E., Trazzi, S., Fuchs, C., Erriquez, D., Bartesaghi, R., Perini, G., & Ciani, E. (2012). CDKL5, a novel MYCN-repressed gene, blocks cell cycle and promotes differentiation of neuronal cells. *Biochim Biophys Acta*, 1819(11-12), 1173-1185.

21) Martynoga, B., Morrison, H., Price, D. J., & Mason, J. O. (2005). Foxg1 is required for specification of ventral telencephalon and region-specific regulation of dorsal telencephalic precursor proliferation and apoptosis. *Dev Biol*, *283*(1), 113-127.

22) Georgel PT, Georgel PT, Horowitz-Scherer RA, Adkins N, Woodcock CL, Wade PA, Hansen JC. (2003). Chromatin compaction by human MeCP2. Assembly of novel secondary chromatin structures in the absence of DNA methylation. *J Biol Chem*. 278(34):32181-8. PMID: 12788925

23) Cheng TL, Cheng TL , Wang Z, Liao Q, Zhu Y, Zhou WH, Xu W, Qiu Z. (2014). MeCP2 suppresses nuclear microRNA processing and dendritic growth by regulating the DGCR8/Drosha complex. *Dev Cell*. 28(5):547-560. PMID: 24636259

24) Zha AS, Li Z, Chen S, Liu F, Wang F. (2019). MeCP2 inhibits cell functionality through FoxO3a and autophagy in endothelial progenitor cells. *Aging (Albany NY)*. 11.17: 6714.PMID: 31477637

25) Sbardella D, Tundo GR, Campagnolo L, Valacchi G, Orlandi A, Curatolo P, *et al*. (2017). Retention of mitochondria in mature human red blood cells as the result of autophagy impairment in Rett syndrome. *Sci Rep*. 7.1: 1-12. PMID: 28951555

26) Ricciardi S, Boggio EM, Grosso S, Lonetti G, Forlani G, Stefanelli G, *et al*. (2011). Reduced AKT/mTOR signaling and protein synthesis dysregulation in a Rett syndrome animal model. *Hum Mol Genet*. 20.6: 1182-1196.PMID: 21212100

27) Boutouja, F., Stiehm, C. M., & Platta, H. W. (2019). mTOR: a cellular regulator interface in health and disease. *Cells*, *8*(1), 18.

28) Tsujimura, K., Irie, K., Nakashima, H., Egashira, Y., Fukao, Y., Fujiwara, M., ... & Yamashita, Y. (2015). miR-199a links MeCP2 with mTOR signaling and its dysregulation leads to Rett syndrome phenotypes. *Cell reports*, *12*(11), 1887-1901.

29) Patriarchi, T., Amabile, S., Frullanti, E., Landucci, E., Rizzo, C. L., Ariani, F., ... & Renieri, A. (2016). Imbalance of excitatory/inhibitory synaptic protein expression in iPSC-derived neurons from FOXG1+/− patients and in foxg1+/− mice. *Eur J Hum Genet*, *24*(6), 871-880.

30) Manuel, M. N., Martynoga, B., Molinek, M. D., Quinn, J. C., Kroemmer, C., Mason, J. O., & Price, D. J. (2011). The transcription factor Foxg1 regulates telencephalic progenitor proliferation cell autonomously, in part by controlling Pax6 expression levels. *Neural Dev*, *6*(1), 1-12.

31) Livide, G., Patriarchi, T., Amenduni, M., Amabile, S., Yasui, D., Calcagno, E., ... & Mari, F. (2015). GluD1 is a common altered player in neuronal differentiation from both MECP2-mutated and CDKL5-mutated iPS cells. *Eur J Hum Genet*, *23*(2), 195-201.

32) Motil, K. J., Caeg, E., Barrish, J. O., Geerts, S., Lane, J. B., Percy, A. K., ... & Neul, J. L. (2012). Gastrointestinal and nutritional problems occur frequently throughout life in girls and women with Rett syndrome. *J Pediatr Gastroenterol Nutr*, *55*(3), 292.

33) Sampson, T. R., & Mazmanian, S. K. (2015). Control of brain development, function, and behavior by the microbiome. *Cell Host Microbe*, *17*(5), 565-576.

34) Strati, F., Cavalieri, D., Albanese, D., De Felice, C., Donati, C., Hayek, J., ... & Rizzetto, L. (2016). Altered gut microbiota in Rett syndrome. *Microbiome*, *4*(1), 41.

35) Budden, S. S., & Gunness, M. E. (2003). Possible mechanisms of osteopenia in Rett syndrome: bone histomorphometric studies. *J Child Neurol*, *18*(10), 698-702.

36) Heilstedt, H. A., Shahbazian, M. D., & Lee, B. (2002). Infantile hypotonia as a presentation of Rett syndrome. *Am J Med Genet*, *111*(3), 238-242.

37) Jefferson, A. L., Woodhead, H. J., Fyfe, S., Briody, J., Bebbington, A., Strauss, B. J., ... & Leonard, H. (2011). Bone mineral content and density in Rett syndrome and their contributing factors. *Pediatr Res*, *69*(4), 293-298.

38) Pfrieger, F. W., & Ungerer, N. (2011). Cholesterol metabolism in neurons and astrocytes. *Prog Lipid Res*, *50*(4), 357-371.

39) Zlokovic, B. V. (2008). The blood-brain barrier in health and chronic neurodegenerative disorders. *Neuron*, *57*(2), 178-201.

40) Justice, M. J., Buchovecky, C. M., Kyle, S. M., & Djukic, A. (2013). A role for metabolism in Rett syndrome pathogenesis: New clinical findings and potential treatment targets. *Rare Diseases*, *1*(1), 1013-20.

41) Buchovecky, C. M., Turley, S. D., Brown, H. M., Kyle, S. M., McDonald, J. G., Liu, B., ... & Shendure, J. (2013). A suppressor screen in Mecp2 mutant mice implicates cholesterol metabolism in Rett syndrome. *Nat Genet*, *45*(9), 1013.

42) Hagberg, B., Witt-Engerström, I., Opitz, J. M., & Reynolds, J. F. (1986). Rett syndrome: a suggested staging system for describing impairment profile with increasing age towards adolescence. *Am J Med Genet*, *25*(S1), 47-59.

43) Galupa, R., & Heard, E. (2018). X-chromosome inactivation: a crossroads between chromosome architecture and gene regulation. *Annu Rev Genet*, *52*, 535-566.

44) Hagberg, B. (2002). Clinical manifestations and stages of Rett syndrome. *Ment Retard Dev Disabil Res Rev*, *8*(2), 61-65.

45) Ariani, F., Hayek, G., Rondinella, D., Artuso, R., Mencarelli, M. A., Spanhol-Rosseto, A., ... & Meloni, I. (2008). FOXG1 is responsible for the congenital variant of Rett syndrome. *Am J Med Genet*, *83*(1), 89-93.

46) Jan, M. M., Dooley, J. M., & Gordon, K. E. (1999). Male Rett syndrome variant: application of diagnostic criteria. *Pediatr Neurol*, *20*(3), 238-240.

47) Moog, U., Smeets, E. E., van Roozendaal, K. E., Schoenmakers, S., Herbergs, J., Schoonbrood-Lenssen, A. M., & Schrander-Stumpel, C. T. (2003). Neurodevelopmental disorders in males related to the gene causing Rett syndrome in females (MECP2). *Eur J Paediatr Neurol*, *7*(1), 5-12.

48) Ben Zeev, B., Yaron, Y., Schanen, N. C., Wolf, H., Brandt, N., Ginot, N., ... & Orr-Urtreger, A. (2002). Rett syndrome: clinical manifestations in males with MECP2 mutations. *J Child Neurol*, *17*(1), 20-24.

49) Neul, J. L., Kaufmann, W. E., Glaze, D. G., Christodoulou, J., Clarke, A. J., Bahi-Buisson, N., ... & Renieri, A. (2010). Rett syndrome: revised diagnostic criteria and nomenclature. *Annals of neurology*, *68*(6), 944-950.

50) Hagberg, B., Hanefeld, F., Percy, A., & Skjeldal, O. L. A. (2002). An update on clinically applicable diagnostic criteria in Rett syndrome. Comments to Rett Syndrome Clinical Criteria Consensus Panel Satellite to European Paediatric Neurology Society Meeting, Baden Baden, Germany, 11 September 2001. *Eur J Paediatr Neurol*, *6*(5), 293.

51) Tarquinio, D. C., Hou, W., Neul, J. L., Lane, J. B., Barnes, K. V., O'Leary, H. M., ... & Skinner, S. A. (2015). Age of diagnosis in Rett syndrome: patterns of recognition among diagnosticians and risk factors for late diagnosis. *Pediatric neurology*, *52*(6), 585-591.

52) Jobe, E. M., & Zhao, X. (2017). DNA methylation and adult neurogenesis. *Brain Plast*, *3*(1), 5-26.

53) Bergmann, O., Spalding, K. L., & Frisén, J. (2015). Adult neurogenesis in humans. *Cold Spring Harb Perspect Biol*, *7*(7), a018994.

54) Costello, J. F. (2003). DNA methylation in brain development and gliomagenesis. *Front Biosci*, *8*, s175.

55) Guoping, F. A. N., & Hutnick, L. (2005). Methyl-CpG binding proteins in the nervous system. *Cell Res*, *15*(4), 255-261.

56) Meehan, R. R., Lewis, J. D., McKay, S., Kleiner, E. L., & Bird, A. P. (1989). Identification of a mammalian protein that binds specifically to DNA containing methylated CpGs. *Cell*, *58*(3), 499-507.

57) Ehrhart, F., Coort, S. L., Cirillo, E., Smeets, E., Evelo, C. T., & Curfs, L. M. (2016). Rett syndrome–biological pathways leading from MECP2 to disorder phenotypes. *Orphanet J Rare Dis*, *11*(1), 158.

58) Shahbazian, M. D., Antalffy, B., Armstrong, D. L., & Zoghbi, H. Y. (2002). Insight into Rett syndrome: MeCP2 levels display tissue-and cell-specific differences and correlate with neuronal maturation. *Hum Mol Genet*, *11*(2), 115-124.

59) Kaufmann, W. E., Johnston, M. V., & Blue, M. E. (2005). MeCP2 expression and function during brain development: implications for Rett syndrome's pathogenesis and clinical evolution. *Brain Dev*, *27*, S77-S87.

60) Gulmez Karaca, K., Brito, D. V., & Oliveira, A. M. (2019). MeCP2: a critical regulator of chromatin in neurodevelopment and adult brain function. *Int J Mol Sci*, *20*(18), 4577.

61) Shah, R. R., & Bird, A. P. (2017). MeCP2 mutations: progress towards understanding and treating Rett syndrome. *Genome Med*, *9*(1), 17.

62) Wan, M., Lee, S. S. J., Zhang, X., Houwink-Manville, I., Song, H. R., Amir, R. E., ... & Zoghbi, H. Y. (1999). Rett syndrome and beyond: recurrent spontaneous and familial MECP2 mutations at CpG hotspots. *Am J Med Genet*, *65*(6), 1520-1529.

63) Nan, X., Ng, H. H., Johnson, C. A., Laherty, C. D., Turner, B. M., Eisenman, R. N., & Bird, A. (1998). Transcriptional repression by the methyl-CpG-binding protein MeCP2 involves a histone deacetylase complex. *Nature*, *393*(6683), 386-389.

64) Schmidt, A., Zhang, H., & Cardoso, M. C. (2020). MeCP2 and Chromatin Compartmentalization. *Cells*, *9*(4), 878.

65) Ballas, N., Lioy, D. T., Grunseich, C., & Mandel, G. (2009). Non–cell autonomous influence of MeCP2-deficient glia on neuronal dendritic morphology. *Nat Neurosci*, *12*(3), 311-317.

66) Bienvenu, T., & Chelly, J. (2006). Molecular genetics of Rett syndrome: when DNA methylation goes unrecognized. *Nat Rev Genet*, *7*(6), 415-426.

67) Bredenkamp, N., Seoighe, C., & Illing, N. (2007). Comparative evolutionary analysis of the FoxG1 transcription factor from diverse vertebrates identifies conserved recognition sites for microRNA regulation. *Dev Genes Evol*, *217*(3), 227-233.

68) Tian, C., Gong, Y., Yang, Y., Shen, W., Wang, K., Liu, J., ... & Zhao, C. (2012). Foxg1 has an essential role in postnatal development of the dentate gyrus. *J Neurosci*, *32*(9), 2931-2949.

69) Shen, W., Ba, R., Su, Y., Ni, Y., Chen, D., Xie, W., ... & Zhao, C. (2019). Foxg1 regulates the postnatal development of cortical interneurons. *Cereb Cortex*, *29*(4), 1547-1560.

70) Pauley, S., Lai, E., & Fritzsch, B. (2006). Foxg1 is required for morphogenesis and histogenesis of the mammalian inner ear. *Dev Dyn*, *235*(9), 2470-2482.

71) Kawauchi, S., Santos, R., Kim, J., Hollenbeck, P. L., Murray, R. C., & Calof, A. L. (2009). The role of foxg1 in the development of neural stem cells of the olfactory epithelium. *Ann N Y Acad Sci*, *1170*, 21.

72) Kortüm, F., Das, S., Flindt, M., Morris-Rosendahl, D. J., Stefanova, I., Goldstein, A., ... & Rauch, A. (2011). The core FOXG1 syndrome phenotype consists of postnatal microcephaly, severe mental retardation, absent language, dyskinesia, and corpus callosum hypogenesis. *J Med Genet*, *48*(6), 396-406.

73) Manuel, M. N., Martynoga, B., Molinek, M. D., Quinn, J. C., Kroemmer, C., Mason, J. O., & Price, D. J. (2011). The transcription factor Foxg1 regulates telencephalic progenitor proliferation cell autonomously, in part by controlling Pax6 expression levels. *Neural Dev*, *6*(1), 1-12.

74) Pratt, T., Quinn, J. C., Simpson, T. I., West, J. D., Mason, J. O., & Price, D. J. (2002). Disruption of early events in thalamocortical tract formation in mice lacking the transcription factors Pax6 or Foxg1. *J Neurosci*, *22*(19), 8523-8531.

75) López-Bendito, G., & Molnár, Z. (2003). Thalamocortical development: how are we going to get there? *Nat Rev Neurosci*, *4*(4), 276-289.

76) He, Z., Fang, Q., Li, H., Shao, B., Zhang, Y., Zhang, Y., ... & Shi, L. (2019). The role of FOXG1 in the postnatal development and survival of mouse cochlear hair cells. *Neuropharmacology*, *144*, 43-57.

77) Adesina, A. M., Veo, B. L., Courteau, G., Mehta, V., Wu, X., Pang, K., ... & Peters, L. (2015). FOXG1 expression shows correlation with neuronal differentiation in cerebellar development, aggressive phenotype in medulloblastomas, and survival in a xenograft model of medulloblastoma. *Hum Pathol*, *46*(12), 1859-1871.

78) Danesin, C., Peres, J. N., Johansson, M., Snowden, V., Cording, A., Papalopulu, N., & Houart, C. (2009). Integration of telencephalic Wnt and hedgehog signaling center activities by Foxg1. *Dev Cel*, *16*(4), 576-587.

79) Chen, J., Wu, X., Xing, Z., Ma, C., Xiong, W., Zhu, X., & He, X. (2018). FOXG1 expression is elevated in glioma and inhibits glioma cell apoptosis. *J Cancer*, *9*(5), 778.

80) Wong, L. C., Singh, S., Wang, H. P., Hsu, C. J., Hu, S. C., & Lee, W. T. (2019). FOXG1-Related Syndrome: From Clinical to Molecular Genetics and Pathogenic Mechanisms. *Int J Mol Sci*, *20*(17), 4176.

81) Bahi-Buisson, N., & Bienvenu, T. (2011). CDKL5-related disorders: from clinical description to molecular genetics. *Mol Syndromol*, *2*(3-5), 137-152.

82) Lin, C., Franco, B., & Rosner, M. R. (2005). CDKL5/Stk9 kinase inactivation is associated with neuronal developmental disorders. *Hum Mol Genet*, *14*(24), 3775-3786.

83) Rusconi, L., Salvatoni, L., Giudici, L., Bertani, I., Kilstrup-Nielsen, C., Broccoli, V., & Landsberger, N. (2008). CDKL5 expression is modulated during neuronal development and its subcellular distribution is tightly regulated by the C-terminal tail. *J Biol Chem*, *283*(44), 30101-30111.

84) Fichou, Y., Nectoux, J., Bahi-Buisson, N., Chelly, J., & Bienvenu, T. (2011). An isoform of the severe encephalopathy-related CDKL5 gene, including a novel exon with extremely high sequence conservation, is specifically expressed in brain. *J Hum Genet*. *56*(1), 52-57.

85) Williamson, S. L., Giudici, L., Kilstrup-Nielsen, C., Gold, W., Pelka, G. J., Tam, P. P., ... & Christodoulou, J. (2012). A novel transcript of cyclin-dependent kinase-like 5 (CDKL5) has an alternative C-terminus and is the predominant transcript in brain. *Hum Genet*, *131*(2), 187-200.

86) Mari, F., Azimonti, S., Bertani, I., Bolognese, F., Colombo, E., Caselli, R., ... & Ariani, F. (2005). CDKL5 belongs to the same molecular pathway of MeCP2 and it is responsible for the early-onset seizure variant of Rett syndrome. *Hum Mol Genet*, *14*(14), 1935-1946.

87) Bertani, I., Rusconi, L., Bolognese, F., Forlani, G., Conca, B., De Monte, L., ... & Kilstrup-Nielsen, C. (2006). Functional consequences of mutations in CDKL5, an X-linked gene involved in infantile spasms and mental retardation. *J Biol Chem*, *281*(42), 32048-32056.

88) Kameshita, I., Sekiguchi, M., Hamasaki, D., Sugiyama, Y., Hatano, N., Suetake, I., ... & Sueyoshi, N. (2008). Cyclin-dependent kinase-like 5 binds and phosphorylates DNA methyltransferase 1. *Biochem Biophys Res Commun*, *377*(4), 1162-1167.

89) Wang, I. T. J., Allen, M., Goffin, D., Zhu, X., Fairless, A. H., Brodkin, E. S., ... & Zhou, Z. (2012). Loss of CDKL5 disrupts kinome profile and event-related potentials leading to autistic-like phenotypes in mice. *Proc Natl Acad Sci U S A*, *109*(52), 21516-21521.

90) Amendola, E., Zhan, Y., Mattucci, C., Castroflorio, E., Calcagno, E., Fuchs, C., ... & Ciani, E. (2014). Mapping pathological phenotypes in a mouse model of CDKL5 disorder. *PloS one*, *9*(5), e91613.

91) Jhang, C. L., Huang, T. N., Hsueh, Y. P., & Liao, W. (2017). Mice lacking cyclin-dependent kinase-like 5 manifest autistic and ADHD-like behaviors. *Human Mol Genet*, *26*(20), 3922-3934.

92) Tang, S., Wang, I. T. J., Yue, C., Takano, H., Terzic, B., Pance, K., ... & Zhou, Z. (2017). Loss of CDKL5 in glutamatergic neurons disrupts hippocampal microcircuitry and leads to memory impairment in mice. *J Neurosci*, *37*(31), 7420-7437.

93) Okuda, K., Takao, K., Watanabe, A., Miyakawa, T., Mizuguchi, M., & Tanaka, T. (2018). Comprehensive behavioral analysis of the Cdkl5 knockout mice revealed significant enhancement in anxiety-and fear-related behaviors and impairment in both acquisition and long-term retention of spatial reference memory. *PloS one*, *13*(4), e0196587.

94) Barbiero, I., Valente, D., Chandola, C., Magi, F., Bergo, A., Monteonofrio, L., ... & Rinaldo, C. (2017). CDKL5 localizes at the centrosome and midbody and is required for faithful cell division. *Sci Rep*, *7*(1), 1-12.

95) Marchetto, M. C., Carromeu, C., Acab, A., Yu, D., Yeo, G. W., Mu, Y., ... & Muotri, A. R. (2010). A model for neural development and treatment of Rett syndrome using human induced pluripotent stem cells. *Cell*, *143*(4), 527-539.

96) Takahashi, K., & Yamanaka, S. (2006). Induction of pluripotent stem cells from mouse embryonic and adult fibroblast cultures by defined factors. *cell*, *126*(4), 663-676.

97) Grobarczyk, B., Franco, B., Hanon, K., & Malgrange, B. (2015). Generation of isogenic human iPS cell line precisely corrected by genome editing using the CRISPR/Cas9 system. *Stem Cell Rev Rep*, *11*(5), 774-787.

98) Ananiev, G., Williams, E. C., Li, H., & Chang, Q. (2011). Isogenic pairs of wild type and mutant induced pluripotent stem cell (iPSC) lines from Rett syndrome patients as in vitro disease model. *PloS one*, *6*(9), e25255.

99) Cheung, A. Y., Horvath, L. M., Grafodatskaya, D., Pasceri, P., Weksberg, R., Hotta, A., ... & Ellis, J. (2011). Isolation of MECP2-null Rett Syndrome patient hiPS cells and isogenic controls through X-chromosome inactivation. *Human Mol Genet*, *20*(11), 2103-2115.

100) Kim, K. Y., Hysolli, E., & Park, I. H. (2011). Neuronal maturation defect in induced pluripotent stem cells from patients with Rett syndrome. *Proc Natl Acad Sci U S A*, *108*(34), 14169-14174.

101) Brown, K., Selfridge, J., Lagger, S., Connelly, J., De Sousa, D., Kerr, A., ... & Bird, A. (2016). The molecular basis of variable phenotypic severity among common missense mutations causing Rett syndrome. *Human Mol Genet*, *25*(3), 558-570.

102) Cuddapah, V. A., Pillai, R. B., Shekar, K. V., Lane, J. B., Motil, K. J., Skinner, S. A., ... & Percy, A. K. (2014). Methyl-CpG-binding protein 2 (MECP2) mutation type is associated with disease severity in Rett syndrome. *J Med Genet*, *51*(3), 152-158.

103) Guy, J., Gan, J., Selfridge, J., Cobb, S., & Bird, A. (2007). Reversal of neurological defects in a mouse model of Rett syndrome. *Science*, *315*(5815), 1143-1147.

104) Guy, J., Hendrich, B., Holmes, M., Martin, J. E., & Bird, A. (2001). A mouse Mecp2-null mutation causes neurological symptoms that mimic Rett syndrome. *Nat Genet*, *27*(3), 322-326.

105) Chen, R. Z., Akbarian, S., Tudor, M., & Jaenisch, R. (2001). Deficiency of methyl-CpG binding protein-2 in CNS neurons results in a Rett-like phenotype in mice. *Nat Genet*, *27*(3), 327-331.

106) Hanashima, C., Li, S. C., Shen, L., Lai, E., & Fishell, G. (2004). Foxg1 suppresses early cortical cell fate. *Science*, *303*(5654), 56-59.

107) Eagleson, K. L., McFadyen-Ketchum, L. S., Ahrens, E. T., Mills, P. H., Does, M. D., Nickols, J., & Levitt, P. (2007). Disruption of Foxg1 expression by knock-in of cre recombinase: effects on the development of the mouse telencephalon. *Neuroscience*, *148*(2), 385-399

108) Striano, P., Paravidino, R., Sicca, F., Chiurazzi, P., Gimelli, S., Coppola, A., ... & Operto, F. (2011). West syndrome associated with 14q12 duplications harboring FOXG1. *Neurology*, *76*(18), 1600-1602.

109) Chen, Q., Zhu, Y. C., Yu, J., Miao, S., Zheng, J., Xu, L., ... & Xiong, Z. Q. (2010). CDKL5, a protein associated with rett syndrome, regulates neuronal morphogenesis via Rac1 signaling. *J Neurosci*, *30*(38), 12777-12786.

110) Della Sala, G., Putignano, E., Chelini, G., Melani, R., Calcagno, E., Ratto, G. M., ... & Pizzorusso, T. (2016). Dendritic spine instability in a mouse model of CDKL5 disorder is rescued by insulin-like growth factor 1. *Biol Psychiatry*, *80*(4), 302-311.

111) Ishino, Y., Shinagawa, H., Makino, K., Amemura, M., & Nakata, A. (1987). Nucleotide sequence of the iap gene, responsible for alkaline phosphatase isozyme conversion in Escherichia coli, and identification of the gene product. *J Bacteriol*, *169*(12), 5429-5433.

112) Jansen, R., Embden, J. D. V., Gaastra, W., & Schouls, L. M. (2002). Identification of genes that are associated with DNA repeats in prokaryotes. *Mol Microbiol*, *43*(6), 1565-1575.

113) Bolotin, A., Quinquis, B., Sorokin, A., & Ehrlich, S. D. (2005). Clustered regularly interspaced short palindrome repeats (CRISPRs) have spacers of extrachromosomal origin. *Microbiology*, *151*(8), 2551-2561.

114) Barrangou, R., Fremaux, C., Deveau, H., Richards, M., Boyaval, P., Moineau, S., ... & Horvath, P. (2007). CRISPR provides acquired resistance against viruses in prokaryotes. *Science*, *315*(5819), 1709-1712.

115) Hille, F., & Charpentier, E. (2016). CRISPR-Cas: biology, mechanisms and relevance. *Philos Trans R Soc Lond B Biol Sci*, *371*(1707), 20150496.

116) Barrangou, R., & Marraffini, L. A. (2014). CRISPR-Cas systems: prokaryotes upgrade to adaptive immunity. *Molecular cell*, *54*(2), 234-244.

117) Tyson, G. W., & Banfield, J. F. (2008). Rapidly evolving CRISPRs implicated in acquired resistance of microorganisms to viruses. *Environ Microbiol*, *10*(1), 200-207.

118) Rath, D., Amlinger, L., Rath, A., & Lundgren, M. (2015). The CRISPR-Cas immune system: biology, mechanisms and applications. *Biochimie*, *117*, 119-128;

119) Doudna, J. A., & Charpentier, E. (2014). The new frontier of genome engineering with CRISPR-Cas9. *Science*, *346*(6213

120) Ran, F. A., Hsu, P. D., Lin, C. Y., Gootenberg, J. S., Konermann, S., Trevino, A. E., ... & Zhang, F. (2013). Double nicking by RNA-guided CRISPR Cas9 for enhanced genome editing specificity. *Cell*, *154*(6), 1380-1389.

121) Jiang, F., & Doudna, J. A. (2017). CRISPR–Cas9 structures and mechanisms. *Annu Rev Biophys*, *46*, 505-529.

122) Nishiyama, J., Mikuni, T., & Yasuda, R. (2017). Virus-mediated genome editing via homology-directed repair in mitotic and postmitotic cells in mammalian brain. *Neuron*, *96*(4), 755-768.

123) Ribeil, J. A., Hacein-Bey-Abina, S., Payen, E., Magnani, A., Semeraro, M., Magrin, E., ... & Bartolucci, P. (2017). Gene therapy in a patient with sickle cell disease. *N Engl J Med*, *376*(9), 848-855.

124) Eichler, F., Duncan, C., Musolino, P. L., Orchard, P. J., De Oliveira, S., Thrasher, A. J., ... & Raymond, G. V. (2017). Hematopoietic stem-cell gene therapy for cerebral adrenoleukodystrophy. *N Engl J Med*, *377*(17), 1630-1638.

125) Liang, P., Xu, Y., Zhang, X., Ding, C., Huang, R., Zhang, Z., ... & Sun, Y. (2015). CRISPR/Cas9-mediated gene editing in human tripronuclear zygotes. *Protein & cell*, *6*(5), 363-372.

126) Yang, Y., Zhang, X., Yi, L., Hou, Z., Chen, J., Kou, X., ... & Wang, Y. (2016). Naïve induced pluripotent stem cells generated from β-thalassemia fibroblasts allow efficient gene correction with CRISPR/Cas9. *Stem Cells Transl Med*, *5*(1), 8-19.

127) Ma, W. G., Zhang, W., Zhu, J. M., Ziganshin, B. A., Zhi, A. H., Zheng, J., ... & Sun, L. Z. (2017). Long-term outcomes of frozen elephant trunk for type A aortic dissection in patients with Marfan syndrome. *J Thorac Cardiovasc Surg*, *154*(4), 1175-1189.

128) Prondzynski, M., Mearini, G., & Carrier, L. (2019). Gene therapy strategies in the treatment of hypertrophic cardiomyopathy. *Pflugers Arch*, *471*(5), 807-815.

129) Charlesworth, C. T., Deshpande, P. S., Dever, D. P., Camarena, J., Lemgart, V. T., Cromer, M. K., ... & Behlke, M. A. (2019). Identification of preexisting adaptive immunity to Cas9 proteins in humans. *Nat Med*, *25*(2), 249-254.

130) Chew, W. L., Tabebordbar, M., Cheng, J. K., Mali, P., Wu, E. Y., Ng, A. H., ... & Church, G. M. (2016). A multifunctional AAV–CRISPR–Cas9 and its host response. *Nat Methods*, *13*(10), 868-874.

131) Kleinstiver, B. P., Pattanayak, V., Prew, M. S., Tsai, S. Q., Nguyen, N. T., Zheng, Z., & Joung, J. K. (2016). High-fidelity CRISPR–Cas9 nucleases with no detectable genome-wide off-target effects. *Nature*, *529*(7587), 490-495.

132) Adachi, K., & Nakai, H. (2016). 540. Identification of a 16 Amino Acid-Long Motif in the N-Terminal Half of the AAV9 Capsid Essential for Persistence in the Blood for an Extended Period of up to 3 Days. *Molecular Therapy*, *24*, S216.

133) Chan, K. Y., Jang, M. J., Yoo, B. B., Greenbaum, A., Ravi, N., Wu, W. L., ... & Gradinaru, V. (2017). Engineered AAVs for efficient noninvasive gene delivery to the central and peripheral nervous systems. *Nat Neurosci*, *20*(8), 1172-1179.

134) Al-Zaidy, S. A., & Mendell, J. R. (2019). From clinical trials to clinical practice: practical considerations for gene replacement therapy in SMA type 1. *Pediatr Neurol*, *100*, 3-11.

135) Sehara, Y., Fujimoto, K. I., Ikeguchi, K., Katakai, Y., Ono, F., Takino, N., ... & Muramatsu, S. I. (2017). Persistent expression of dopamine-synthesizing enzymes 15 years after gene transfer in a primate model of Parkinson's disease. *Hum Gene Ther Clin Dev*, *28*(2), 74-79.

136) Guy, J., Gan, J., Selfridge, J., Cobb, S., & Bird, A. (2007). Reversal of neurological defects in a mouse model of Rett syndrome. *Science*, *315*(5815), 1143-1147.

137) Castro, J., Garcia, R. I., Kwok, S., Banerjee, A., Petravicz, J., Woodson, J., ... & Sur, M. (2014). Functional recovery with recombinant human IGF1 treatment in a mouse model of Rett Syndrome. *Proc Natl Acad Sci U S A*, *111*(27), 9941-9946.

138) Khwaja, O. S., Ho, E., Barnes, K. V., O'Leary, H. M., Pereira, L. M., Finkelstein, Y., ... & Khatwa, U. (2014). Safety, pharmacokinetics, and preliminary assessment of efficacy of mecasermin (recombinant human IGF-1) for the treatment of Rett syndrome. *Proc Natl Acad Sci U S A*, *111*(12), 4596-4601.

139) Gadalla, K. K., Vudhironarit, T., Hector, R. D., Sinnett, S., Bahey, N. G., Bailey, M. E., ... & Cobb, S. R. (2017). Development of a novel AAV gene therapy cassette with improved safety features and efficacy in a mouse model of Rett syndrome. *Mol Ther Methods Clin Dev*, *5*, 180-190.

140) Vangipuram, M., Ting, D., Kim, S., Diaz, R., & Schüle, B. (2013). Skin punch biopsy explant culture for derivation of primary human fibroblasts. *J Vis Exp*, (77), e3779.

141) Hotta, A., Cheung, A. Y., Farra, N., Vijayaragavan, K., Séguin, C. A., Draper, J. S., ... & Bhatia, M. (2009). Isolation of human iPS cells using EOS lentiviral vectors to select for pluripotency. *Nat Methods*, *6*(5), 370-376.

142) Auricchio, A., Hildinger, M., O'Connor, E., Gao, G. P., & Wilson, J. M. (2001). Isolation of highly infectious and pure adeno-associated virus type 2 vectors with a single-step gravity-flow column. *Hum Gene Ther*, *12*(1), 71-76.

143) Swiech, L., Heidenreich, M., Banerjee, A., Habib, N., Li, Y., Trombetta, J., ... & Zhang, F. (2015). In vivo interrogation of gene function in the mammalian brain using CRISPR-Cas9. *Nat Biotechnol*, *33*(1), 102-106.

144) Niccheri, F., Pecori, R., & Conticello, S. G. (2017). An efficient method to enrich for knock-out and knock-in cellular clones using the CRISPR/Cas9 system. *Cell Mol Life Sci 74*(18), 3413-3423.

145) Dracopoli, N. C., Haines, J. L., & Korf, B. R. (1994). Current protocols in human genetics.

146) Li, X. L., Li, G. H., Fu, J., Fu, Y. W., Zhang, L., Chen, W., ... & Chen, W. V. (2018). Highly efficient genome editing via CRISPR–Cas9 in human pluripotent stem cells is achieved by transient BCL-XL overexpression. *Nucleic Acids Res*, *46*(19), 10195-10215.

147) Park, J., Lim, K., Kim, J. S., & Bae, S. (2017). Cas-analyzer: an online tool for assessing genome editing results using NGS data. *Bioinformatics*, *33*(2), 286-288.

148) Tsai, S. Q., Zheng, Z., Nguyen, N. T., Liebers, M., Topkar, V. V., Thapar, V., ... & Aryee, M. J. (2015). GUIDE-seq enables genome-wide profiling of off-target cleavage by CRISPR-Cas nucleases. *Nat Biotechnol*, *33*(2), 187-197.

149) Casini, A., Olivieri, M., Petris, G., Montagna, C., Reginato, G., Maule, G., ... & Inga, A. (2018). A highly specific SpCas9 variant is identified by in vivo screening in yeast. *Nat Biotechnol*, *36*(3), 265-271.ù

150) Gabel, H. W., Kinde, B., Stroud, H., Gilbert, C. S., Harmin, D. A., Kastan, N. R., ... & Greenberg, M. E. (2015). Disruption of DNA-methylation-dependent long gene repression in Rett syndrome. *Nature*, *522*(7554), 89-93.

151) Zhou, Z., Hong, E. J., Cohen, S., Zhao, W. N., Ho, H. Y. H., Schmidt, L., ... & Hu, L. (2006). Brain-specific phosphorylation of MeCP2 regulates activity-dependent Bdnf transcription, dendritic growth, and spine maturation. *Neuron*, *52*(2), 255-269

152) Yasui, D. H., Peddada, S., Bieda, M. C., Vallero, R. O., Hogart, A., Nagarajan, R. P., ... & LaSalle, J. M. (2007). Integrated epigenomic analyses of neuronal MeCP2 reveal a role for long-range interaction with active genes. *Proc Natl Acad Sci U S A*, *104*(49), 19416-19421.

153) Jordan, C., Li, H. H., Kwan, H. C., & Francke, U. (2007). Cerebellar gene expression profiles of mouse models for Rett syndrome reveal novel MeCP2 targets. *BMC Med Genet*, *8*(1), 36.

154) Runkel, F., Rohlmann, A., Reissner, C., Brand, S. M., & Missler, M. (2013). Promoter-like sequences regulating transcriptional activity in neurexin and neuroligin genes. *J Neurochem*, *127*(1), 36-47.

155) Gibson, J. H., Slobedman, B., Harikrishnan, K. N., Williamson, S. L., Minchenko, D., El-Osta, A., ... & Christodoulou, J. (2010). Downstream targets of methyl CpG binding protein 2 and their abnormal expression in the frontal cortex of the human Rett syndrome brain. *BMC Neurosci*, *11*(1), 53.

156) Delgado, I. J., Kim, D. S., Thatcher, K. N., LaSalle, J. M., & Van den Veyver, I. B. (2006). Expression profiling of clonal lymphocyte cell cultures from Rett syndrome patients. *BMC Med Genet*, *7*(1), 61.

157) Ballestar, E., Ropero, S., Alaminos, M., Armstrong, J., Setien, F., Agrelo, R., ... & Monros, E. (2005). The impact of MECP2 mutations in the expression patterns of Rett syndrome patients. *Hum Genet*, *116*(1-2), 91-104.

158) Traynor, J., Agarwal, P., Lazzeroni, L., & Francke, U. (2002). Gene expression patterns vary in clonal cell cultures from Rett syndrome females with eight different MECP2 mutations. *BMC Med Genet*, *3*(1), 12.

159) Fazzari, P., Paternain, A. V., Valiente, M., Pla, R., Luján, R., Lloyd, K., ... & Rico, B. (2010). Control of cortical GABA circuitry development by Nrg1 and ErbB4 signalling. *Nature*, *464*(7293), 1376-1380.

160) Ting, A. K., Chen, Y., Wen, L., Yin, D. M., Shen, C., Tao, Y., ... & Mei, L. (2011). Neuregulin 1 promotes excitatory synapse development and function in GABAergic interneurons. *J Neurosci*, *31*(1), 15-25.

161) Li, H., Chou, S. J., Hamasaki, T., Perez-Garcia, C. G., & O'Leary, D. D. (2012). Neuregulin repellent signaling via ErbB4 restricts GABAergic interneurons to migratory paths from ganglionic eminence to cortical destinations. *Neural Dev*, *7*(1), 1-17.

162) Tong, X. J., Hu, Z., Liu, Y., Anderson, D., & Kaplan, J. M. (2015). A network of autism linked genes stabilizes two pools of synaptic GABAA receptors. *elife*, *4*, e09648.

163) Tapia, M., Wandosell, F., & Garrido, J. J. (2010). Impaired function of HDAC6 slows down axonal growth and interferes with axon initial segment development. *PloS one*, *5*(9), e12908.

164) Yee, A. J., Bensinger, W. I., Supko, J. G., Voorhees, P. M., Berdeja, J. G., Richardson, P. G., ... & Tamang, D. L. (2016). Ricolinostat plus lenalidomide, and dexamethasone in relapsed or refractory multiple myeloma: a multicentre phase 1b trial. *Lancet Oncol*, *17*(11), 1569-1578.

165) Haapaniemi, E., Botla, S., Persson, J., Schmierer, B., & Taipale, J. (2018). CRISPR–Cas9 genome editing induces a p53-mediated DNA damage response. *Nat Med*, *24*(7), 927-930.

166) Thomas, M., Kalita, A., Labrecque, S., Pim, D., Banks, L., & Matlashewski, G. (1999). Two polymorphic variants of wild-type p53 differ biochemically and biologically. *Mol Cell Biol*, *19*(2), 1092-1100.

167) Naso, M. F., Tomkowicz, B., Perry, W. L., & Strohl, W. R. (2017). Adeno-associated virus (AAV) as a vector for gene therapy. *BioDrugs*, *31*(4), 317-334.

168) Park, J., Lim, K., Kim, J. S., & Bae, S. (2017). Cas-analyzer: an online tool for assessing genome editing results using NGS data. *Bioinformatics*, *33*(2), 286-288.

169) Saraiva, J., Nobre, R. J., & de Almeida, L. P. (2016). Gene therapy for the CNS using AAVs: the impact of systemic delivery by AAV9. *J Control Release*, *241*, 94-109.

170) Landucci, E., Brindisi, M., Bianciardi, L., Catania, L. M., Daga, S., Croci, S., ... & Furini, S. (2018). iPSC-derived neurons profiling reveals GABAergic circuit disruption and acetylated α-tubulin defect which improves after iHDAC6 treatment in Rett syndrome. *Exp Cell Res*, *368*(2), 225-235.

171) Le, T. T. H., Tran, N. T., Dao, T. M. L., Nguyen, D. D., Do, D. H., Ha, L. T., ... & Chu, V. T. (2019). Efficient and precise CRISPR/Cas9-mediated MECP2 modifications in human induced pluripotent stem cells. *Front Genet*, *10*, 625.

172) Martufi, M., Good, R. B., Rapiteanu, R., Schmidt, T., Patili, E., Tvermosegaard, K., ... & Maratou, K. (2019). Single-step, high-efficiency CRISPR-Cas9 genome editing in primary human disease-derived fibroblasts. *CRISPR J*, *2*(1), 31-40.

173) Xie, N., Gong, H., Suhl, J. A., Chopra, P., Wang, T., & Warren, S. T. (2016). Reactivation of FMR1 by CRISPR/Cas9-mediated deletion of the expanded CGG-repeat of the fragile X chromosome. *PloS one*, *11*(10), e0165499.

174) Mendell, J. R., Al-Zaidy, S., Shell, R., Arnold, W. D., Rodino-Klapac, L. R., Prior, T. W., ... & Kissel, J. T. (2017). Single-dose gene-replacement therapy for spinal muscular atrophy. *N Engl J Med*, *377*(18), 1713-1722.

175) Koerner, M. V., FitzPatrick, L., Selfridge, J., Guy, J., De Sousa, D., Tillotson, R., ... & Bird, A. (2018). Toxicity of overexpressed MeCP2 is independent of HDAC3 activity. *Genes Dev*, *32*(23-24), 1514-1524.

176) Lombardi, L. M., Baker, S. A., & Zoghbi, H. Y. (2015). MECP2 disorders: from the clinic to mice and back. *J Clin Invest*, *125*(8), 2914-2923.

177) Bowers, W. J., Breakefield, X. O., & Sena-Esteves, M. (2011). Genetic therapy for the nervous system. *Hum Mol Genet*, *20*(R1), R28-R41.

178) Daya, S., & Berns, K. I. (2008). Gene therapy using adeno-associated virus vectors. *Clin Microbiol Rev*, *21*(4), 583-593.

179) Kaplitt, M. G., Feigin, A., Tang, C., Fitzsimons, H. L., Mattis, P., Lawlor, P. A., ... & During, M. J. (2007). Safety and tolerability of gene therapy with an adeno-associated virus (AAV) borne GAD gene for Parkinson's disease: an open label, phase I trial. *The Lancet*, *369*(9579), 2097-2105.

180) Foust, K. D., Nurre, E., Montgomery, C. L., Hernandez, A., Chan, C. M., & Kaspar, B. K. (2009). Intravascular AAV9 preferentially targets neonatal neurons and adult astrocytes. *Nat Biotechnol*, *27*(1), 59-65.

181) Hareendran, S., Balakrishnan, B., Sen, D., Kumar, S., Srivastava, A., & Jayandharan, G. R. (2013). Adeno-associated virus (AAV) vectors in gene therapy: immune challenges and strategies to circumvent them. *Rev Med Virol*, *23*(6), 399-413.

182) Sinnett, S. E., Hector, R. D., Gadalla, K. K., Heindel, C., Chen, D., Zaric, V., ... & Gray, S. J. (2017). Improved MECP2 gene therapy extends the survival of MeCP2-null mice without apparent toxicity after intracisternal delivery. *Mol Ther Methods Clin Dev*, *5*, 106-115.

183) Senís, E., Fatouros, C., Große, S., Wiedtke, E., Niopek, D., Mueller, A. K., ... & Grimm, D. (2014). CRISPR/Cas9-mediated genome engineering: an adeno-associated viral (AAV) vector toolbox. *Biotechnol J*, *9*(11), 1402-1412.

184) Bak, R. O., & Porteus, M. H. (2017). CRISPR-mediated integration of large gene cassettes using AAV donor vectors. *Cell Rep*, *20*(3), 750-756.

185) Gray, S. J., Kalburgi, S. N., McCown, T. J., & Samulski, R. J. (2013). Global CNS gene delivery and evasion of anti-AAV-neutralizing antibodies by intrathecal AAV administration in non-human primates. *Gene Ther*, *20*(4), 450-459.

186) Maguire, C. A., Ramirez, S. H., Merkel, S. F., Sena-Esteves, M., & Breakefield, X. O. (2014). Gene therapy for the nervous system: challenges and new strategies. *Neurotherapeutics*, *11*(4), 817-839.

187) Büning, H., & Srivastava, A. (2019). Capsid modifications for targeting and improving the efficacy of AAV vectors. *Mol Ther Methods Clin Dev*, *12*, 248-265.

188) Ruan, G. X., Barry, E., Yu, D., Lukason, M., Cheng, S. H., & Scaria, A. (2017). CRISPR/Cas9-mediated genome editing as a therapeutic approach for Leber congenital amaurosis 10. *Mol Ther*, *25*(2), 331-341.

189) Gong, H., Liu, M., Klomp, J., Merrill, B. J., Rehman, J., & Malik, A. B. (2017). Method for dual viral vector mediated CRISPR-Cas9 gene disruption in primary human endothelial cells. *Sci Rep*, *7*, 42127.

190) Chu, H. W., Rios, C., Huang, C., Wesolowska-Andersen, A., Burchard, E. G., O'Connor, B. P., ... & Seibold, M. A. (2015). CRISPR–Cas9-mediated gene knockout in primary human airway epithelial cells reveals a proinflammatory role for MUC18. *Gene Ther*, *22*(10), 822-829.

191) Voets, O., Tielen, F., Elstak, E., Benschop, J., Grimbergen, M., Stallen, J., ... & Essrich, C. (2017). Highly efficient gene inactivation by adenoviral CRISPR/Cas9 in human primary cells. *PLoS One*, *12*(8), e0182974.

192) Chapman, J. R., Taylor, M. R., & Boulton, S. J. (2012). Playing the end game: DNA double-strand break repair pathway choice. *Mol Cell*, *47*(4), 497-510.

193) Cox, D. B. T., Platt, R. J., & Zhang, F. (2015). Therapeutic genome editing: prospects and challenges. *Nat Med*, *21*(2), 121-131.

194) Ishizu, T., Higo, S., Masumura, Y., Kohama, Y., Shiba, M., Higo, T., ... & Hikoso, S. (2017). Targeted genome replacement via homology-directed repair in non-dividing cardiomyocytes. *Sci Rep*, *7*(1), 1-11.

195) Keimling, M., & Wiesmüller, L. (2009). DNA double-strand break repair activities in mammary epithelial cells—influence of endogenous p53 variants. *Carcinogenesis*, *30*(7), 1260-1268.

196) Moureau, S., Luessing, J., Harte, E. C., Voisin, M., & Lowndes, N. F. (2016). A role for the p53 tumour suppressor in regulating the balance between homologous recombination and non-homologous end joining. *Open Biol*, *6*(9), 160225.

197) Hustedt, N., & Durocher, D. (2017). The control of DNA repair by the cell cycle. *Nat Cell Biol*, *19*(1), 1-9.

198) Ihry, R. J., Worringer, K. A., Salick, M. R., Frias, E., Ho, D., Theriault, K., ... & Randhawa, R. (2018). p53 inhibits CRISPR–Cas9 engineering in human pluripotent stem cells. *Nat Med*, *24*(7), 939-946.

199) Conti, A., & Di Micco, R. (2018). p53 activation: a checkpoint for precision genome editing?. *Genome Med*, *10*(1), 66.

200) Zhang, X. H., Tee, L. Y., Wang, X. G., Huang, Q. S., & Yang, S. H. (2015). Off-target effects in CRISPR/Cas9-mediated genome engineering. *Mol Ther Nucleic Acids*, *4*, e264.

201) Daga, S., Donati, F., Capitani, K., Croci, S., Tita, R., Giliberti, A., ... & Baldassarri, M. (2020). New frontiers to cure Alport syndrome: COL4A3 and COL4A5 gene editing in podocyte-lineage cells. *Eur J Hum Genet*, *28*(4), 480-490.

7. List of abbreviations

RTT = Rett syndrome

KO = knock-out

XCI = X Chromosome Inactivation

ASD = Autism Spectrum Disorders

MECP2 = Methyl-CpG- binding protein 2

CVS = Chorionic villus sampling

MBD = CpG-Binding Domain

NID = NCoR domain

TRD = Transcriptional Repression Domain

NLS = Nuclear Localization Signal

FOXG1 = Fork-head box protein G1

CDKL5 = Cyclin-Dependent Kinase-like-5

DNMT1 = DNA methyltransferase I

CNS = Central Nervous System

FOXG1-RD = FOXG1-Related Disorders

iPSCs = Induced Pluripotent Stem Cell

CRISPR = Clustered Regularly Interspaced Short Palindromic Repeats

PAM = Protospacer Adjacent Motif

sgRNA = single guide RNA

NHEJ = Non-Homologous End Joining

HDR = Homology-Directed Repair

DSB = Double Strand Breaks

HCM = Hypertrophic Cardiomyopathy

BBB = Blood Brain Barrier

AAV = Adeno Associated Virus

3PN zygotes = three-pronuclear zygotes

TP53 = tumor protein 53

Bp = base pairs